University of Liège

Faculty of Applied Sciences
Aerospace and Mechanical Engineering Department (LTAS)

Oufti-1 : flight system configuration and structural analysis.

Master Thesis — June 2009

Supervisor : Prof. Gaëtan Kerschen

Gauthier Pierlot
2nd Master in Aerospace Engineering

Academic Year 2008 – 2009

Abstract

$OUFTI-1$ is the first satellite ever equipped with a recently developed amateur radio digital-communication technology: the D-STAR protocol. This system represents both the satellite's communication system and its payload.

This thesis focuses on the mechanical structure of $OUFTI-1$. It intends to precise the structural functions and requirements according to the mission objectives. It develops a flight system configuration that highlights the environmental constraints due to the particular orbit imposed by the Vega Maiden Flight. Another objective of this thesis is to ensure the structural reliability during launch as well as in orbit. Several finite element analysis demonstrate the ability of $OUFTI-1$ to sustain the structural loads. A free-free modal survey is carried out and the corresponding modal analysis is correlated. The first vibrations tests on shaker are also presented.

Keywords : OUFTI-1, CubeSat, LEODIUM, D-STAR, amateur radio, STRU, Configuration, Structure.

Acknowledgment

First of all, I would like to express my gratitude to my advisor Professor Gaëtan Kerschen for its precious help and support. I appreciated its advices and its confidence in me.

Many thanks go to Professors Grigorios Dimitriadis, Jean-Claude Golinval, Jacques Verly, and Amandine Denis who accepted to participate in the examination committee of this master thesis. I am more than thankful to Amandine for her comments and suggestions throughout the writing of this dissertation.

I am pleased to acknowledge my friends of the $OUFTI-1$ team who created a pleasant working atmosphere. Special thanks go to Jonathan and Amandine for their kindness and their motivation.

Finally and foremost, I would like to express my love and gratitude to Audrey for her constant help and for always being there for me during these five years.

Contents

Abbreviated terms

ADCS	Attitude determination and control system
Al	Aluminum
ATOX	Atomic oxygen
BOL	Begin of life
CalPoly	California polytechnic state university
COG	Center of gravity
COM	Electronic card for communication
CDS	CubeSat design specification
CFRP	Carbon fiber reinforced plastic
COTS	Commercial off the shell
CSG	Centre spatial de Guyane
CSK	CubeSat kit
CSL	Centre spatial de Liège
CTE	Coefficient of thermal expansion
CVCM	Collected volatile condensable material
ECFM	Electronic card's flight model
ECSS	European cooperation for space standarization
EMC	Electromagnetic compatibility
EMI	Electromagnetic interference
EPS1	Main electrical power supply
EPS2	Experimental electrical power supply
ESA	European space agency
FEA	Finite element analysis
FEM	Finite element model
FM430	Electronic flight module 430 card
FOS	Factor of safety
FR4	Flame resistant 4
GFRP	Glass fiber reinforced plastic
ICD	Interface control document
ITD	Ibrahim time domain
KISS	Keep It Simple and Smart
KS	Kill switch
LEO	Low earth orbit
LiPo	Lithium-polymer batteries
LSCE	Least-squares complex exponential
LSFD	Least-squares frequency domain
LV	Launch vehicle
LPTM	Low power transmission mode

MAC	Modal Assurance Criterion
MIAS	Mission analysis subsystem
MECH	Antenna's deployment subsystem
MOS	Margin of safety
MSO	Midplane standoff
MTP	Mission test plan
OBC2	Second on-board computer
PCB	Printed circuit board
PFC	Pass fail criteria
PSD	Power spectral density
RBF	Remove before flight
RT	Room temperature
SP	Spring plungers
SPOF	Single point of failure
SM	Structural model
SNR	Signal to noise ratio
STRU	Structural subsystem
TBD	To be determined
TBC	To be confirmed
TID	Total irradiation dose
TML	Total mass loss
THER	Thermal subsystem
UHF	Ultra high frequency
VHF	Very high frequency

Introduction 1

1.1 Introduction

$OUFTI-1$ is the first satellite developed at the University of Liège as well as the first nanosatellite ever made in Belgium. The purpose of this thesis is to present the developments and advancements in the structural subsystem of the $OUFTI-1$ project during the academic year $2008-2009$ at the University of Liège (ULg).

Written in the framework of the 2nd master in aerospace engineering, this master thesis develops the flight system configuration, the structural study and the preliminary vibration testing of $OUFTI-1$ in order to make one step closer to its realization.

The mechanical structure plays a major role during the launch because it is the backbone of the mechanical system. It has to withstand the static and dynamic loading as well as the noise during the flight and the shocks during stage separation, ignition and fairing jettisoning. Once in orbit, the structure will protect the main payload against the harsh space environment : radiations, debris, thermal variations, etc. Therefore, a complete structural analysis is necessary to provide a pledge on the satellite structural reliability.

1.2 CubeSat program

The CubeSat program, which started 10 years ago, aims to facilitate the access to space by creating a standard easier to design and develop such it can be used as secondary payload on space launcher. This new trend within the aerospace community allows to flight a real spacecraft under much less cost and development time than many other solutions.

This program is jointly led by the California Polytechnic State University, well-known for its "learn by doing´´ principles, and Stanford University. Year after year, it is becoming a complete success with the universities and the industries all over the world, and takes more and more extent in many sectors. At the moment, at least 80 institutions are involved in a CubeSat project.

Moreover, seeing that the CubeSat program facilitates the space access to a larger sector of developers such as the universities, it also promotes

the educational purposes by giving hands-on experience to engineering students in aerospace. It is in this way that the University of Liège develops its first nanosatellite called $OUFTI - 1$.

1.3 CubeSat concept

The fundamental features of the CubeSat standard are its physical constraints : 1 kilogram mass in 1 dm^3 volume with an average power of approximately 1 watt. This small 10 x 10 x 10 cm unit represents a technical challenge just by those restrictions.

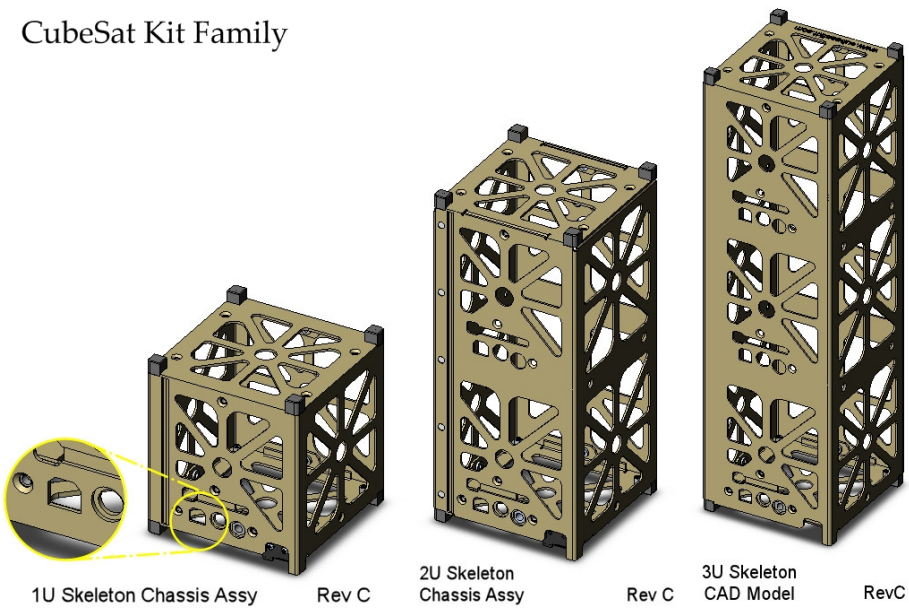

Figure 1.1 – *CubeSat formats*

3 formats come from this definition (Figure 1.1). 1 structural unit, the most simple and probably the most used. 2 structural units, simply obtained by stacking up 2 single structures, and finally the 3 units CubeSats, the largest format. Although many commercial structures exist (e.g. Pumpkin, Boeing, Isis, etc.), the most popular remains the CubeSat Kit (CSK) structure from Pumpkin.

The CubeSat philosophy is quite different compared to larger satellites. While a typical spacecraft often costs millions of dollars and needs many years to be designed and launched, a CubeSat project can start with a budget less than 100000€ and 2 years of developments (19) (80), from the first steps to the launch.

This philosophy is also different in regard to the development process. Instead of using space qualified and very expensive technology, a student nanosatellite tries as much as possible to integrate Commercial Of The Shelf (COTS) materials and components to reduce the cost and the development time. For the same reasons, official requirements are lightened. Thus, there is a management of failures rather than using expensive solution to minimize them.

Since the beginning, CalPoly develops standards and procedures to design, build and qualify structure for space launch. Thus, any nanosatellite has to respect several technical specifications and guidelines (47) to be validated as a CubeSat. Those ensure that the CubeSat definition is compatible with the launcher's interface and that it will not interfere with other satellites or payloads by describing the requirements (e.g., outer dimensions and restrictions, recommended materials).

CalPoly also develops a standard solution for the deployment interface : the P-POD or Poly Pico-Satellite Orbital Deployer (Figure 1.2). It enables 1 to 3 units CubeSats to be deployed in orbit by a smart system that uses the under utilized space inside the launch vehicle. Its utilization greatly simplifies the CubeSats integration and limits the undesirable interactions with the surrounding environment. Further details can be found in reference(6).

Figure 1.2 – *Poly Pico Satellite Orbital Deployer (P-Pod)*

1.4 State of art

CubeSats projects are now widespread and range from meteorological or space environment studies to telecommunications. The following list is not exhaustive but it gives an overview of their applications (18).

SwissCube is the first nanosatellite developed at the Swiss Federal Institute of Technology Lausanne (Switzerland). Its objective is to take optical measurements of the airglow phenomenon over all latitudes and longitudes for at least 3 months. (66)

Delfi-C3 is the first CubeSat student project from the Delft University of Technology (the Netherlands). It carries new thin film solar cells and an autonomous wireless sun sensor experiment. (54)

Compass-1 is developed at Aachen University of Applied Sciences, in Germany. The mission purpose is to allow everyone to take and download pictures of the earth (51).

Can-X2 tests a set of solutions (propulsion system, custom radios, attitude sensors and actuators and a commercial GPS receiver) that will be used on their next satellites. It is the second CubeSat project initiated at the University of Toronto (55).

C.A.P.E 1's purpose is to gather data from terrestrial receivers in Gulf of Mexico and transmit them to the ground station at the University of Louisiana at Lafayette. (53)

CP6 is made at its Californian cradle of CalPoly. This nanosatellite implements an attitude control system using magnetic torquers embedded within the side panels. It also carries a scientific payload for electron measurements in orbit. (11)

Kumu A'o CubeSat is designed at the University of Hawaii. This CubeSat has only an educational purpose by providing opportunities to Hawaiian engineering students to develop a real space project. (13)

CalPoly understood that the exchange of information is key to the CubeSat concept success. The CubeSat community was then created to facilitate the communications between developers and official standard (12).

1.5 OUFTI-1 Project

1.5.1 Genesis

$OUFTI-1$ project began in September 2007 following an idea of Luc Halbach (Spacebel) : the use inside a nanosatellite of the innovative digital telecommunications protocol D-STAR. Within a few weeks, a team of students and academics was created and the project was on track : $OUFTI-1$ was born. OUFTI, which stands for Orbital Utility For Telecommunications Innovations, is a common expression in Liège (Belgium) that means : " WAW! ´´. At the moment, 13 students from three engineering schools are doing their master theses on $OUFTI-1$.

1.5.2 Mission objectives

$OUFTI-1$ intends to demonstrate in orbit the feasibility of 3 payloads (30) :

1. D-STAR digital telecommunications protocol
2. Azurspace's solar cells with 30% efficiency BOL
3. An innovative electrical power system

D-STAR, which stands for Digital Smart Technology for Amateur Radio, is a digital protocol from the Japan Amateur Radio League (JARL) and is $OUFTI-1$'s main payload . This protocol brings many advances compared to conventional radio system such as a much better Signal to Noise Ratio (SNR), a simultaneous transmission of data (e.g. GPS data) and voice, and a direct connection to the internet thanks to the D-STAR repeater at ULg. Moreover, D-STAR is widespread within the ham-radio community, especially in the United States and now in Europe.

A new digital power supply will be aboard $OUFTI-1$. This power supply, developed in collaboration with Thales Alenia Space (76), is based on a fly back converter which is digitally controlled. It will supply the $3,3\ V$ bus but it will never take the control over the main power supply.

Finally, high-efficiency solar cells will be tested. Provided by Azurspace (5), they have 30% efficiency at their begin of life (BOL) which is the highest efficiency available on the market at the moment.

1.5.3 CubeSat Kit and development philosophy

To accelerate the development of this challenging CubeSat, the University of Liège bought a 1U CubeSat Kit last year (37). The structure is conform to the standard developed at CalPoly and integrates the first electronic card (Figure 1.3). Because this kit has already flown, it is a reliable starting point for the rest of the developments.

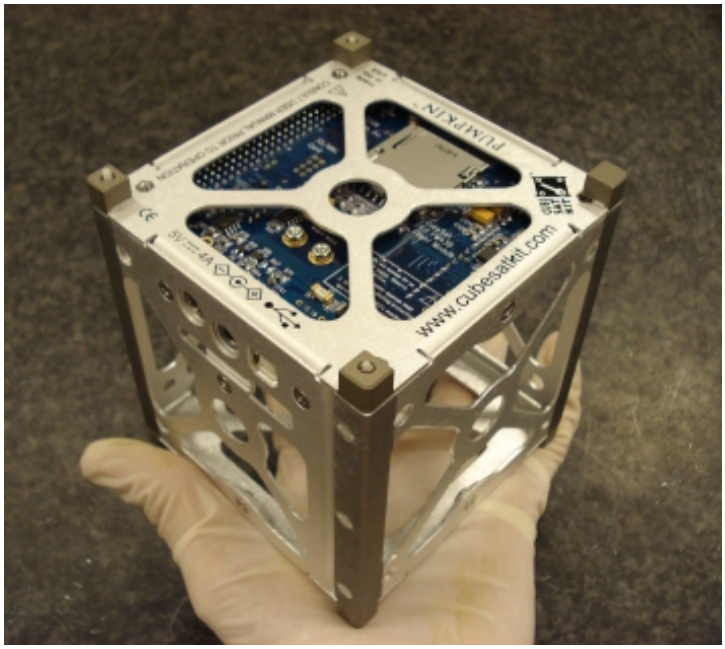

Figure 1.3 – *CubeSat Kit Structure and Flight Module 430 card*

The philosophy followed at ULg is KISS : Keep It Simple and Stupid. The simpler the concept, the better the solution! Many problems will be then solved by choosing the simpler concept to save time and money.

1.5.4 Requirements

The structural subsystem has to fulfill many functions to ensure mission success. They are summarized in Figure 1.4. The division of the structural subsystem is done with a primary structure, the CubeSat Kit (CSK), which cannot be manufactured easily. The secondary structure represents any part that will not directly sustain the structural loads from Launch Vehicle (LV), i.e. solar panels, screws, Printed Circuit Boards (PCBs), etc. Finally, the interface with P-POD includes the rails, the feet, a Remove Before Flight pin (RBF), etc.

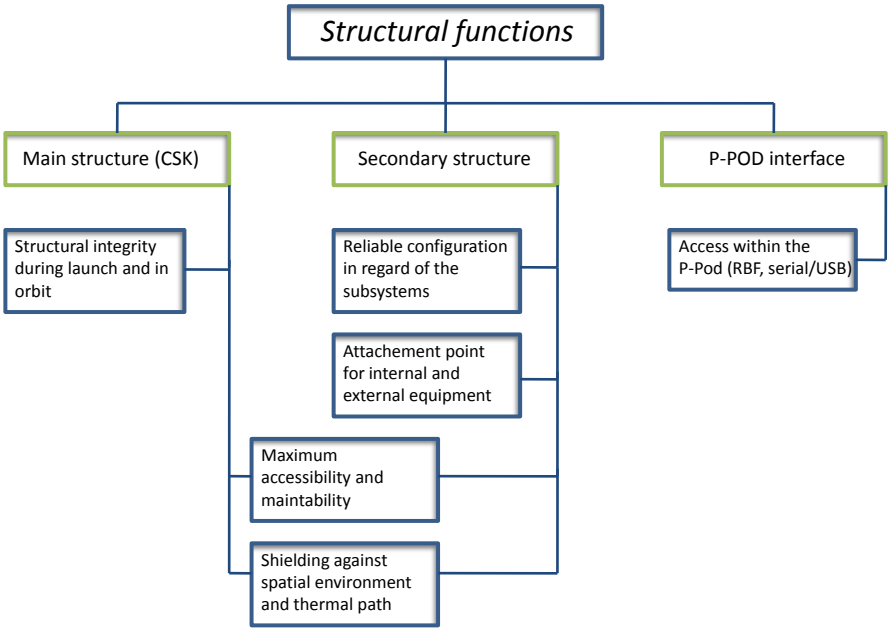

Figure 1.4 – *Structural functionalities*

On the basis of these functions and reference (25), a set of structural requirements can be written in subsection 1.5.4.1.

The equipment necessary to the mission success (e.g. EPS, permanent magnet and hysteresis rods) is added. It has to fulfill many requirements from official institutions such as ESA (56), CalPoly (47) and ArianeSpace (7). These are presented in subsection 1.5.4.2, 1.5.4.3, 1.5.4.4 and 1.5.4.5.

1.5.4.1 Structural Requirements

1. **STRU-1**: Structural subsystem shall protect mechanically the spacecraft equipment during launch.
2. **STRU-2**: Structural subsystem shall shield spacecraft equipment against space environment.
3. **STRU-3**: Structural subsystem shall be designed to survive its temperature range as described in (35).

4. **STRU-4**: Structural subsystem shall align the spacecraft according to the ADCS purpose(31).
5. **STRU-5**: Structural subsystem shall integrate the spacecraft equipment.
6. **STRU-6**: Structural subsystem shall connect mechanically and electrically the spacecraft equipment.
7. **STRU-7**: Structural subsystem shall ensure the integration within the P-POD and test pod.
8. **STRU-8**: Structural subsystem shall apply the management choice.

1.5.4.2 Mass Requirements

1. **STRU-MR-1**: Each single CubeSat shall not exceed 1 kg mass (47).
2. **STRU-MR-2**: Center of mass shall be located within 2 cm of its geometric center (47).

1.5.4.3 Design Requirements

1. **STRU-DR-1**: The CubeSat shall have an access port area placed on a side face (61).
2. **STRU-DR-2**: The external components other than the rails shall not touch the inside of the P-Pod (47).
3. **STRU-DR-3**: Components on shaded sides shall not extend more than $6,5$ mm normal to the surface (47).
4. **STRU-DR-4**: Deployables shall be constrained by the CubeSat. Note that the P-POD rails and walls are NOT to be used to constrain deployables (47).
5. **STRU-DR-5**: NASA/ESA approved materials should be used whenever possible (47), (43).
6. **STRU-DR-6**: The use of Aluminum $7075 - T73$ or $6061 - T6$ is suggested for the main structure (47).
7. **STRU-DR-7**: Minimum safety factor shall be used for standard metallic materials (56).
8. **STRU-DR-8**: Margins of safety (MOS) shall be positive (47).
9. **STRU-DR-9**: The CubeSats shall not generate any debris or separate parts during any post-delivery activity or during the flight mission on LARES System (Including release operations) (56).
10. **STRU-DR-10**: The max outgassing values for each material used on P-POD/CubeSat shall be (56) :
    - TML : less than $0,1$ %
    - CVCM : less than $0,01$ %

1.5.4.4 Launcher Requirements

1. **STRU-1-LR-1**: The CubeSat shall support static acceleration from LV (7).
2. **STRU-1-LR-2**: The CubeSat shall not have structural modes at frequencies lower than to be determined (TBD) Hz in hard mounted configuration (56).
3. **STRU-1-LR-3**: Random vibrations spectrum, sine spectrum, shock response spectrum and acoustic vibrations spectrum shall be performed at the levels described by the current Interface Control Document (ICD) (56).
4. **STRU-1-LR-4**: Random vibration testing and shocks tests procedures shall be done in accord with ESA's approach (28).
5. **STRU-1-LR-5**: The structural subsystem shall be able to support a thermal test that simulate Vega's mission profile (7).
6. **STRU-1-LR-6**: The structural subsystem shall be able to support a thermal vacuum bake out to ensure proper outgassing of components. The test cycle and duration shall be outlined in the mission test plan (MTP) (47), (56), (7).
7. **STRU-1-LR-7**: The depressurization rate under the fairing shall not exceed 5 kPa/s (7).
8. **STRU-1-LR-8**: CubeSats shall NOT be disassembled or modified after qualification testing (56).

1.5.4.5 Operational Requirements

1. **STRU-1-OR-1**: CubeSats shall not present any danger to neighboring CubeSats in the P-POD, the Launch Vehicle, or primary payloads (47), (7), (56).
2. **STRU-1-OR-2**: CubeSats with rechargeable batteries shall have the capability to receive a transmitter shutdown command, as per Federal Communications Commission (FCC) regulation (47).
3. **STRU-1-OR-3**: Time intervals for scheduled maintenance operations on CubeSats shall be no less than 3 months (56).
4. **STRU-1-OR-4**: Storage life shall be at least 24 months (with possible maintenance operations) (56).
5. **STRU-1-OR-5**: The CubeSats shall be completely passive during all ground activities and during the flight mission before release (56).
6. **STRU-1-OR-6**: On ground only the CubeSats should be active only during functional check-out/maintenance operations performed by the P-POD/CubeSat provider (56).
7. **STRU-1-OR-7**: The Cubesats shall conform to a Class 100000 clean environment (56).

8. **STRU-1-OR-8**: The Cubesats shall conform to Guiana Space Center (CSG) safety regulations (56), (7).

9. **STRU-1-OR-9**: Cal Poly will conduct a minimum of one fit check in which developer hardware will be inspected and integrated into the P-POD. A final fit check will be conducted prior to launch. The CubeSat Acceptance Checklist (CAC) will be used to verify compliance of the specifications (47).

1.6 Thesis outline

According its mission's objectives, $OUFTI-1$ intends to demonstrate in orbit the D-STAR technology, Azruspace's solar cells and an experimental EPS.

To achieve this goal, the purpose of the structural subsystem is to design a suitable and reliable mechanical structure, in accordance with the aforementioned requirements and functionalities. The starting point will be the CSK structure and the components will be integrated in agreement with the constraints from each subsystem.

Chapter 2 will start with a brief description of the different mechanical and electrical components. The flight system configuration and the proposed integration procedure will then be discussed. A detailed structural analysis, which includes finite element computations, will be carried out in Chapter 3. These numerical results will be verified using preliminary experimental vibration tests in Chapter 4. Finally, the conclusions of this study will be drawn in Chapter 5.

Flight System Configuration 2

2.1 Introduction

This chapter gives a detailed description of the $OUFTI-1$'s mechanical and electrical components. Another objective of this chapter is to define the flight system configuration whose purpose is to arrange each component according to the existing requirements. Finally, this chapter will present and discuss the configuration of $OUFTI-1$.

2.2 Catia modeling

A detailed geometric model was carried out using the commercial Catia V5 software (74). This model, shown in Figures 2.1 and 2.2, gives a detailed view of $OUFTI-1$ and of its components.

2.2.1 Why a Catia modeling?

A Catia model presents several important advantages for designing a structure, which certainly explains its widespread use in the mechanical industry.

Firstly, the study of the CSK with Catia allows a good understanding of the components included in the kit.

Secondly, Catia can be used to verify the suitability of new concepts. For example, if there are dimensional problems with a particular design, Catia modeling will warn the user by identifying the parts that may collide.

Catia can also calculate several physical properties such as the total mass, the center of gravity (COG) location and the inertia properties. A complete material database has been created to enable Catia to calculate these properties from the geometry.

Finally, the software facilitates the creation of technical drawings and the FEM's geometry which considerably simplifies the work.

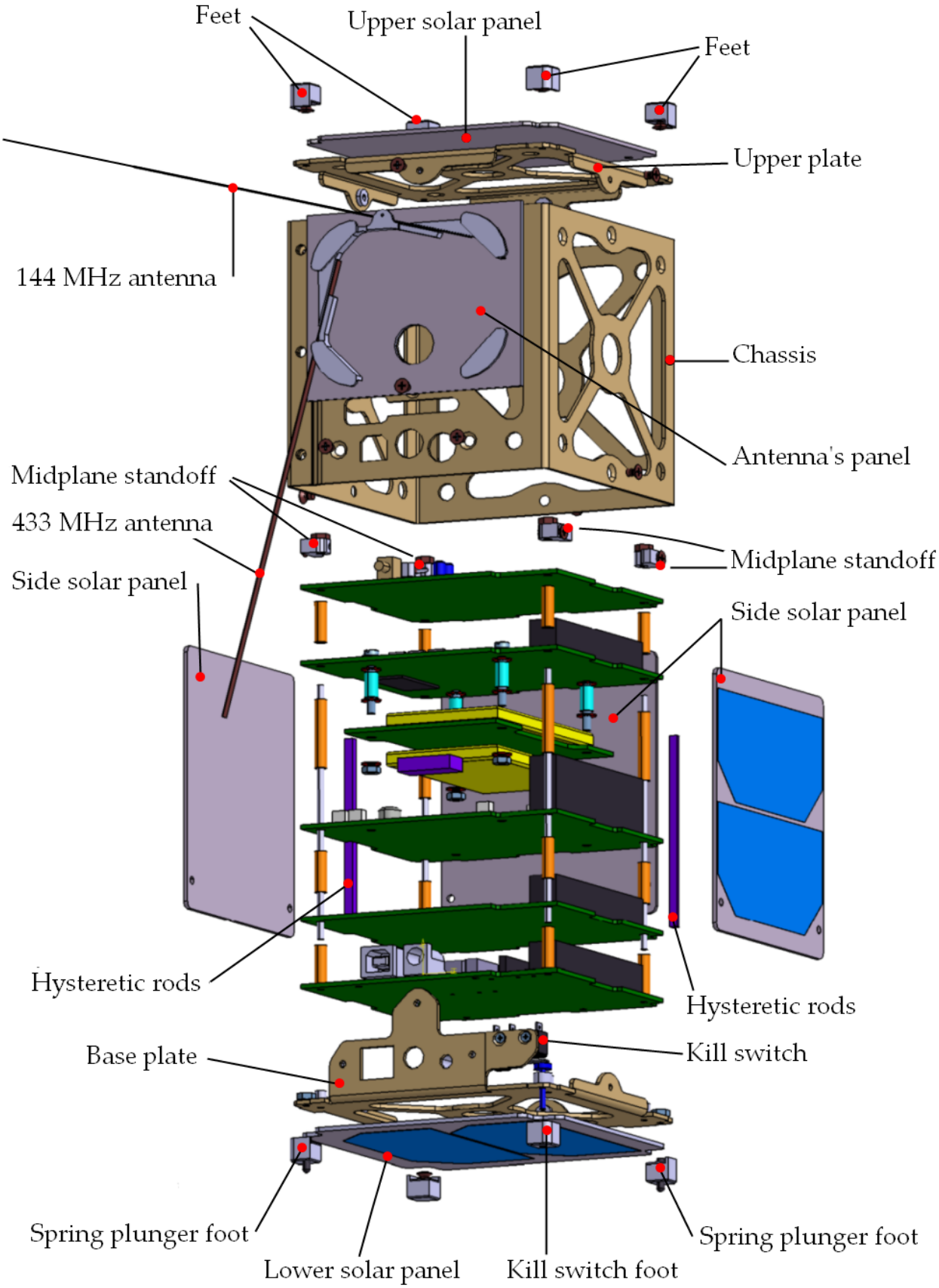

Figure 2.1 – *Exploded view of OUFTI-1*

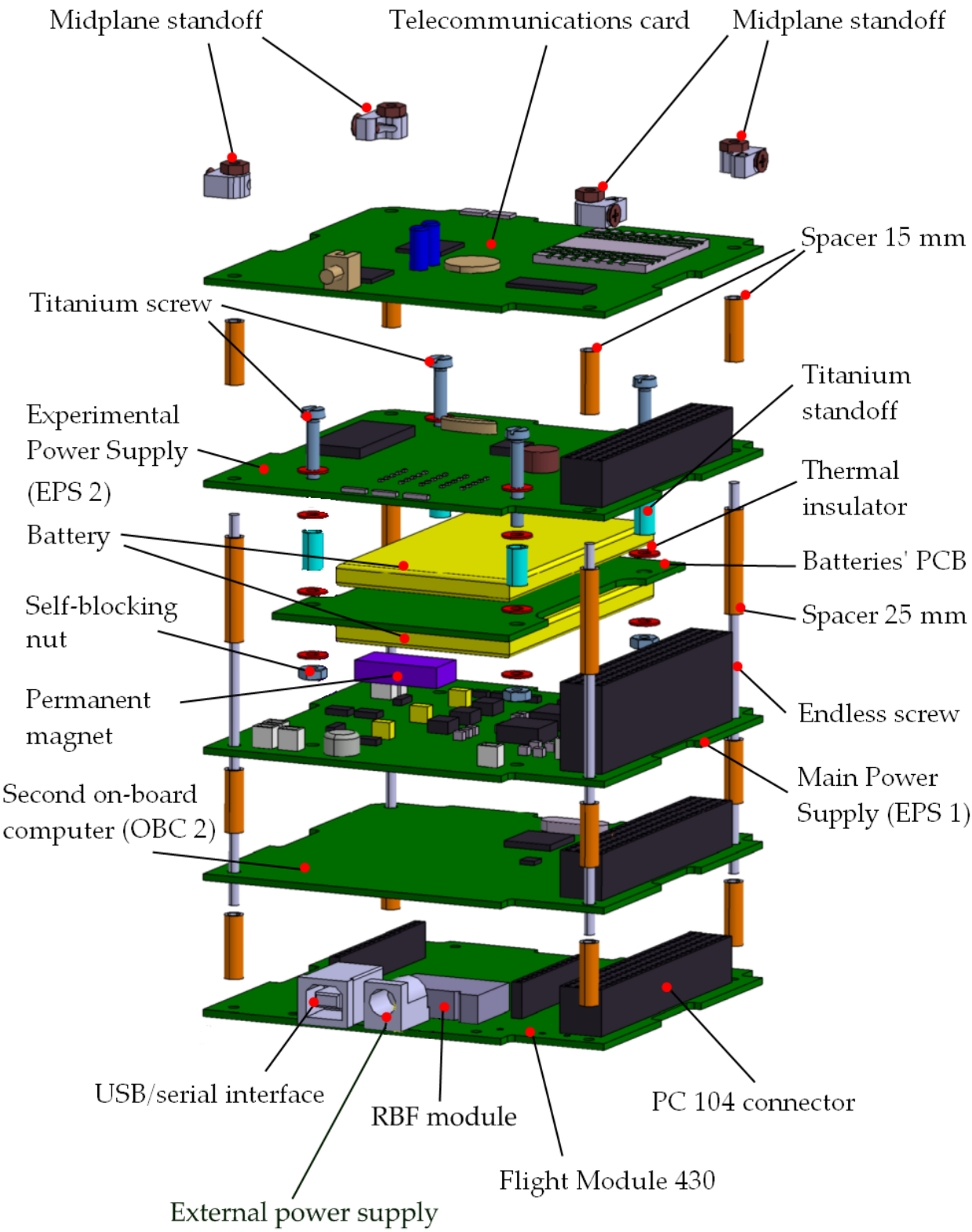

Figure 2.2 – *Exploded view of OUFTI-1's internal components*

2.2.2 Implementation

2 main sources of information were available regarding CSK's dimensions : official drawings (38) (61) and step files downloaded from Pumpkin website (37). For intellectual property, both are willingly amputated from a part of information.

Hence, the main dimensions were missing, and it was not possible to create a reliable model on this basis. Therefore, we decide to take measurements on our kit to establish an accurate model. As the CSK machining tolerances are wider than any other space application, we decide to limit the accuracy in the range of 1 to 5/100 mm.

The end result is presented in Figures 2.1 and 2.2 : 113 components (without washers), 253 location constraints and 262 contacts without any interference.

2.2.3 Frame

A frame must be defined to facilitate the description of the components' location. Its origin is chosen at the Cubesat's geometric center, oriented using a right hand set rule as shown in Figure 2.3.

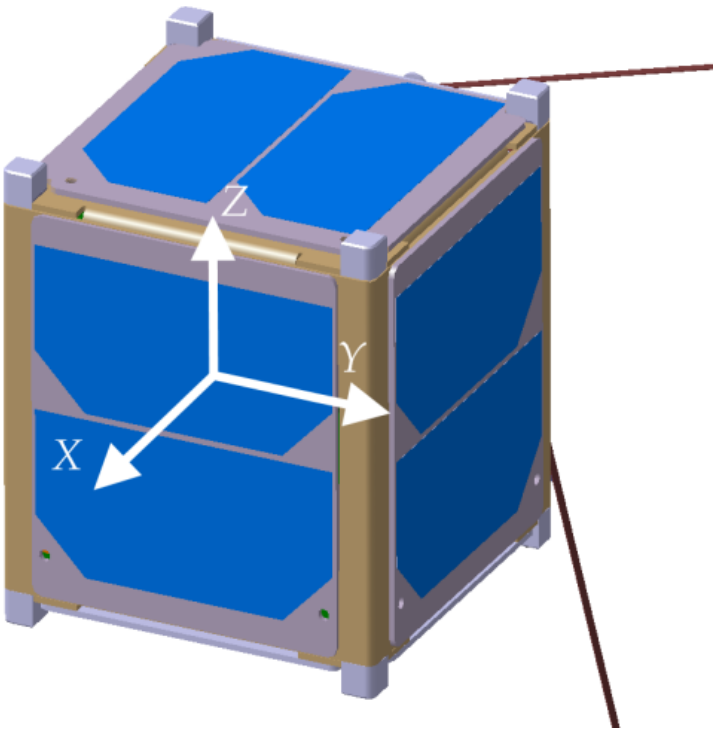

Figure 2.3 – *Reference frame*

This particular frame presents 3 majors advantages :

1. it is the same as the one given in the official documents (61).
2. a direct evaluation of the center of gravity (COG) location in regard to the geometrical center can be done.

3. each panel can be easily identified with the following rule : the name associated to the current panel is the name of its normal axis, according to its direction (e.g., the panel with the communication's ports is referred to as $-X$ face).

2.3 Mechanical components

This section describes components with a mechanical function, even if some of them are strongly linked to electrical functions.

2.3.1 CubeSat structure

One year ago, the University of Liège bought a CSK structure to accelerate the developments of the $OUFTI-1$ project. It is made to be as multipurpose as possible and many commercial solutions exist to simplify the advancements (14) (37). Thus, certain designs (e.g. solar panels) will also be dictated by the existing structure.

The CubeSat Kit comprises 3 main parts, all made in $Al-5052\ H32$ (38) :

1. an upper plate, also known as end plate, screwed on the chassis with 4 $M3\ x\ 5$ stainless steel screws. It supports 4 feet.
2. a chassis that is drilled on $-X$ to create a serial/USB interface with the $FM430$ electronic card. The remove before flight (RBF) pin and the external electrical power supply are also located on this face.
3. a lower plate or base plate. It carries two important components : 2 spring plungers and 1 deployment switch. It is screwed on the chassis with 6 $M3\ x\ 5$ stainless steel screws.

The chassis' corners and the feet are hard anodized to prevent cold welding and to have good anti-friction properties. The remaining parts are alodined and constitute the electrical ground of the structure. Figures 2.4 and 2.5 show the details of Pumpkin's structure.

2.3.2 Feet

Feet are made of $Al-6061\ T6$, which is a common aluminum in aerospace industry and recommended by (47). A foot can be decomposed in 4 parts : the foot itself which is hard anodized, a stainless steel "shym´´ that has to be removed if $OUFTI-1$ uses solar panels clips, a stainless steel screw and a grower washer (Figure 2.6). Note that their dimensions are prescribed in (61).

The "normal´´ feet are not drilled and have no protuberances at their basis. The CSK upper and base plates support 5 normal feet : 4 on the end plate and 1 on the base plate.

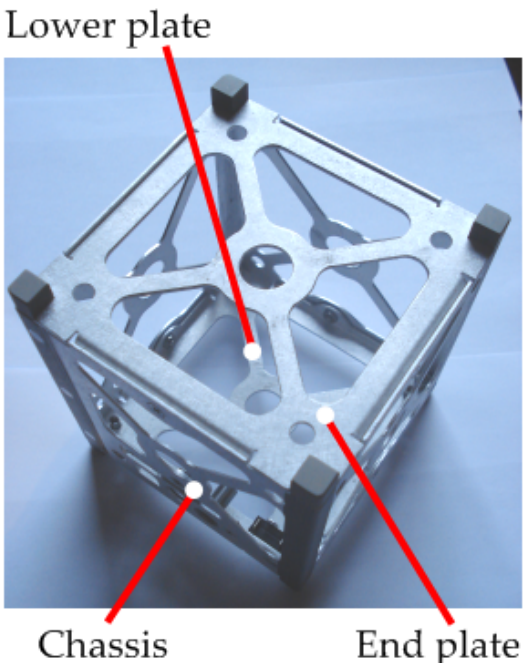

Figure 2.4 – *Mechanical structure provided with the CubeSat Kit*

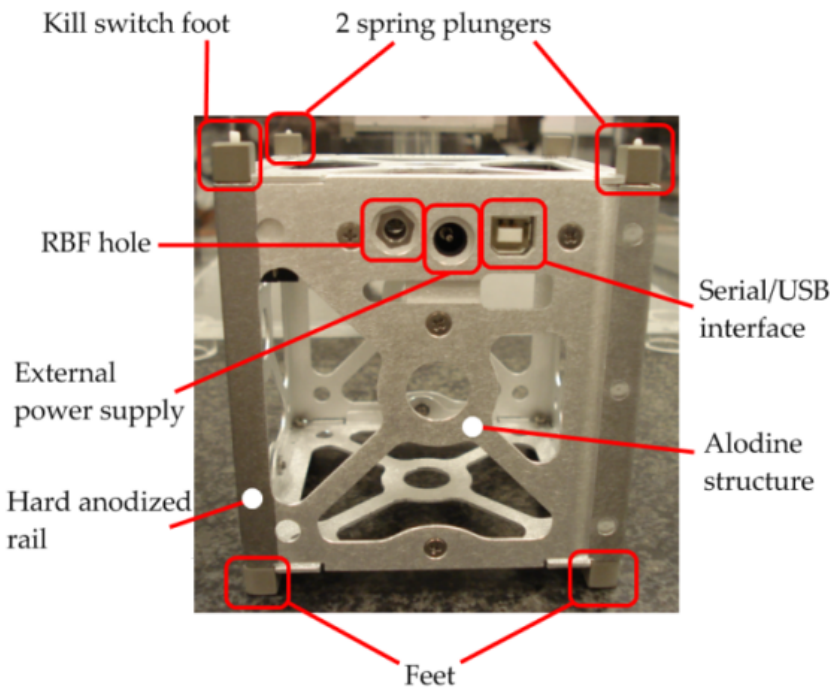

Figure 2.5 – *Close-up of -X face*

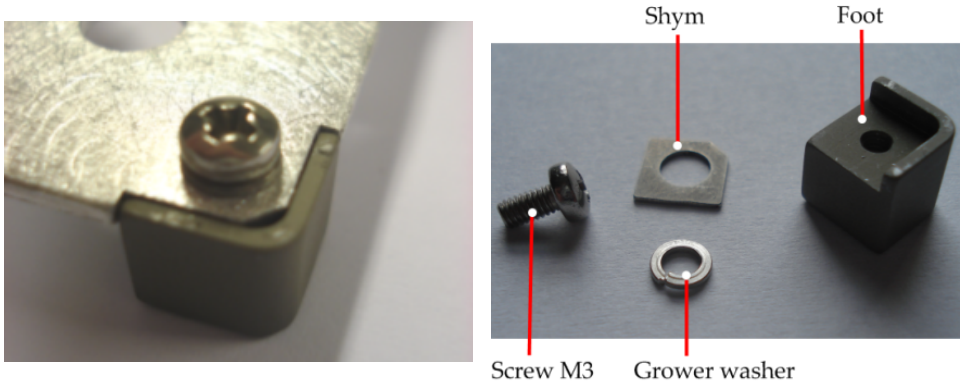

Figure 2.6 – *Left plot : assembled foot; right plot : different components of a foot*

2.3.3 Spring plungers

Spring plungers, or more commonly spring loaded device, add value to a classical spring by encapsulating it into a CubeSat foot and providing a plunger tip on one end. In this way, the spring plunger allows much more accurate and repeatable end force than an usual spring. Their aim is to provide a relative velocity to separate $OUFTI - 1$ from the 2 others P-Pod's CubeSats.

2 of the 4 base plate feet posses the spring plungers (Figure 2.1). Their placement inside the feet must respect a particular procedure to avoid any damage (39). A spring plunger foot can also be decomposed in 4 parts : the foot (hard anodized), a stainless steel "shym´´, a $M3$ nut and the spring plungers (Figure 2.7).

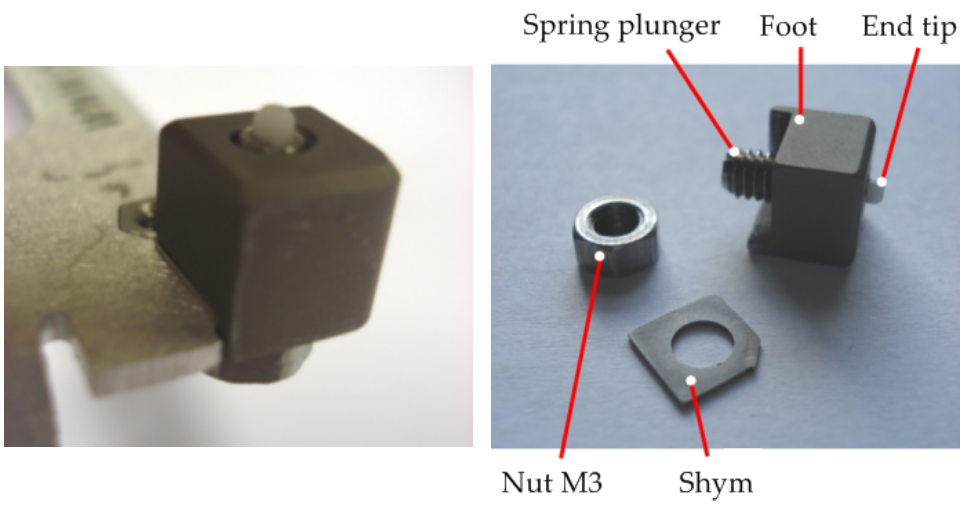

Figure 2.7 – *Left plot : spring's end tip; right plot : spring plunger's components*

2.3.4 Deployment switch

One requirement inside the P-Pod is that all satellite's functions must be shutdown to avoid any problem (e.g. premature antennas deployment).

This is the deployment switch purpose which disconnects the electrical contacts when it is mechanically engaged. The CSK structure contains 2 switch modules.

The first is placed on the $FM430$ electronic card from Pumpkin (Figure 2.8, left plot) and can be switched on/off thanks to the RBF pin. It is used to disconnect batteries' power supply during ground transportation, maintenance or tests.

The second is fixed on the base plate (in black in Figure 2.1) and is used inside the deployer, after the satellite integration.A small plastic shaft activates the switch and cut off power supply when it is stacked inside the deployer. Once in orbit, the deployment mechanism releases all CubeSats and in the same time, the shaft and the switch. This mechanism is placed in the last foot on the lower plate, just at the corner $-X/-Y$.

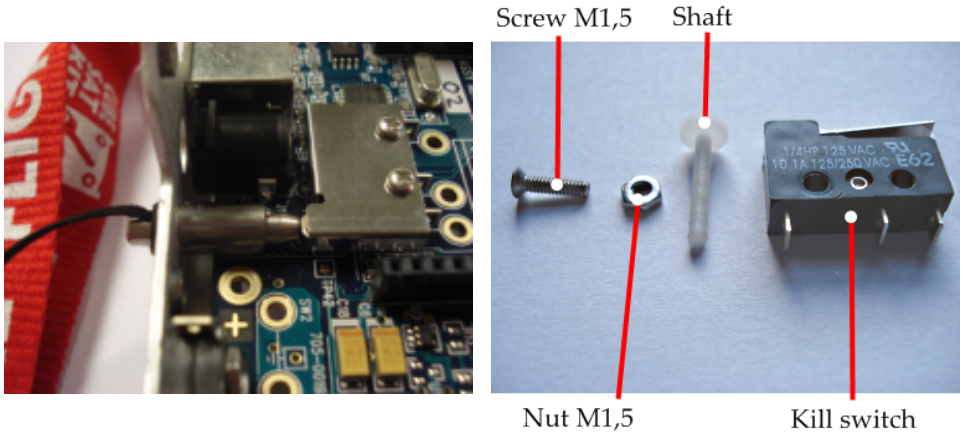

Figure 2.8 – *Left plot : switch mechanism with the RBF pin; Right plot : base plate's switch components*

2.3.5 Spacers and endless screws

Spacers are represented in orange in Figure 2.1 and 2.2. They are made of $Al-6061\ T6$ and have inner and outer diameter of $3\ mm$ and $4,5\ mm$ respectively. Spacers are stacked up around $M3$ stainless steel endless screw, alternately with electronic cards. They can be $15\ mm$ or $25\ mm$ height (see PC-104 specifications (33)) and provide an equal distance between 2 adjacent PCBs.

The endless screws spread from 4 lugs in the base plate until the midplane standoff. Their role is to provide a positioning pattern to the PC-104 electronic card. Global view of both spacers and endless screw is presented in Figure 2.9.

2.3.6 Midplane standoff

Midplanes are the mechanical connections between the endless screws and the chassis. As the electronic cards' positioning is not symmetric in-

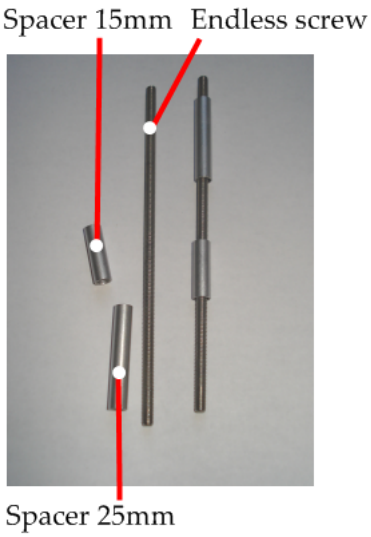

Figure 2.9 – *Spacers of 15/25 mm and/around the endless screws*

side the CubeSat structure, four different $Al - 6061\ T6$ standoffs are used. They are named from A to D and their placement is described in reference (40).

Midplanes are drilled with 2 holes : one through the height and the other on the longer lateral side. The first is for the endless screw that should be bolted just above the midplane, and the second is used to screw the midplane on the $+/-\ Y$ chassis' face. They are represented in Figure 2.10.

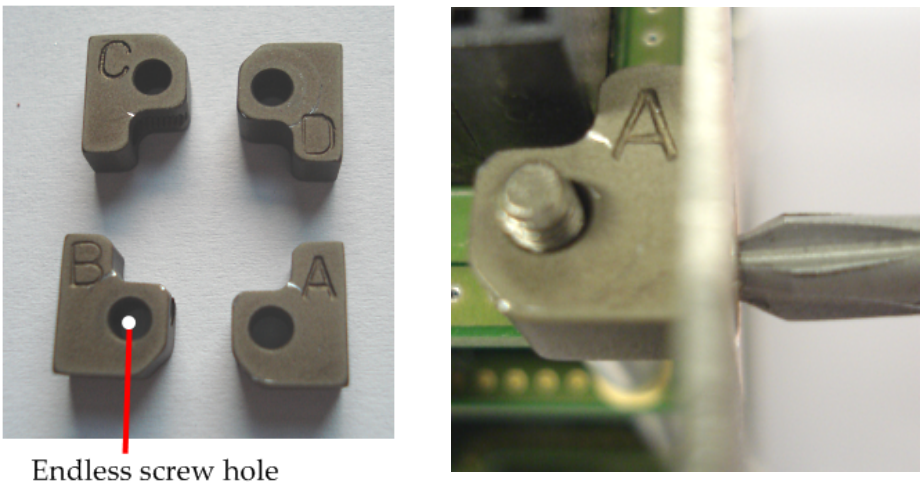

Figure 2.10 – *Left plot : the 4 different midplanes; right plot : midplane A during mounting*

2.3.7 Batteries' PCB

A sixth PCB is mounted between EPS1 and EPS2. It supports and thermally insulates the batteries, as it can be shown in Figure 2.2.

This PCB is attached to EPS2 via 4 titanium screws $M3\ x\ 20\ mm$ bolted with 4 self-blocking nuts (Figure 2.11). 16 polyamide washers are added to the assembly to increase the thermal resistance. Four spacers of 9 mm height (in pale blue in Figure 2.2),and also made of titanium, place the PCB to the right height.

1 heater is placed between each battery and the PCB, on or inside the PCB (TBD) and a thermal sensor is placed on both batteries' sides to ensure they respect their temperature operating range. On the other hand, PCB has to be large enough to support the heater control transistor, batteries' protection circuit and charger connected to the external power supply.

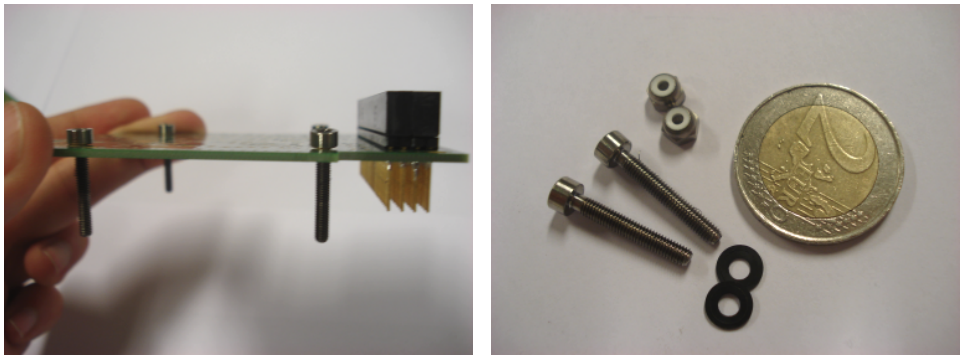

Figure 2.11 – *Left plot : connection to EPS2; right plot : screws,nuts and washers*

At the moment, this subsystem is still under design.

2.3.8 Magnet and hysteresis rods

$OUFTI-1's$ attitude control system is based on the passive use of the earth's magnetic field to create a 2 axis stabilization. Actually, one axis of the spacecraft will follow magnetic field's line all along the orbit. Then, ADCS subsystem (31) defines the elements that will be taken on-board : one permanent magnet and a damping material.

The permanent magnet is made of $Al-Ni-Co-5$, which are a common ferrous alloy that can be found easily on the market. At the moment, the last evaluation of the ADCS subsystem leads to 1 cm^3 as the necessary volume to align the spacecraft with a good accuracy. The permanent magnet will be stuck or mechanically attached (TBD) because it cannot be drilled without destroying the magnetic domains.

$OUFTI-1$ has to use a damping material made of $Hy-Mu-80$ or Permanorm $5000-H2$, both being nickel-iron soft magnetic alloy. It draws its energy into the rotating movement to travel through the material's hysteresis cycle. In this way, it decelerates the rotating movement and limits the modulation effect on ground station. Last assessments lead to $0,1\ cm^3$ of damping material. At least 2 hysteresis rods are placed on-board, at the $+X$ face internal corners (Figure 2.1). They will be stuck or mechanically attached (TBD).

2.3.9 Solar panels

The solar panels are made of $Al - 7075 - T73$ and they provide the surface for mounting the solar cells from AzurSpace (see Annex B). 3 kinds of panel are used :

- 3 side panels with a rectangular shape of 82 x 96 mm^2, and a thickness of $1,5$ mm. These panels are drilled with 2 holes of 3 mm for the cabling path.
- 1 top panel with a particular shape with external dimensions of 90 x 96 mm^2. This design is done to get a compromise between the cabling path and CSK dimensions, as explained later.
- 1 lower panel without any hole but similar to the upper panel's form.

The first and second types are represented in Figure 2.12. Solar panels take also an important role in the $OUFTI - 1$ mission : they are also designed to shield equipment against spatial radiations and thermal variations.

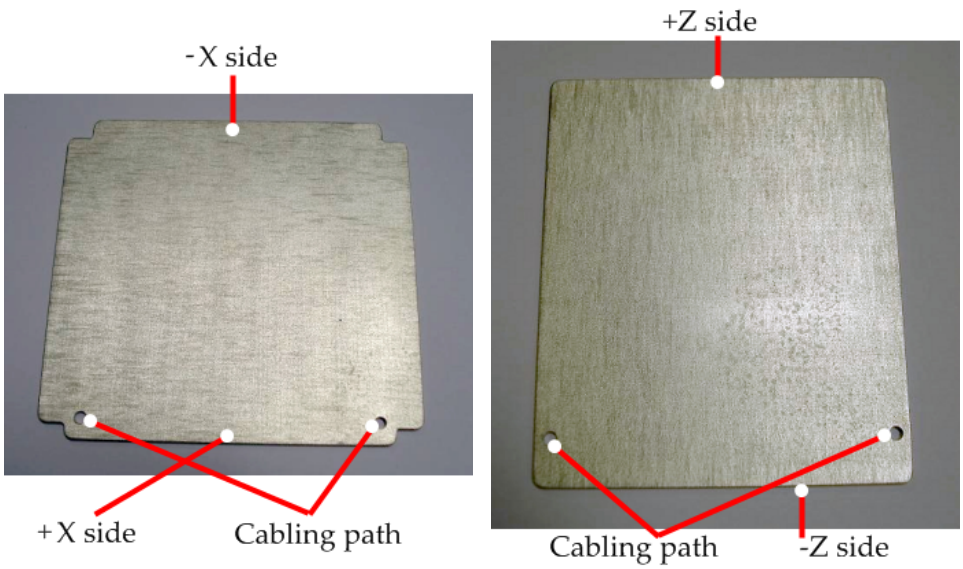

Figure 2.12 – *Aluminum substrate; Left plot : +Z panel ; right plot : +X and +/-Y panel*

2.3.10 Antennas

The antennas' deployment mechanism is managed by the MECH subsystem (81). Made of aluminum, the antennas' panel is mounted on $-X$ and is hard anodized to ensure electrical insulation to the antennas.

As already mentioned, $OUFTI - 1$ has 2 channels of telecommunications : the downlink transmission in the VHF band at 144 MHz and the uplink transmission in the UHF band at 433 MHz, both frequencies being usual within the ham radio community.

The antennas are made of a cupro-beryllium alloy and correspond to the frequencies by the quarter length wave : 50 cm for the downlink and

17 *cm* for the uplink. Concerning the width, it has been chosen to respect the structural requirements and to create a simple system of deployment.

Antennas' fixation on the aluminum panel is designed to be as reliable as possible. In addition to be bonded at the base of the guide rails,each antenna can be folded in 2 notches created on the panel's back side.

The deployment mechanism works as follows : both antennas are rolled around the guide rails and are attached thanks to a wire in "Dyneema´´, wich is a modified polyethylene. When appropriate, an electrical impulse from EPS1 will deliver a current to a thermal knife that will reach the Dyneema's melting point. After its fusion, the antennas will deploy. The mechanical interface and the uplink antenna are represented in Figure 2.13.

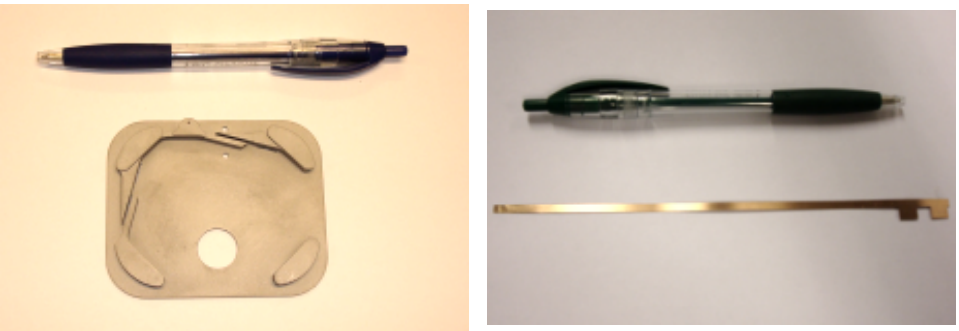

Figure 2.13 – *Deployment interface and uplink antenna*

2.4 Electrical components and electronics

2.4.1 PC-104 standard

Electronic cards used in $OUFTI-1$ project are all in the PC-104+ format size (see Annex A). First of all, it should be noted that it exists slight differences between the consortium's definition (33), Pumpkin PCB (62) and the real $FM430$ from the kit.

PCB are made of FR4, which stands for Flame Resistant 4, that belongs to the Glass Fiber Reinforced Plastic (GFRP) class of material. A PCB is produced by inserting continuous glass woven fabric impregnated with an epoxy resin binder while forming the sheet under high pressure. An usual PCB is often made with 4 to 6 layers and generally includes different electrical grounds. The electrical components can be connected to a particular potential within the card or to the common ground on the chassis. On the other hand, the electronic cards can include special components such as the "via´´, in copper or aluminum, that spread thermal activity on the whole PCB.

Each PCB has a common device : the PC-104 connector. This allows a direct connection with all cards through 104 pins welded in it. The connectors are made of GFRP and are 11 *mm* height (83). They can be extended to

21 mm thanks to an additional connector (82) (68). Note that all connectors are chosen as the low insertion force versions to facilitate the integration.

Finally, it will be noted that these PCBs will be protected by a thin film to avoid outgassing of sensitive components such as chemical capacitors.

2.4.2 Electronic cards

A preliminary assessment from Pumpkin's drawings gives $62,5\ mm^2$ of free surface for the integration of components, with an estimated margin of security of 5%. As this area is large enough to support all the electrical functions, only 5 cards will be used : OBC1 (from CSK), OBC2, EPS1, EPS2 and COM.

This section briefly describes the electronic card functionalities. For further details, references (49) (77) (45) (75) (26) can be consulted.

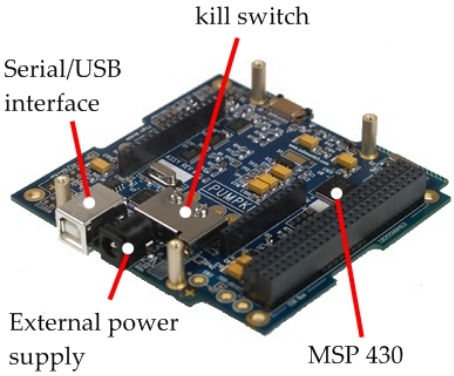

FM430 card also known as OBC1. This card comes from the CSK and is a reliable solution. One note that several functions will not be used aboard (e.g. the MHX). This card is managed by OBC (75).

OBC2 card is developed to be redundant with OBC1. It integrates in an efficient way all the functions used on the OBC1 thanks to a $MSP430$. This card is also managed by OBC (75).

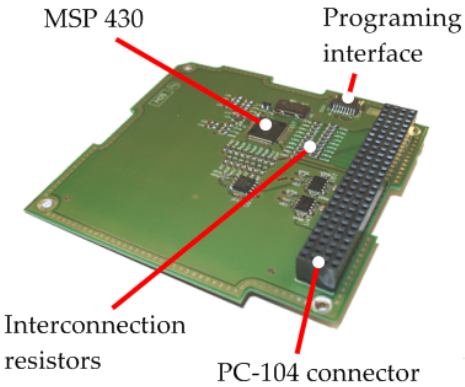

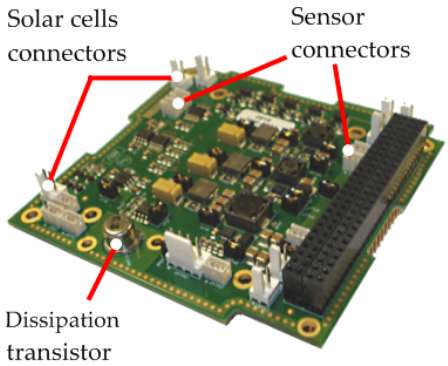

EPS1 card is the main power supply. It manages and supplies clients with the power available from solar cells. Batteries must be integrated near this card. It is managed by EPS1 (77) and the measurements by reference (26).

EPS2 card or experimental EPS is a digitally controlled EPS with a flyback module. It constitutes a secondary payload, but it cannot supply the overall system. A strong interaction with battery module arises from thermal simulation (35). This card is managed by EPS2 (45).

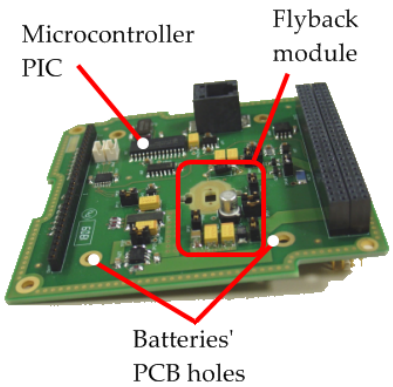

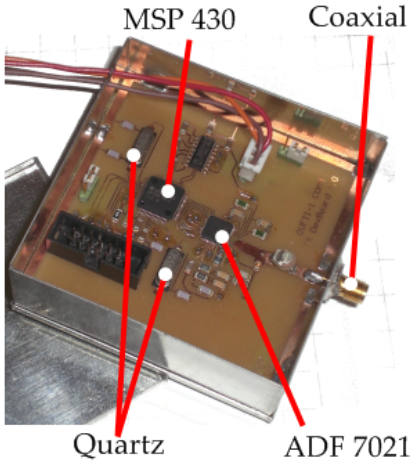

COM card integrates the $AX-25$ (32) and D-STAR telecommunication protocols. It brings high frequencies that could disturb the OBC2. This card is managed by the COM team (49) (34).

2.4.3 Batteries

The main criteria for the selection of this component are : mass, volume, reliability and specific electrical capacity.

Lithium-polymer type has been chosen by EPS team, mainly because it provides the best specific capacity as well as a compact form. Thus, a complete set of COTS Li-Po batteries has been bought on the basis of their flight experience. They are presented in Table 2.1 and are listed by descending order of preference.

Manufacturer	Model	Tested
Kokam	603870H	Done
	554374H	Done
Panasonic	CGA633450B	Ongoing
Varta	PLF 463759C	Done

Table 2.1 – *Batteries considered*

Structural characteristics are described in details in datasheets (59), (60), (79) and (70), respectively (see Annex C). Protection circuits will be used too.

2 batteries will be used in the flight model as redundant solution. An agreement was made between Dresde (52) and ULg to test different batteries : ULg performed a testing campaign on the electrical capacity of

Kokam's batteries. Dresde will test the Panasonic battery using the same protocol and the results will be exchanged.

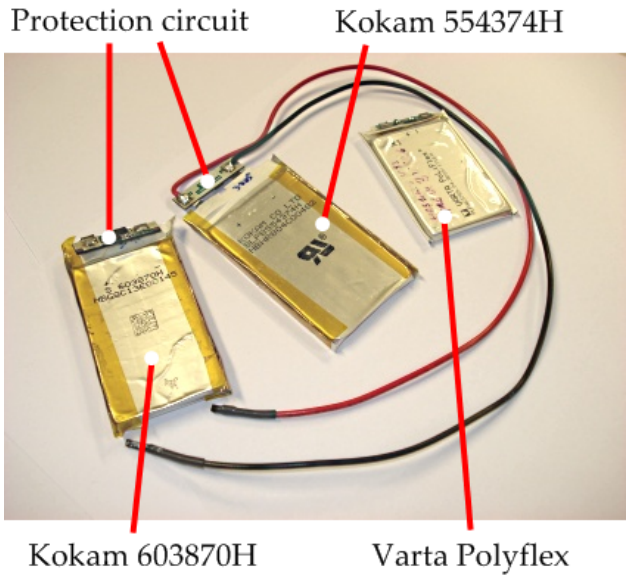

Figure 2.14 – *Batteries and their protection circuits*

Kokam batteries have good spatial experience on CubeSat (77). However, the first tests performed at the CSL showed that thermal cycling combined with high vacuum induces large deformations of the cells' envelope. To counteract this effect and avoid dramatical lost in performance, batteries will be placed inside an aluminum box. The space between cells and box could be filled with epoxy resin. Besides the good protection against spatial environment, this solution also brings a mechanical fastening of the batteries to the structure. Batteries could be thermally insulated from the main structure (TBD), depending on the experimental and theoretical results from thermal subsystem (35).

Panasonic's batteries are tested at Dresde at the moment. They are thinner and narrower than Kokam's batteries but have less capacity. Depending on the results, this type could be used on $OUFTI-1$. However, mechanical design can be concentrated on Kokam's batteries with a comfortable margin of security. Indeed, Kokam's external dimensions are greater than the Panasonic one.

It will be noted that Varta Polyflex batteries are of less interest because several uncertainties remain on their electrical capacity evolution in time.

2.4.4 Solar cells

Since 1964, AzurSpace powered more than 340 satellites such as XMM, Herschel, Planck or Mars Express (5). The most advanced solar cells technology are developed on experience of more than 40 years and several million solar cells. The range of products covers various types of silicon and $III-V$ solar cells on germanium for space application (72). Therefore, its strong industrial experience is a reliable solution to power $OUFTI-1$.

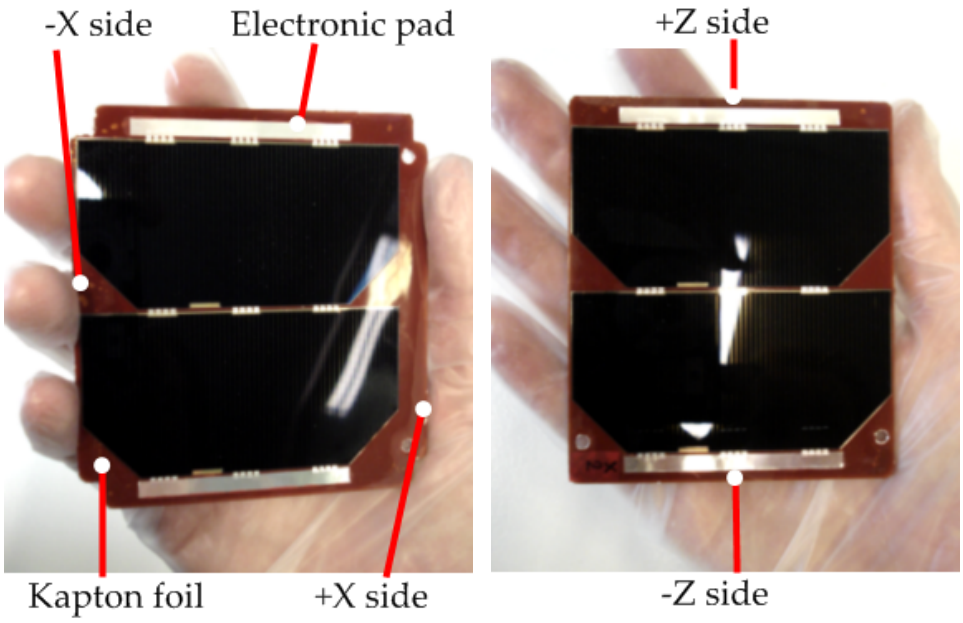

Figure 2.15 – *OUFTI-1's GaAs solar cells (30% efficiency BOL)*

The new generation of triple-junction Gallium-Arsenide solar cell of thirty percent BOL efficiency will be used on $OUFTI-1$ and measurements will be done in orbit. On the other hand, integration on the main structure will be led by EADS Astrium, as recommended by AzurSpace.

Solar cells, whose size is 80 mm wide for 40 mm height with cropped corners, are connected in series which explains their location on the panel. It is also recommended to use same cells on all panels to avoid any short-circuit problems within EPS1 subsystem. Once again, the simplest solution is to integrate only new solar cells on-board.

Astrium has integrated cells on the aluminum substrate with the following layout : aluminum panel - adhesive - Kapton - adhesive - solar cell - cover glass. Indeed, the complete surface is covered with 50 microns thick Kapton foil for electrical insulation reason and the cover glass protects solar cells against space environment. All adhesives are typical silicone type and have a thickness around 50 micron. Figure 2.15 presents 2 solar panels after integration.

It can be observed that upper and lower area are covered with electronic pads to weld cables. One pad corresponds to the electrical mass while the other represents the useful electrical voltage, both being connected to the EPS1. One pad has 6 mm height and around 60 mm wide. The interstice between cells is only 1 mm height.

2.5 OUFTI-1 Flight system configuration

2.5.1 Objective and procedure

The purpose of the flight system configuration is to arrange all the spacecraft elements by respecting a set of requirements. The first difficulty is then to define accurately the requirements.

For each group of components, the main problems involving the configuration (e.g. environmental, dimensional, physical) are investigated. The constraints associated to these problems are defined and translated into requirements that can be linked to the structural requirements (see section 1.5.4.1).

Finally, a configuration will be proposed and discussed to see weither the requirements are satisfied. Note that this section only looks at the configuration problem. The discussion concerning the design, operational and launch requirements will be done in chapters 3 and 4.

2.5.2 Groups

Six groups of elements can be defined :

1. **The CSK structure** which includes the main structure, endless screws and midplanes standoffs.
2. **The** 5 **electronic cards** and spacers associated.
3. **The** 2 **batteries**, cables, protection circuit and their mechanical connections.
4. **The magnet and** 2 **hysteresis rods** and their mechanical connections.
5. **The solar panels** which include the aluminum panel, solar cells, cables and their mechanical connections.
6. **The antenna's deployment mechanism** with its panel, both antennas, electrical and mechanical connections.

These groups are strongly mechanically, thermally and electrically interconnected. They also interact with the space environment, i.e. the radiation, thermal cycling and earth's magnetic field. The next section will describe the main constraints associated to these elements.

2.5.3 Constraints

2.5.3.1 Product assurance constraints

The product assurance constraints concern the safety and the quality of material/product used. They ensure the satellite's reliability and impose the basic configuration layout.

Hence, the CSK structure will be used to integrate the Azurspace solar cells and the FM430 while the electronic cards will follow the PC-104 format. The corresponding requirements are :

- **STRU-8-PAR-1**: The CubeSat structure shall be the CSK structure.
- **STRU-8-PAR-2**: The $FM430$ electronic card defined in reference (41) from the CSK shall be used.
- **STRU-8-PAR-3**: The PC-104 format shall be used as defined in reference (33).
- **STRU-8-PAR-4**: The AzurSpace solar cells defined in reference (73) shall be used.

2.5.3.2 Environmental constraints

The environmental constraints are linked to the system environment during its life cycle. This includes the environment in orbit such as the radiations, thermal cycling and vacuum but also the environment induced within the satellite, i.e. the electromagnetic interferences (EMI), electronic's thermal dissipation and the permanent magnet's field.

Radiations in space

With an apogee altitude of 1447 km, the satellite's revolutions through the Van Allen inner belt can induce a total irradiation dose (TID) around 10000 kilorads (9) without shielding. As $OUFTI-1$'s lifetime will be determined by the shielding against these radiations , the solar panels and the batteries, which represent the main hardening components, will be located to ensure a total mission duration of 1 year.

- **STRU-2-ENV-1**: Solar panels shall shield electronic components against space radiations for 1 year lifetime.
- **STRU-2-ENV-2**: Batteries shall shield electronic components against space radiations for 1 year lifetime.

Space vacuum

In space, the pressure can lie between 10^{-11} to 10^{-15} Pa. The main problem is linked with the batteries that can expand and lose more than 15% of their mass (46), as shown in Figure 2.16. Thus, they will be encapsulated within a thin aluminum box.

- **STRU-2-ENV-3**: Both batteries shall be encapsulated within an aluminum box.

Electromagnetic compatibility

Even if accurate measurements within $OUFTI-1$ are not yet available, the telecommunications card (49) (34) should generate strong electromagnetic interferences (EMI) during D-Star functioning. The resulting bad signal to noise ratio (SNR) could lead to loss of data or erroneous command. These interferences varying as $\frac{1}{D^2}$ where D is the distance to the COM card, they will be minimized if the COM is placed away from the other cards, i.e. in extremal position (nearest the base or end plate).

Figure 2.16 – *Batteries during and after high vacuum test. Courtesy (52)*

- **STRU-2-ENV-4**: COM card shall be nearest the base or end plate.

Thermal environment in space

The 14 revolutions per day may induce temperatures that can range from $-30°C$ to $70°C$. The batteries are the most critical components and they should be situated within $[0°C - 40°C]$ during the charge and within $[-20°C - 60°C]$ during the discharge. The thermal subsystem ensures better thermal conditions if a sixth PCB is directly connected to an existing electronic card. Moreover, its location near the geometric center should contribute to limit the thermal variations.This batteries' PCB shall be thermally insulated from the electronic card.

- **STRU-3-ENV-1**: Batteries shall be situated at the center of the satellite.
- **STRU-3-ENV-2**: Batteries shall be integrated on a sixth PCB attached to an electronic card.
- **STRU-3-ENV-3**: Batteries' PCB shall be thermally insulated from the electronic card.

Thermal environment induced by electronics

The EPS1 card uses a dissipation transistor to transform in heat the energy that cannot be stored during sunlight period (77). Its temperature can reach $120°C$ which constitutes a problem for the batteries. It will be placed in such a way that it will not heat up the batteries over $40°C$ (35). Thermal subsystem ensures this condition if the transistor is connected to the main structure on $-X$ with an aluminum square and a "patch´´ resistor (35). In addition, batteries should be not be connected to the EPS1 to limit the transistor influence.

- **STRU-3-ENV-4**: The dissipative transistor placed on the EPS1 shall be connected to the $-X$ panel with an aluminum square.

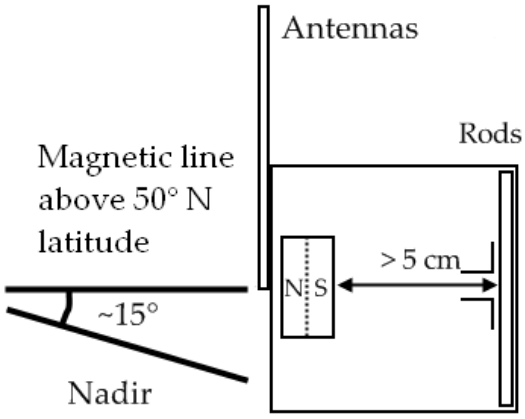

Figure 2.17 – *Permanent magnet's alignment and rods location*

- **STRU-3-ENV-5**: The dissipative transistor placed on the EPS1 shall be connected to the $-X$ panel with a patch.
- **STRU-3-ENV-6**: The batteries shall not be connected to the EPS1.

Earth's magnetic field

The plane defined by the omnidirectional antennas is taken as perpendicular as possible to the nadir axis above latitude of Liège (around $50°N$) as shown in Figure 2.17. This is chosen to keep an antennas' gain around 1 dBi. The angle between nadir axis and the magnetic lines at this point being around 15°, we can consider them as similar (31) in a first approach and the permanent magnet axis can be set parallel to the normal X to align the spacecraft.

- **STRU-4-ENV-1**: The permanent magnet axis will be parallel to the normal X.

Magnetic field induced by the permanent magnet

If the permanent magnet's field induces the magnetic saturation in the hysteresis rods, their efficiency decreases and the rods become useless. According to the ADCS (31), it is necessary to limit the magnetic field to values under $0,1\ A/m$ in the rods, which requires at least 5 cm between rods and magnet (Figure 2.17).

- **STRU-4-ENV-2**: Permanent magnet shall be situated at least 5 cm from the hysteresis rods.

2.5.3.3 Configuration constraints

In a strict sense, these constraints are linked to the composition of the product or its organization within the CubeSat format.

PC-104 format

The electronic cards, whose the external dimensions follow the PC-104 format (92 x 96 mm^2), are integrated inside the 98 x 98 mm^2 structure. In addition to the 5 electronic cards, the PC-104 format should be slightly modified to let pass 1 permanent magnet (1 cm^3), 2 hysteresis rods ($0,1$ cm^3), 1 deployment switch ($1,5$ x $0,6$ cm^2) and cables from solar cells. To ensure reliability, the batteries' PCB will be attached mechanically using screws (see Chapter 3). This implies 4 holes in the card that supports the batteries assembly.

- **STRU-5-CONF-1**: The PC-104 shall include notches of at least 2 x $0,25$ cm^2 for the cabling path.
- **STRU-5-CONF-2**: The PC-104 shall include a notch of at least 2 x $0,8$ cm^2 for the deployment switch.
- **STRU-5-CONF-3**: The PC-104 shall include notches of at least 2 x 2 mm^2 to let pass the hysteresis rods.
- **STRU-5-CONF-4**: The PC-104 shall include notches to let pass the permanent magnet.
- **STRU-5-CONF-5**: The PC-104 that supports the batteries shall include 4 holes (dimensions available in Chapter 3).

Hysteresis rods

The hysteresis rods have to be perpendicular to the permanent magnet polarization axis in order to stabilize the CubeSat during the transitional phase (Figure 2.17).

- **STRU-5-CONF-6**: The magnet polarization axis will be perpendicular to the hysteresis rods axis.

FM430

The satellite has the data ports (i.e. the serial/USB port and 5 V power supply) on $-X$ panel. Thus, the $FM430$ has to be connected on the base plate to allow external connections.

- **STRU-5-CONF-7**: $FM430$ shall be connected on the base plate.

2.5.3.4 Interface constraints

The interface constraints refer to the interconnections or relationship characteristics between 2 devices. This definition includes electrical and mechanical interface.

Mechanical connections

The 2 rods and the magnet cannot be drilled without modifying their magnetic properties and they will be bonded or attached (TBD). Each solar panel requires at least 93 x 80 mm^2 for only 87 x 80 mm^2 available on

$-X$ side : it will be used to integrate the antennas' deployment mechanism. The combination of Astrium's integration layout and CSK structure directly interferes with the solar panels clips use (64). The clips cover up at least one cell on the top/bottom panel, as shown in Figure 2.18. Therefore, adhesives will be used.

- **STRU-6-INTER-1**: The magnet shall be fixed rigidly within the satellite
- **STRU-6-INTER-2**: The hysteresis rods shall be fixed rigidly within the satellite.
- **STRU-6-INTER-3**: The solar panels shall be bonded on the satellite.
- **STRU-6-INTER-4**: The antennas' deployment mechanism shall be bonded on the satellite.

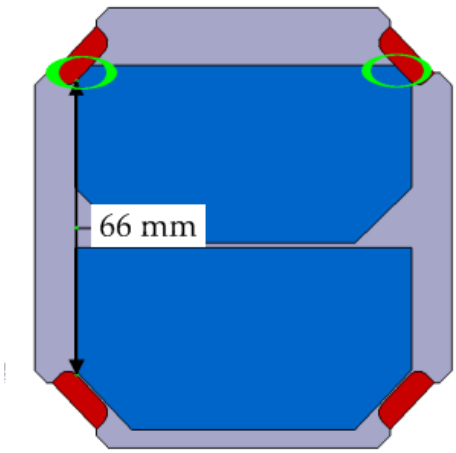

Figure 2.18 – *Top panel with solar clips*

Electrical connections

The batteries require at least 6 cables while the solar panels need 10, both will be connected to EPS1 whereas the antennas will be connected to the COM by using one coaxial cable. They will be preferably the ribbon cables with silver plate connectors described in reference (66). They are designed for ultrahigh vacuum up to $0,5 \cdot 10^{-10}$ *mbar*, resist to 10^4 *krad* whereas they have a density of 1530 kg/m^3.

- **STRU-6-INTER-5**: The batteries shall be connected to EPS1 using 6 cables.
- **STRU-6-INTER-6**: The solar cells shall be connected to EPS1 using 10 cables.
- **STRU-6-INTER-7**: The antennas' deployment mechanism shall be connected with the COM card using 1 coaxial cable.

2.5.3.5 Physical constraints

These constraints establish the boundary conditions to ensure physical compatibility because they are not defined by the interface constraints.

Cabling path

The main problem is that the structure could not be drilled or manufacture and only few holes are available (Figure 2.19). The lateral sides of the structure are drilled of 4 holes in the corners but both corners situated near the end plate (in red) are already occupied on $+/-Y$ by midplane standoffs. The base plate has no holes whereas the upper plate has 4 holes free. In our case, the solar cells' cables length will be taken in such a way that, among all cabling path available with these holes, the chosen cabling path will be the shortest. The same remark can be done in regard of the batteries and the antennas' deployment mechanism.

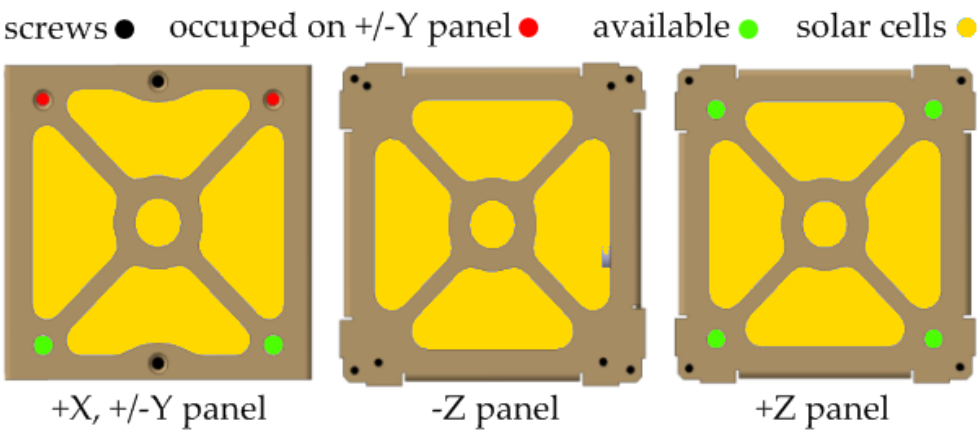

Figure 2.19 – *Available holes on the CSK structure skeleton*

- **STRU-6-PHY-1**: The solar cells cables shall be the shortest.
- **STRU-6-PHY-2**: The batteries cables shall be the shortest.
- **STRU-6-PHY-3**: The coaxial connection on the antennas' panel shall be the shortest.

2.5.4 OUFTI-1 flight system configuration

Using the KISS philosophy, we proposed the solution described in Table 2.2. The requirements fulfilled are highlighted in the right column while those placed between brackets will be discussed in section 2.5.5.

Electronic cards	
Description	**Requirements**
The 5 electronic cards are stack up through 4 endless screws fastened in the CSK structure's base plate. The $FM430$ card is placed with its components facing to the base plate's ports while the COM card is situated at the opposite, close to the end plate. The EPS2 is situated just below the COM while EPS1 and OBC2 are stacked on the $FM430$ (Figure 2.20).	(STRU-2-ENV-4); STRU-5-CONF-6; STRU-8-PAR-1/2
All cards (Figure 2.21) follow the format PC-104. They have upper and lower right corners cropped to place hysteresis rods. Lower left corner is removed to let pass the deployment switch module on OBC2 and can guide the cables on EPS1, EPS2 and COM. Notches are created in each side and serve as guideline to the cables whereas EPS2 is drilled to integrate batteries' module.	STRU-5-CONF-1/2/3/4/5; STRU-8-PAR-3
Solar cells connectors are placed at the EPS1 corners while the dissipation transistor on EPS1 is placed near $-X$ where it is mechanically connected to antennas' panel thanks to an aluminum square and a patch resistor.	(STRU-3-ENV-4/5); STRU-5-INTER-1; STRU-6-PHY-1

Batteries	
Description	**Requirements**
As shown in Figure 2.20, the batteries are placed on each side of a PCB that is fixed on EPS2 thanks to 4 titanium screws and spacers. 16 polyamide washers are placed to the contact point. Batteries are encapsulated into an aluminum box that surrounds the entire PCB and 6 cables directly connect the batteries to EPS1.	(STRU-2-ENV-2); (STRU-2-ENV-3); (STRU-3-ENV-1/2/3/6); STRU-6-INTER-5; STRU-6-PHY-2

Magnets and hysteresis rods	
Description	**Requirements**
The magnet is fixed on the lower side of batteries' PCB near the $-X$ face. Its polarization axis is perpendicular to the $-X$ face whereas the hysteresis rods are situated at the opposite corners of $+X$ as it can be shown on Figure 2.22. They will be bonded in the Z direction and will be perpendicular to the normal X.	STRU-4-ENV-1/2; STRU-5-CONF-6; STRU-6-INTER-1/2

Antenna's deployment mecanism	
Description	**Requirements**
Bonded on $-X$, the panel developed by MECH subsystem is connected to the COM with 1 cable.	STRU-6-INTER-4; STRU-6-INTER-7; STRU-6-PHY-3

Solar panels	
Description	**Requirements**
Solar cells from Azurspace are integrated on panels that are bonded on the CSK structure $+X$, $+/-\ Y$ and $+/-\ Z$ panels.	(STRU-2-ENV-1); STRU-6-INTER-3; STRU-8-PART-4
The cables from the 3 lower solar cells on lateral panels and both cables from the $-Z$ solar panel can pass through the 6 lower holes on the $+/-\ Y$ and X panel. The upper part with 5 cables pass inside the structure by using 2 holes on the upper plate near $+X$ side. Cabling path configuration is schematically represented in Figures 2.23 and 2.24.	STRU-6-INTER-6; STRU-6-PHY-1

Table 2.2 – *OUFTI-1's configuration description*

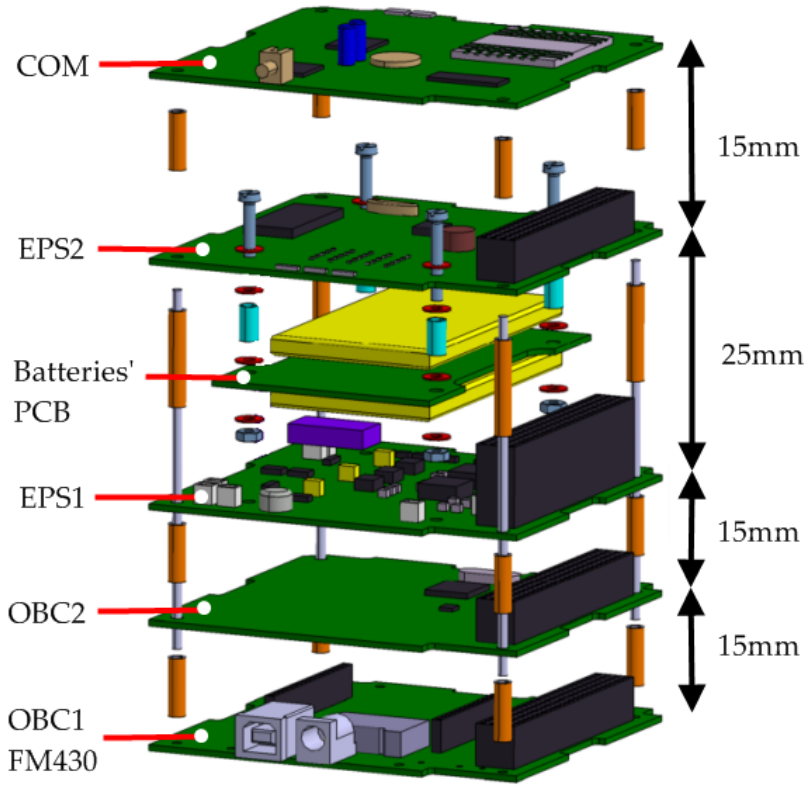

Figure 2.20 – *OUFTI-1 electronic cards' configuration*

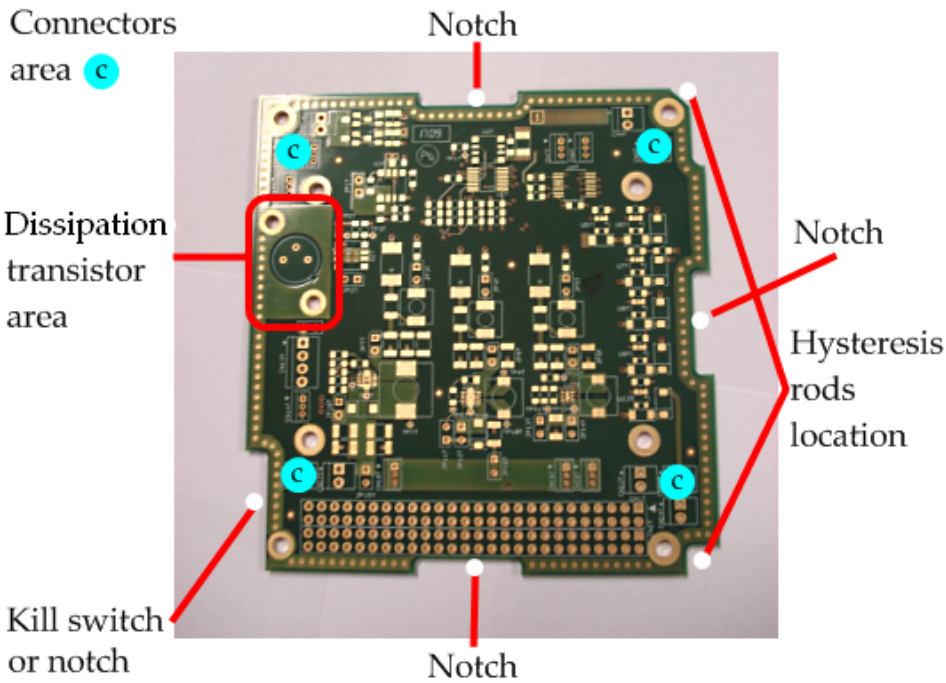

Figure 2.21 – *PC-104's layout*

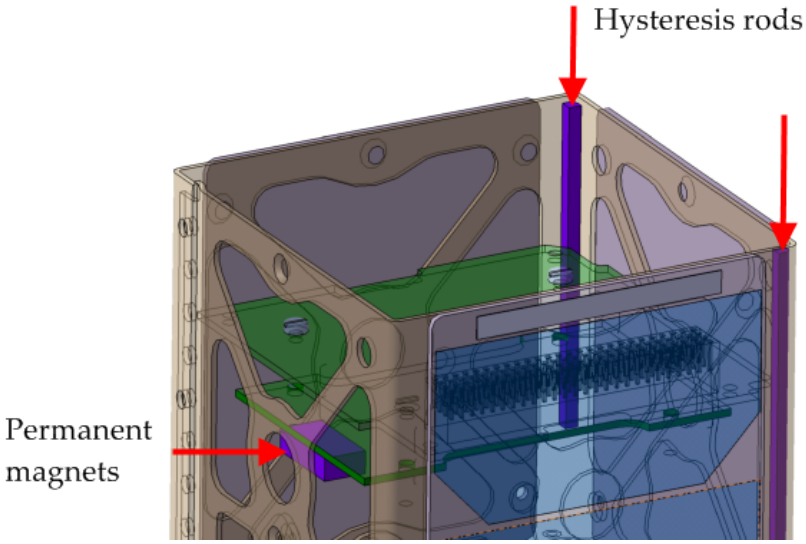

Figure 2.22 – *Magnet and rods configuration*

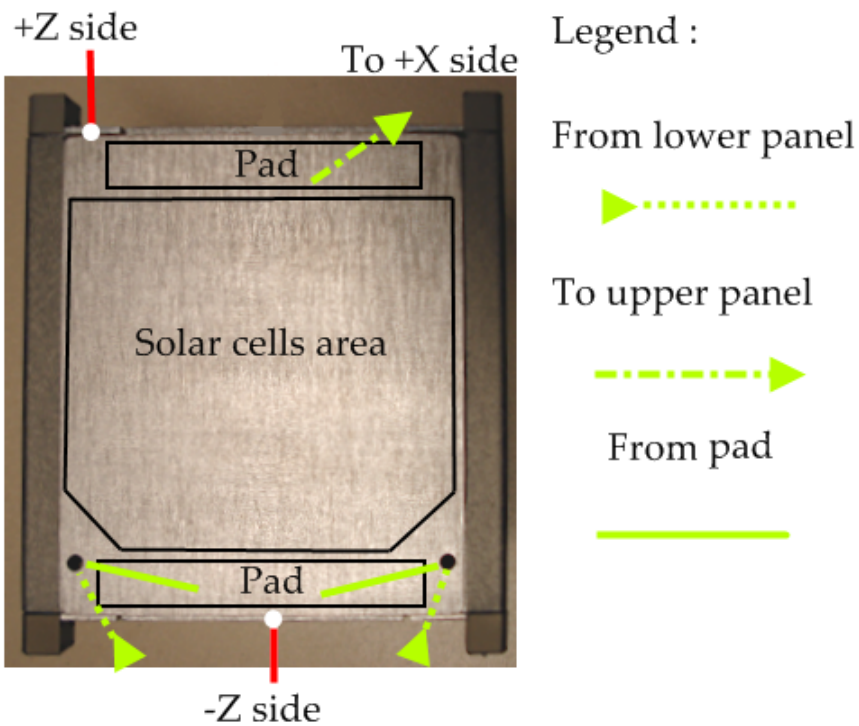

Figure 2.23 – *Cabling path on the lateral face*

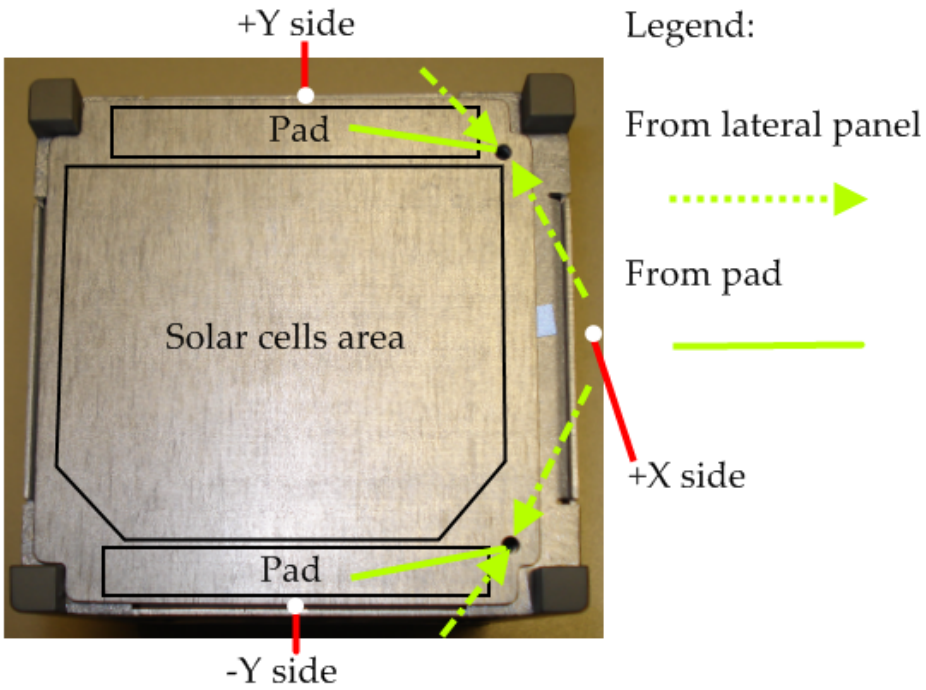

Figure 2.24 – *Cabling path on the upper face*

2.5.5 Discussion

2.5.5.1 Requirement STRU-2-ENV-2

The shielding is obtained on 5 faces with the solar panel and on the sixth face with the antennas' panel. Their thickness will be chosen to provide a 1 year lifetime to the electronic equipment in chapter 3. In addition to this, the solar panels' material could be choose to limit the thermal variations : this idea will be investigated in Chapter 3.

In addition to this global protection, the batteries can shield locally the electronic equipment. It could be interesting to list the most sensitive electronic components (e.g. MSP430) in order to align them above and under the batteries area. Note that an individual protection with a sandwich sheet aluminum/tantalum/aluminum can also be envisaged.

2.5.5.2 Requirement STRU-2-ENV-4

If the FM430 and the COM card locations are fixed by the requirements, the 3 remaining cards can be placed in the order of our choice. Seeing that EPS2 is not always switched on, it can be placed just below the COM card to limits the EMI. On the other hand, the EPS1 location to limit the cable length to the batteries, which finally explains the cards' order proposed. However, a complete electromagnetic compatibility study should be performed as soon the COM card will be available to confirm this order.

Note that the aluminum coverage of modulator/demodulator $ADF7021$ is interesting because it combines both radiations and EMI shielding. Thus, it should be investigated in the next steps of developments.

2.5.5.3 Requirement STRU-3-ENV-1 to 3

The batteries' assembly represents a concentrate mass that can be dangerous during the vibration tests and launch. A finite element model will be performed in Chapter 3 to ensure its mechanical reliability. The mechanical assembly will also be studied to ensure the thermal insulation required (see Chapter 3 too).

On the other hand, this assembly is the most compact and adjustable solution to place the permanent magnet. Indeed, we can provide an accurate positioning by using the free volume under the PCB's lower face and EPS1 (around 15 mm). This accuracy should not be possible on the main structure seeing the fixations availability.

2.5.5.4 Requirement STRU-3-ENV-4 to 6

Many problems arise from these requirements : the transistor has been moved near $-X$ to dissipate its power, the batteries PCB has been relocated on the EPS2, an additional aluminum square and a patch resistor have been placed on the antennas' panel, which complicates greatly the final integration.

Thus, we can wonder if the dissipation circuit is really necessary and other solutions should be investigated in the next developments.

2.5.5.5 Requirement STRU-6-INTER-2

The hysteresis rods have been placed at the corners of $+X$, but the requirement STRU-DR-2 forbids any mechanical fastening on the corners. Therefore, the rods will be bond as well as the solar panels and we can give a new requirement :

- **STRU-6-INTER-2-DES-1**: the hysteresis rods shall be bonded in the corners of $+X$

2.6 Integration

2.6.1 Objectives and methodology

The main purpose of the integration description is to create a detailed road map to become accustomed to this complex procedure. On the other hand, the integration procedure allows to verify the feasibility of the proposed configuration and tries to forecast the problems that could arise during the final integration.

A first procedure has been created with the engineering model of the CSK structure and 5 motherboards (Figure 2.25). It has been tested by the team members and the main difficulties were highlighted. The last update of this document is given in reference (57).

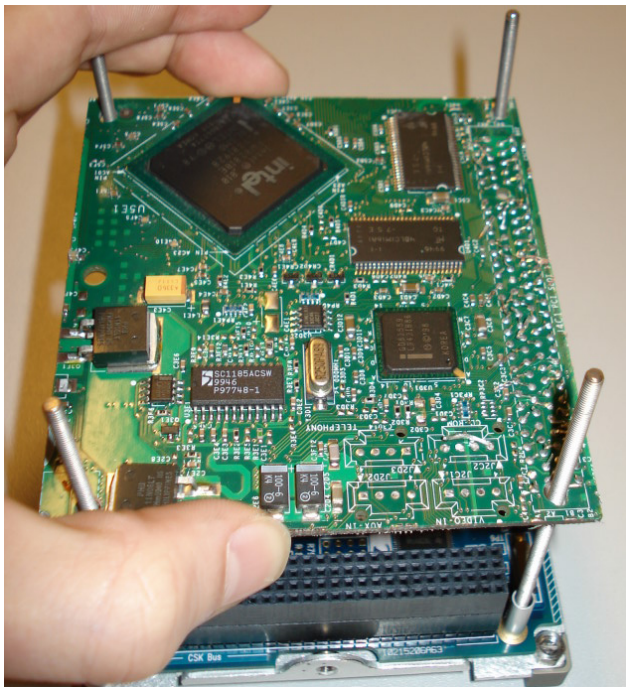

Figure 2.25 – *Integration of the engineering model with 5 motherboards*

2.7 Concluding remarks

The purpose of this chapter was to define a flight system configuration compatible with the listed requirements.

After the presentation of the mechanical and electrical components, the interconnections' problems associated to the assemblies were investigated. The constraints were identified and requirements have been written. The configuration proposed fulfills all these requirements and further considerations about the future improvements have been done. Finally, the integration has verified that this concept was possible.

We can then conclude that the proposed flight system configuration is suitable and reliable. The next step consists in verifying the mass, the design and operational requirements described in section 1.5.4. The solar panels' material has to be defined as well as the dynamic behavior of the CSK structure and the batteries' PCB.

Structural Analysis 3

3.1 Introduction

This chapter outlines the structural analysis of satellite $OUFTI-1$. It intends to assess the structural integrity and ensure that the satellite fulfills all the requirements defined in section 1.5.4.

This chapter starts with the verification of the mass requirement and the calculation of the inertia properties. The solar panels design will be presented. The choice of the material and adhesives will be studied. Another objective is to discuss the batteries' PCB design and to ensure its thermal insulation and mechanical reliability. Finally, the first finite element analyses (FEA) will be presented.

3.2 Mass budget

3.2.1 Objective and methodology

According to the requirement **STRU-MR-1**, it is important to know and update the satellite's mass throughout the advances to ensure that $OUFTI-1$ does not exceed 1 kg mass.

All the components presented in Chapter 2 were weighted, but as some designs are not yet finished (e.g. COM card, batteries' PCB) the -mass budget can variate greatly. Both worst and best case have been considered whereas the letter E represents an estimation when the elements are not yet available. The final result is presented in table 3.1.

The mass budget is divided into minor mass budgets for the subassemblies and major components in order to identify main mass consuming parts. All the tables are rounded to nearest $0,1$ gr and then, the total values may be inconsistent with the sum of the individual parts. The mass budget can be compared with data from reference (63).

3.2.2 Discussion

According to table 3.1, mass budget is large enough to get a comfortable margin : more than 150 gr (15% of the total budget) remain in the best case, and just a bit less than 50 gr (5% of the total budget) in the worst case. Moreover, the "general´´ category is voluntary inflated to stay in safety. We can consider that $OUFTI-1$ meets the requirement **STRU-MR-1**.

Assemblies	Part	Number	Best case (gr)	Worst case (gr)
End plate	end plate	1	26,3	26,3
	foot	4	5,3	5,3
	shym	4	0,6	0,6
	washer M3	4	0,2	0,2
	screw M3	4	1,5	1,5
Total			33,8	33,8
Base plate	base plate	1	35,9	35,9
	foot	1	1,3	1,3
	drilled foot	3	3,6	3,6
	shym	4	0,6	0,6
	spring plungers	2	1,2	1,2
	bolt M3	2	1,1	1,1
	washers	1	0,1	0,1
	screw M3	1	0,4	0,4
	deployment switch	1	2,4	2,4
	screw M1	1	0,4	0,4
	plastic shaft	1	0,1	0,1
Total			47,1	47,1
Contour	Contour	1	63,3	63,3
	screw M3	10	3,2	3,2
Total			66,5	66,5
Side panel	Side panel	3	94	94
	Solar cells	6	/	/
	Kapton film	3	/	/
	Adhesive	3	/	/
	Coverglass	3	/	/
Total			125,3	125,3
Top panel	Top panel	1	33	33
	Solar cells	2	/	/
	Kapton film	1	/	/
	Adhesive	1	/	/
	Coverglass	1	/	/
Total			41,9	41,9
Bottom panel	Bottom panel	1	37,5(E)	39,5(E)
	Solar cells	2	/	/
	Kapton film	1	/	/
	Adhesive	1	/	/
	Coverglass	1	/	/
Total			48(E)	50(E)
FM430	Card	1	51,1	51,1
	Endless screw	4	14,6	14,6
	Spacers 15	4	1,1	1,1
Total			66,8	66,8
OBC2	Card	1	50,4	50,4
	Spacers 15	4	1,1	1,1
Total			51,6	51,6

Assemblies	Part	Number	Best case (gr)	Worst case (gr)
EPS1	Card	1	63,8	63,8
	Bus extension	2	10,6	10,6
	Spacers 25	4	1,9	1,9
Total			76,3	76,3
Batteries	K603870H	2	70	70
	or K554374H	2	70	70
	or Varta	2	42,8	42,8
	or Panasonic	2	54(E)	54(E)
	Wires	4	8(E)	10(E)
Total			50,8(E)	80(E)
Sixth PCB	PCB	1	13,3(E)	15,5(E)
	Ti M3 screw	4	2,9	2,9
	Ti M3 nut	4	1	1
	Ti Standoff	4	8,5(E)	8,9(E)
	Washers	16	1,1(E)	1,3(E)
	SC protection	2	2(E)	3(E)
Total			28,4(E)	32,6(E)
EPS2	Card	1	54	54
	Spacers 15	4	1,1	1,1
Total			55,1	55,1
COM	Card	1	50(E)	70(E)
Total			50(E)	70(E)
MSO	MSO	4	3,2	3,2
	M3 nuts	4	1,3	1,3
	M3 screws	4	1,3	1,3
	Washers	4	0,4	0,4
Total			6	6
Antennas	433 Mhz	1	1,2(E)	1,4(E)
	144 Mhz	1	3,6(E)	3,8(E)
	Panel	1	27,1(E)	27,3(E)
	PCB	1	1,5	1,5
Total			33,4(E)	34(E)
ADCS	Magnet	1	7,5(E)	8,5(E)
	Rods	2	0,8(E)	1,5(E)
	Fixation	3	5(E)	7(E)
Total			13,3(E)	17(E)
Subtotal			794,3	854
General	Adhesive	/	15(E)	30(E)
	Cabling	/	15(E)	30(E)
	Sensors	/	20(E)	40(E)
Total			50(E)	100(E)
Total			844,3	954

Table 3.1 – *Oufti-1 mass budget*

The solar panels system is the main mass consumer with around 20% of the mass budget, which can be explained by their radiation shielding purpose. The structure takes about 15% of the total which is little compared to its role of structural load path. The batteries PCB has also an important part with more than 100 gr. Among electronic cards, EPS1 takes the most important part with 8%.

3.3 Center of gravity and inertia

3.3.1 Objectives

The Center of gravity (COG) has to respect the requirement **STRU-MR-2** that imposes its location within 2 cm of the CubeSat's geometric center. On the other hand, the inertia properties are a fundamental feature of a 3 dimensional body and are necessary to the ADCS subsystem's calculus (31).

This section intends to calculate the satellite's inertia and the COG location with a global accuracy of 5%.

3.3.2 Modeling strategy

The model is based on the assumption of an uniform density for the metallic parts (e.g. solar panels, CSK structure). The heavy components on electronic cards (e.g. PC-104 connectors, $5V$ power supply) are weighted thanks to their geometry whereas the distribution of small components' mass (e.g. resistors, capacitors) is supposed uniform over the entire area of PCB.

Only the parts with more than 1% of the total mass (10 gr) are weighted under Catia with an error $\leq$ 2%, in accordance to the mass budget. The others components (e.g. screws, nuts, shyms) are taken into account, but with an error that ranges from 3 to 5%.

When the real weight is estimated (letter E in table 3.1), the average between best and worst cases is considered. Table 3.2 summarizes the main mass consuming parts, their real and estimated weights and the model's error.

A simple method to assess the model quality consists to compare the modeling's weight with the mass budget. As Catia does not model the "general´´ category of the mass budget, it has to be compared to the subtotal : $831,6$ gr for Catia while the mass budget mean is $822,15$ gr. With a mass error of $1,15\%$ on the whole modeling, we can expect a good assessment.

3.3.3 COG location

Three cases are considered :

1. The batteries' PCB upper face is situated at 10 mm from the EPS2 (case 1)

Part	Mass budget (gr)	Catia mass (gr)	Error (%)
End plate	26,3	26,4	+ 0,4
Base plate	35,9	36,6	+ 1,9
Contour	63,3	64,4	+ 1,7
Side panel	125,3	126	+ 0,6
Top panel	41,9	41,8	- 0,2
Bottom panel	49(E)	49,4	+ 0,8
FM430	51,1	51,1	0
Endless screw	14,6	14,5	- 0,7
OBC2	50,4	50,6	+ 0,4
EPS1	74,4	73,9	- 0,7
Kokam	70	69,6	- 0,6
sixth PCB	14,4(E)	14,7	+ 2
EPS2	54	54,1	+ 0,7
COM	60(E)	60,5	+ 0,8
Antenna's panel	27,2(E)	27,2	0

Table 3.2 – *Catia modeling*

2. The batteries' PCB upper face is situated at 18 mm from the EPS2 (case 2)

3. The batteries' PCB upper face is situated at $5,5$ mm from the EPS2 (case 3)

The first case presents the height used on the flight model, the second case has the lower battery on the EPS1 while the third case represents the upper battery on EPS2. The results are presented in table 3.3.

Axis	Case 1 (mm)	Case 2 (mm)	Case 3 (mm)
X	0,61	0,61	0,61
Y	-2,36	-2,36	-2,36
Z	0,24	-0,66	0,75
Geometric center	2,45	2,52	2,55

Table 3.3 – *COG location*

$OUFTI-1$'s COG is separated from its geometric center with less than $2,6$ mm in the 3 cases. The COG location varies only of $1,1$ mm between both extremal cases. This can be interpreted as a uniform distribution of mass along the direction Z.

The COG location along Y axis can be explained by the unsymmetrical properties of the electronic cards and particularly the PC-104's connector. If necessary, this effect can be counteracted by moving the batteries' PCB in $+Y$ direction.

Along X axis, the slight difference can be explained with the mass difference between solar and antennas' panel. From this result, we can conclude that the requirement STRU-MR-1 is largely fulfilled, regardless of the configuration.

3.3.4 Inertia

Inertia can be calculated from any point in the structure, but it is generally preferred to define it from the COG. Thus, the inertia linked to the COG and the frame XYZ are :

$$I_G = \begin{pmatrix} 2,082 & -0,057 & -0,012 \\ -0,057 & 1,765 & -0,096 \\ -0,012 & -0,096 & 2,018 \end{pmatrix} \cdot 10^6 \ \ g\ mm^2 \tag{3.1}$$

Moreover, principal moments and vectors can be found to define completely the system :

$$A_1 = \begin{pmatrix} -0,16 \\ 0,94 \\ 0,31 \end{pmatrix}, \ M_1 = 1,723 \cdot 10^6 \ \ g\ mm^2 \tag{3.2}$$

$$A_2 = \begin{pmatrix} 0,15 \\ -0,29 \\ 0,95 \end{pmatrix}, \ M_2 = 2,049 \cdot 10^6 \ \ g\ mm^2 \tag{3.3}$$

$$A_3 = \begin{pmatrix} 0,98 \\ 0,2 \\ -0,1 \end{pmatrix}, \ M_3 = 2,092 \cdot 10^6 \ \ g\ mm^2 \tag{3.4}$$

These values show that the mass distribution is quite uniform. Finally, note that the COG and inertia should be verified experimentally when a complete spacecraft will be available. From this point of view, reference (71) provides a suitable experimental procedure that allows to retrieve both COG coordinates and inertia from a complex three dimensional body.

3.4 Solar panels design

Solar cells are one of the most important points in a CubeSat design. Then, the structural subsystem shall be able to provide a suitable interface with the solar cells in orbit as well as during launch.

This section will start with a description of the state of art concerning the solar panel. A design will be defined according to the requirements and a material will then be chosen. Finally, a choice of adhesive will be presented.

3.4.1 State of art

It is difficult to follow a guide line to the final design. To our knowledge, no CubeSat combines Azurspace solar cells with a Pumpkin's structure.

Swisscube is of first interest. They designed their own CFRP panels to support the Azurspace's solar cells. Swiss team uses a mono-bloc frame as main structure and the solar panels will be screwed on it.

Würzburg also uses Azurspace's solar cells. They are integrated by Astrium on stainless steel panels as shown in Figure 3.1. Solar panels were screwed on their "home made´´ structure.

ClydeSpace sells ready-to-fly solutions destined to Pumpkin's CSK. However, these solar panels integrate Spectrolab solar cells that are smaller than ours (+/- 70 by 35 mm). Solar panels are made of PCB and can be screwed on the main Pumpkin's structure.

Pumpkin also sells ready-to-fly solution with solar cells from Spectrolab. The integration is done on PCB which are fixed on Cubesat with a set of solar clips (64). This solution was used on the Colombian CubeSat Libertad-1 (Figure 3.2).

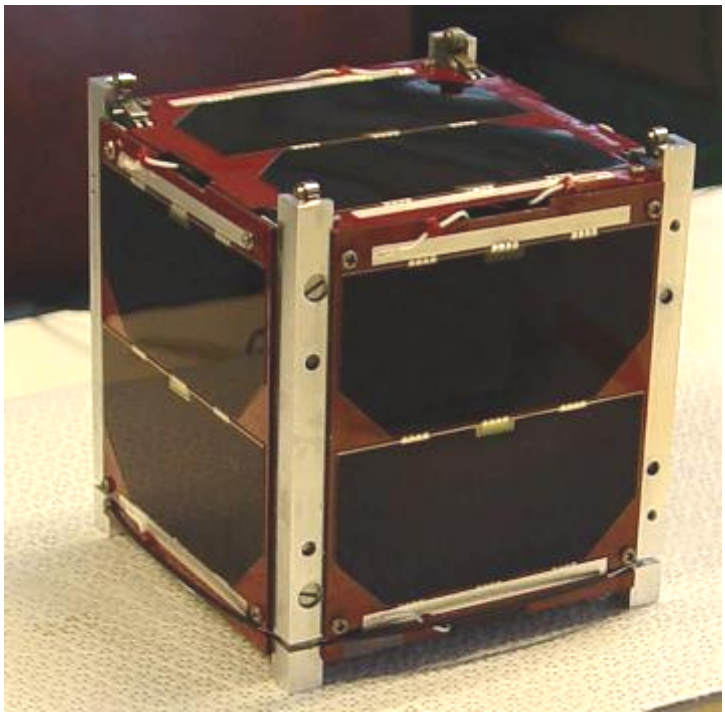

Figure 3.1 – *Würzburg's CubeSat - UWE-1*

3.4.2 Requirements

It is worth recalling that some requirements were imposed on the solar panels during the flight system configuration :

- **STRU-2-ENV-1**: Solar panels shall shield electronic components against space radiations to survive 1 year.
- **STRU-6-INTER-3**: The solar panels shall be bonded on the satellite.
- **STRU-6-INTER-6**: The solar cells shall be connected to EPS1 using 10 cables.
- **STRU-8-PAR-4**: The AzurSpace solar cells defined in reference (73) shall be used.

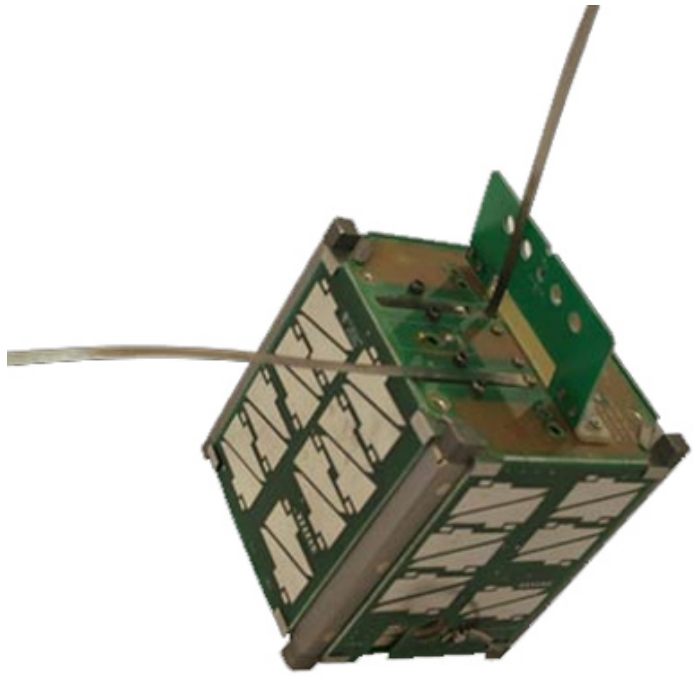

Figure 3.2 – *Colombian CubeSat - Libertad-1*

The solar panels shall also conform to the design requirements. In particular :

1. **STRU-DR-2**: The external components other than the rails shall not touch the inside of the P-Pod (47).
2. **STRU-DR-3**: Components on shaded sides shall not extend more than $6,5\ mm$ normal to the surface (47).
3. **STRU-DR-5**: NASA/ESA approved materials should be used whenever possible (47), (43).
4. **STRU-DR-10**: The max outgassing values for each material used on P-POD/CubeSat shall be (56) :
   - TML : less than $0,1$ %
   - CVCM : less than $0,01$ %

In addition, the solar panels shall be a reliable mechanical solution to the solar cells equipment during launch and in orbit (STRU-1 and STRU-2). They shall be designed to survive their temperature range (STRU-3).

These requirements need to be improved because they are too general to serve as guidelines during the design and the choice of material. The next section defines more precisely the constraints on the design.

3.4.3 Solar panel design

3.4.3.1 STRU-6-INTER-6

- **STRU-6-INTER-6-DES-1**: The side solar panels shall be drilled with 2 holes on their lower parts, according to the cabling path.
- **STRU-6-INTER-6-DES-2**: The top solar panel shall be drilled with 2 holes on the $+X$ side, according to the cabling path.
- **STRU-6-INTER-6-DES-3**: Each holes shall be at least 3 mm wide to let pass 4 cables.

Note that the bottom solar panel is not drilled because its solar cells use the holes on the side panels.

3.4.3.2 STRU-8-PAR-4

Astrium requires a rectangular area of 80 x 93 mm^2 to integrate the solar cells.

- **STRU-8-PAR-4-DES-1** Solar panels substrate shall provide a rectangular area of at least 80 x 93 mm^2 to integrate the solar cells.

3.4.3.3 STRU-DR-2

- **STRU-DR-2-DES-1** Solar panels shall be at the most 82 mm wide.

3.4.3.4 STRU-DR-3

- **STRU-DR-3-DES-1** Solar panels shall be at the most 6 mm thick.

3.4.3.5 Solar panels

The layout of the top and side panels are presented in Figure 3.3, but their thickness remains unknown. They fulfill all the requirements (STRU-6-INTER-6-DES-1; STRU-6-INTER-6-DES-2; STRU-6-INTER-6-DES-3; STRU-8-PAR-4-DES-1; STRU-DR-2-DES-1; STRU-DR-3-DES-1) and then, the concept can be validated.

The next step is then the material selection of the panels' substrate.

3.4.4 Material selection

Let us define accurately the requirements on the material.

3.4.4.1 STRU-1

The first feature of the panels' substrate is its structural integrity during the launch. The solar cells are brittle and a rigid substrate will limit the displacements under harsh vibrations while the strength will ensure the structural integrity of the panel. The toughness is also an important property to sustain the stage ignition/separation, fairing jettisoning and POGO effects during launch.

Then, the general requirement can be expressed as :

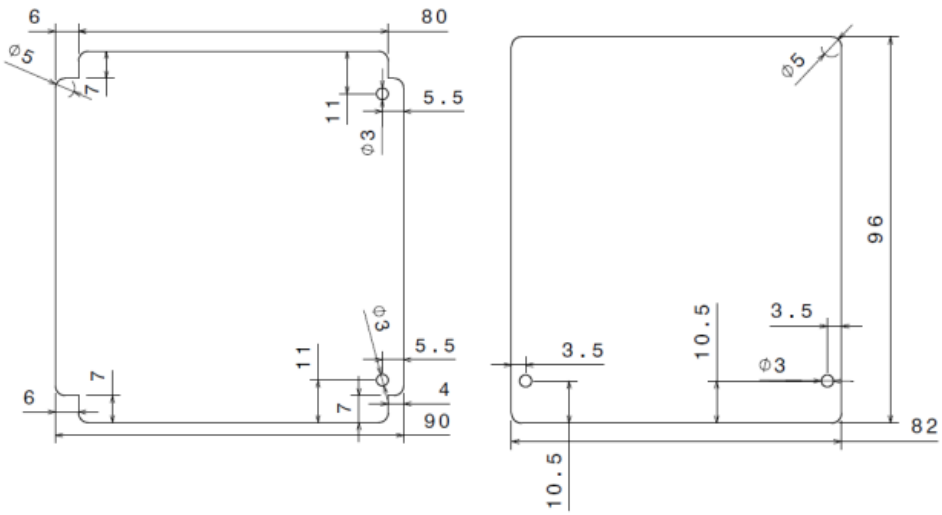

Figure 3.3 – *Geometry of the top panel (left plot) and side panel (right plot)*

- **STRU-1-LR-1**: Solar panels' shall be a reliable mechanical substrate during launch.

We can state more precisely :

- **STRU-1-LR-1-DES-1**: Solar panels' material shall be rigid.
- **STRU-1-LR-1-DES-2**: Solar panels' material shall be resistant in traction/compression.
- **STRU-1-LR-1-DES-3**: Solar panels' material shall have a toughness of at least 25 $MPa.m^{0,5}$.

3.4.4.2 STRU-2-ENV-1

According to the requirement **STUR-2-ENV-1**, the solar panels shall shield the equipment for 1 *year* lifetime.

- **STRU-2-ENV-1-DES-1**: Solar panels' material shall shield electronic components against space radiations for 1 year lifetime.

Note that the thickness of the panels will be defined during the study of the radiative model.

3.4.4.3 STRU-3

The thermal subsystem (35) predicts important thermal variations in LEO that can disturb the batteries. The solar panel substrate can limit these variations by choosing a material with a high thermal inertia. During the eclipse leaving, the cold case simulation indicates that $OUFTI-1$ will limit these variations if the solar panels have also a good thermal conductivity.

The general requirement can be written as :

- **STRU-3-ENV-7**: Solar panels' material shall shield batteries against thermal variations.

And then, typical values of specific heat and thermal conductivity can be given :

- **STRU-3-ENV-7-DES-1**: Solar panels' material shall have a specific heat higher than 750 $J/kg.K$.
- **STRU-3-ENV-7-DES-2**: Solar panels' material shall have a thermal conductivity higher than 50 $W/m.K$.

The thermal cycling can also induce panels' deformations by the adhesive weakening in the interaction structure-glue-panels. This effect can be mitigate if the panel's coefficient of thermal expansion (CTE) is similar to the CSK structure ($Al - 5052 \ : 20 - 25 \ \mu strain/K$).

- **STRU-3-DES-3**: Solar panels' material shall have a CTE that ranges from 20 to 25 $\mu strain/K$.

Finally, the operating range of the solar cells is typically of $[-30°C \ 70°C]$. The material should resist to those temperatures with a security margin of $10°C$.

- **STRU-3-DES-4**: Solar panels' material shall resist to the temperatures range $[-40°C \ 80°C]$.

3.4.4.4 STRU-DR-5

In addition to the radiations, another problem in low earth orbit (LEO) is the atomic oxygen which is an aggressive environment for materials. The main interaction between the high velocity oxygen atoms (around 8 km/s) and the spacecraft is the erosion phenomenon that degrades the material properties and performances (optical, thermal, mechanical and electrical). Erosion rates are usually quoted in terms of yield in units of $10^{24} \ cm^3/atom$. Then, the material substrate will be chosen to resist the atomic oxygen erosion.

- **STRU-DR-5-ENV-1**: Solar panels' material shall be resistant to the atomic oxygen erosion.

3.4.4.5 STRU-DR-10

The outgassing is also taken into account in the choice of the solar panel material. It shall be stable under high vacuum and will be clean of the environmental pollutants. This last condition will be ensure by choosing a suitable post-processing. Further considerations about the adhesives and their poor outgassing properties will be done later.

- **STRU-DR-10-ENV-1**: Solar panels' material shall be conform to the outgassing conditions.
- **STRU-DR-10-ENV-2**: Solar panels' material shall be post-processed.

3.4.4.6 Plasma

A spacecraft in orbit flies through a plasma of particles that are not neutral and can lead to the spacecraft charging, hence electric discharges. A common mean to counteract this effect is to connect electrically the outer surfaces to the same point or keep an electrical conduction on the external structure.

However, the electrical insulation between the solar cells and the structure is made with a kapton foil which limits the surface conductivity. In addition, the adhesives are generally poor electrical conductors and they reinforce the insulation between the panels and the structure. Thus, we can wonder if an electrical conductivity is important seeing the surfaces' poor electrical properties. According to CSL, this effect is particularly important for larger spacecraft of 1 meter or more and our CubeSat, with its 10 *by* 10 *cm* structure, is not influenced by the electrical discharge phenomenon.

3.4.4.7 Methodology

The choice of a particular material and manufacturing process is an iterative and complex problem. The material selection is then done with a systematic procedure described in references (3),(4) and (44).

According to (4), 3 elements have to be defined to perform the material selection :

1. The most important property, also known as objective function, which will be minimized or maximized. This element reflects the principal aim of the material selection, e.g. it can be a minimum cost, minimum mass or maximal rigidity.

2. The primary constraints that define one or several functional material limitations. In other words, primary constraints limit the objective function's evolutions to get a suitable result. For example, a beam with a minimum mass objective could lead to exotic solutions such as foam or nylon. However, if the primary constraint is the resistance, the process will limit solutions to titanium or aluminum alloy.

3. Finally, the secondary constraints describe the numerical limits (e.g. toughness) that are stated in the previous section.

After this complete definition of the problem, performance index can be found from (3), depending on the target function, the primary constraints and the structural purpose (e.g. bar, beam). This indicator reflects the important materials parameters in regard of their purposes.

For technical reasons, this procedure cannot integrate the requirements concerning the radiations (STRU-2-ENV-1-DES-1), atomic oxygen (STRU-DR-5) and outgassing (STRU-DR-10). Then, they will be verified after the selection process.

3.4.4.8 Target function and primary constraints

The target function could be the weight minimization but this objective leads to an incompatibility with the radiation objective. An other drawback is that this target function leads to many complicated and expensive solution, in time and money, because the results fall in the range of very high performances material.

A more convenient objective is to minimize the cost of material, whose is in accord with the KISS philosophy definition. Indeed, many better solutions can be found as the overall price (e.g. material's price, manufacture and finishing touches) of the product is often link to the production's time. Then, the design is said to be "at minimum cost´´.

Primary constraints are linked to the thin geometry of solar panels ($\leq 1,75\ mm$) and the most relevant parameter is the mechanical reliability. As we do not want to limit the material selection to one primary constraint,two properties have been chosen : rigidity and strength. Then, the index can be found by a "stiffness or rigidity-limited design at minimum cost´´ in reference (3).

The constraints of second order come from the rest of technical requirements. They are summarized in table 3.4

Property	Range/value
Toughness	$25\ MPa.m^{0,5}$
Specific heat	$750\ J/kg.K$
Thermal conductivity	$50\ W/m.K$
CTE	$20-25\ \mu strain/K$
Temperature	$[-40°C-80°C]$

Table 3.4 – *Operating limits*

Thus, the problem is completely defined : find a cheap material (objective), which is rigid and resistant (primary constraints), and which respects the requirements concerning the toughness, specific heat, thermal conductivity, CTE, and the temperature operating range (secondary constraints).

3.4.4.9 CES Software

Material selection is simplified thanks to the powerful CES software. This complete material database is coupled with a program that classifies materials from their performance index. CES Software allows a complete selection process in 2 steps :

- **Graph stage**: which allows the comparison of materials in regard of the objective function and the primary constraint through the performance index.
- **Limit stage**: which allows to define the secondary constraints.

3.4.4.10 Selection with CES

According to the objective, the primary constraints and the structural goal, we can retrieve 2 index of performances from reference (3) :

Flat plate, stiffness-limited design at minimum cost $M_{rigidity} = \frac{E^{1/3}}{\rho.C_m}$

Flat plate, strength-limited design at minimum cost $M_{resistance} = \frac{\sigma_{y0}^{1/2}}{\rho.C_m}$

Where M is the performance index, E is the Young's modulus, σ_{y0} is the elastic limit, ρ the density and C_m the material cost per kg.

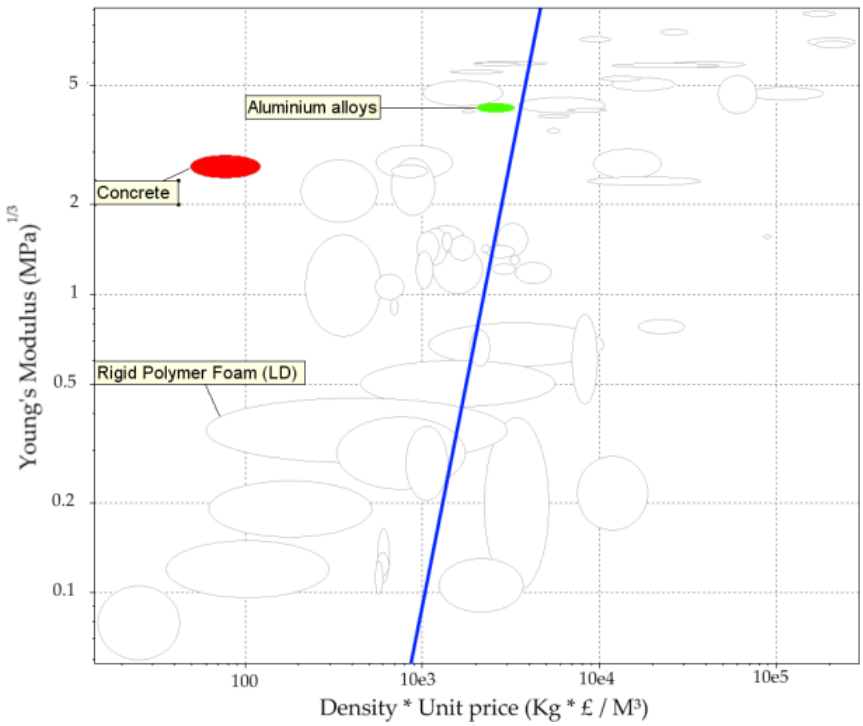

Figure 3.4 – *Stiffness-limited design, first stage*

Through CES, both graphics can be plotted in Figures 3.4 and 3.5. They are both given in logarithmic scale such that iso-performance line can be drawn by the following procedure :

$$M_{rigidity} = \frac{E^{1/3}}{\rho.C_m} \tag{3.5}$$

gives in logarithmic scale :

$$log\ M_{rigidity} + log\ \rho.C_m = \frac{1}{3} \cdot log\ E \tag{3.6}$$

Then, equal performance of the objective function (i.e. M constant) can be found by taking a line of slope 3. This one intersects all the materials that present the same performances. Similarly, a slope of 2 is founded for the strength-limited design.

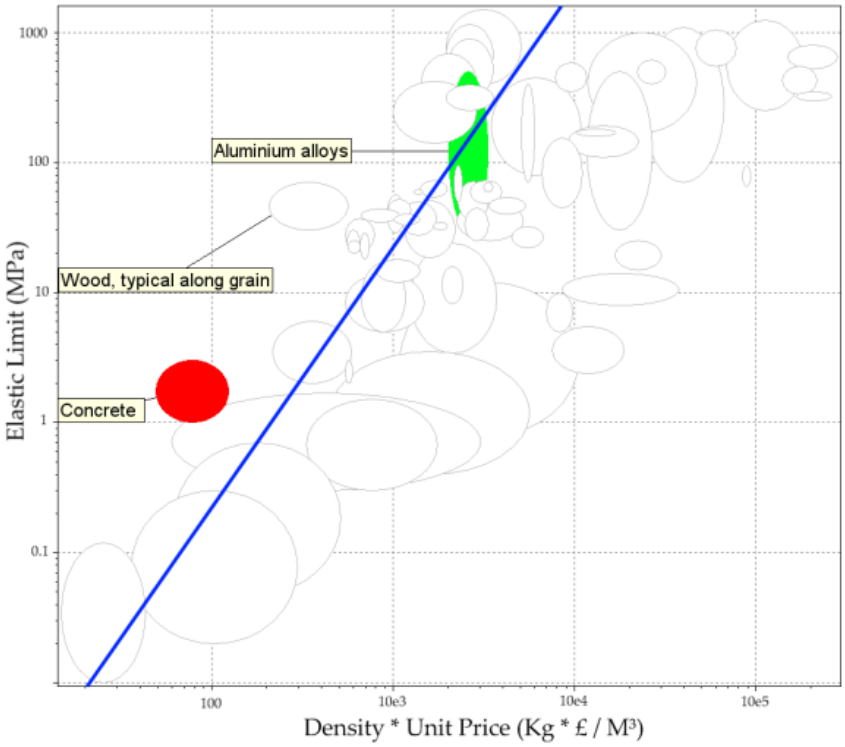

Figure 3.5 – *Strength-limited design, first stage*

As shown in Figure 3.4 and 3.5, aluminum alloy seems to be the solution from both rigidity and strength criterion. As a matter of fact, aluminium alloys are some of the basic building materials of existing spacecraft and appear in many subsystems. They have a wide range of mechanical properties and can be used in heavily loaded structures in circumstance ranging from cryogenic conditions up to $200°C$.

The choice of a particular alloy is almost constrained by industrial's availability, time delay, and overall price. For a first engineering model, the $Al - 7075\ T73$ has been chosen.

3.4.4.11 Validation of material

$Al - 7075\ T73$ is widely used in aerospace structures and recommended by reference (22). Its main mechanical features are displayed in table 3.5 where we can see that requirements **STRU-1-LR-1-DES-3**, **STRU-2-ENV-1-DES-1**, **STRU-3-ENV-7-DES-1/2** and **STRU-3-DES-3/4** are fulfilled. The method itself ensures a material with high specific strength and rigidity satisfying the requirements **STRU-1-LR-1-DES-1/2**.

According to reference (22) (43), and (24), this aluminum alloy is well established in aerospace industry, with many years of application and service experience. In particular, the references (15), (21) and (27) explains that aluminum coated kapton is one of the best hardened material against atomic oxygen with an erosion yield of only $0,05\ ^{\cdot}cm^3/atom$.

Vacuum does not affect aluminum alloys and the outgassing requirement (**STRU-10-DES-1**) are then respected but a post-treatment is neces-

Property	Range/value
Main alloying element	Zn (5,6%)
Young's Modulus	71 GPa
Elastic limit	150 MPa
Fracture toughness	42 $MPa.m^{1/2}$
Maximum service temperature	170°C
Minimum service temperature	$-273°C$
Specific Heat	920 $J/Kg.K$
Thermal Conductivity	160 $W/m.K$
CTE	23 $\mu strain/K$

Table 3.5 – *Aluminum 7075-T73 main properties. Courtesy (29)*

sary to remove the doubtful layer of pollutant. It will be chosen in the next section.

Finally, and from the radiations point of view, reference (8) explains that aluminum is a common technique to shield electronic components in space environment. With this last verification, we conclude that the aluminum is a reliable choice according to the design and environmental requirements. At this point, only the post-treatment and the thickness remain unknown to definitively complete the design.

3.4.4.12 Post-treatment

The roles of post-treatment are numerous and many process exist, depending on the application (67). Two particular procedures are of common use for space applications : hard-anodizing and chemical film ("alodine´´). Both consist in removing the doubtful natural oxide Al_2O_3 and impurities from surface in order to create an other coating, much more uniform and stable, which is desirable for good adhesion and outgassing properties.

Hard-anodizing gives good anti-friction properties that are necessary for structural parts in contact with the P-Pod. The thin oxide layer is characterized by abrasion resistance and film hardness. Typical thick range from 25 to 250 μm and thermal conductivity can be 30 times lower than pure aluminum. Moreover, its melting point extend to more than 2000°C and gives good electrical insulation properties. Most process to hard anodizing are based on sulfuric acid baths.

Alodine, or commonly chem film process, replaces the natural oxide layer with an other one (7 μm in average). Contrarily to sulfuric process, alodine treatment's properties are such as its influence is limited on the mechanical properties of aluminum. The electrical and thermal conduction are also preserved. Although the friction coefficient is a bit better, abrasive properties are weaker than hard anodizing. This process gives a very good surface finishing to the bond process.

Chem film process is generally preferred because it is much more simple and faster than hard-anodizing. Moreover, aluminum panels preserve

a full thermal conduction and the surface finishing to be bonded. Hence, the solar panels substrate will be alodined.

3.4.5 Thickness and radiative model

There exist many different kinds of radiations, but none systematic procedure to perform a radiative model. A common approach consist to take into account only the total irradiation dose (TID), which is an image of the overall radiations' effects on the electronic devices (8) (2) (2) (27). The total irradiation dose is the addition of the effects of the trapped electrons and protons within the radiation belts, the solar protons and the Bremsstrahlung (9).

The only free variable is the solar panels' thickness. It defines the amount of material available to shield $OUFTI-1$ and it will be chosen to ensure a mission lifetime of 1 *year*. The table 3.6 displays the aluminium panels' mass compared to their thickness. We decided to limit the solar panels mass to 200 *gr*. Then, the substrate shall have a thickness lower than $1,75$ *mm* to let a margin to the kapton, glue, pads and cells.

Thickness (mm)	Total mass (mm)
0,5	53,1
0,75	79,7
1	106,2
1,25	132,8
1,5	159,3
1,75	185,9
2	212,9

Table 3.6 – *Solar panels thickness versus substrate's mass*

Then, requirements can be defined on the thickness :

- **STRU-2-ENV-1-DES-2**: Solar panels' thickness shall be chosen for 1 *year* mission lifetime.
- **STRU-2-ENV-1-DES-3**: Solar panels' thickness shall be lower than 175 *gr*.

The total irradiation dose as a function of equivalent aluminum shielding thickness is presented in Figure 3.6. The main assumptions on this study is a maximum solar activity and a spherical shell shield configuration. The equivalent thickness is calculated as the thickness of a closed sphere of 7 *cm* radius which integrates the material volume of the CSK structure, 5 solar panels and antennas' panel.

After $1,5$ *mm* of aluminum panels' thickness, each millimeters does not bring much more significant protection as the Bremsstrahlung plateau is progressively reach. Table 3.7 presents the evolution of the total dose with the solar panel thickness.

Swiss team has already perform several tests on their sensitive devices, and in particular on the MSP430. They concluded that the first problems

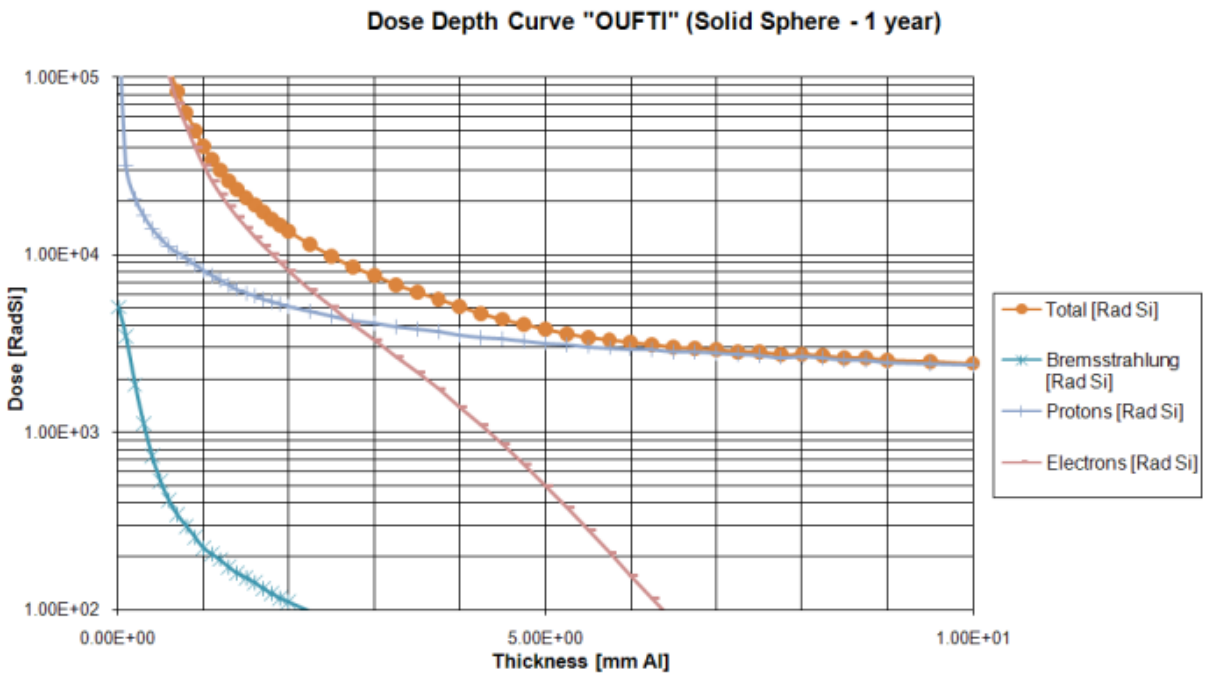

Figure 3.6 – *Total irradiation dose for OUFTI-1's orbit. Courtesy (76)*

Thickness(mm)	Equivalent (mm)	Panels' mass (gr)	TID (krad)
0,2	1,05	22,2	32
0,4	1,19	44,4	27
0,6	1,32	66,6	23
0,8	1,45	88,9	20,5
1	1,59	111,1	19
1,2	1,72	133,3	17
1,4	1,86	155,5	15
1,6	1,99	177,7	13
1,8	2,12	199.9	12
2	2,26	222.1	11

Table 3.7 – *Total dose versus panel thickness*

arise around 25 *krad*. If we take a factor of safety (FOS) of $1,8$, the TID allowed on $OUFTI-1$ will be 14 *krad* and the panels' thickness corresponding is $1,5$ *mm*. By taking this value, the total dose on our electronic equipment is limited to 14 *krad* a year and ensure 1 year mission lifetime with a FOS of $1,8$. Then, the requirements **STRU-2-ENV-1-DES-2/3** are fulfilled and this concludes the solar panels design (Technical drawings available in annex).

An interesting comparison can be done with reference (1) that has performed an accurate radiative model. Spanish team uses 190 *gr* to shield their CubeSat compared to 200 *gr* with $OUFTI-1$ (5 solar panels and 1 antennas' panel).

Finally, let us discuss the quality modeling. A sphere represents a better repartition of mass than a cube and the radiations are underestimate. However, this effect is counteracted because the cube is completely included within the spheroid geometrical approximation : the equivalent thickness is thinner for the same shielding volume.

3.4.6 Adhesive selection

3.4.6.1 Objectives

The mechanical fastening is not always possible and an alternative can be the use of adhesives.

The purpose of this section is the selection of suitable adhesives in both following case :

1. adhesive link between the CSK structure and the solar panels (requirement **STRU-6-INTER-3**).
2. adhesive link between the CSK structure and the hysteresis rods (requirement **STRU-6-INTER-2-DES-1**).

First, the general constraints concerning the adhesive bonding will be presented. Two different types of adhesive will be presented and discussed.

3.4.6.2 General constraints

The first rule to remember is that anything can be bonded, but no adhesive exists that can effectively bond everything (23). Successful joining by adhesive bonding needs consideration of number factors, as shown in Figure 3.7.

Among these properties, the following factors are particularly important in our case :

- Cure temperature;
- Outgassing;
- Temperature range;

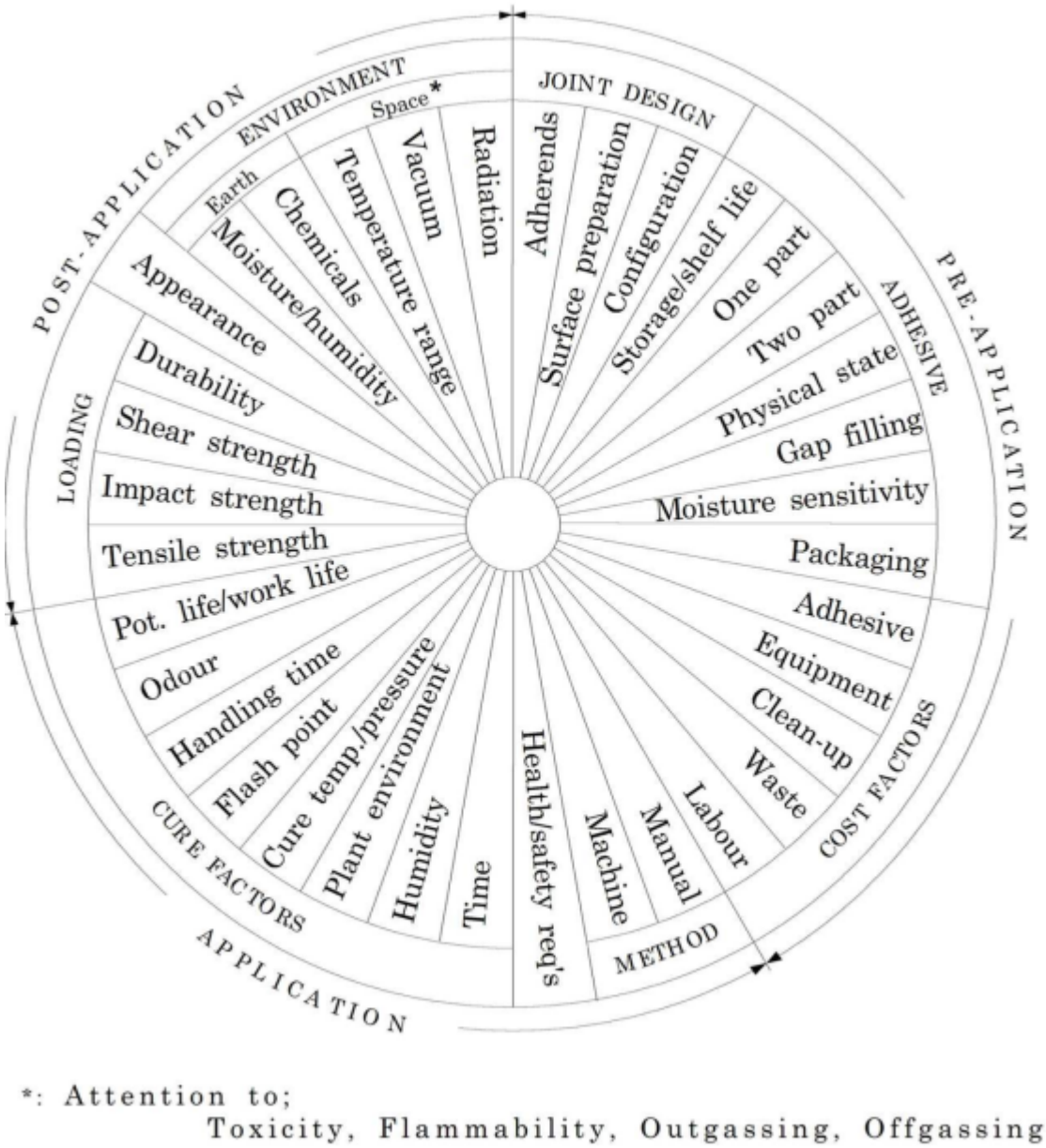

Figure 3.7 – *Factors influencing the adhesive bonding. Courtesy (23)*

- CTE;
- Thermal conductivity;
- Toughness;

Cure temperature

The cure process can be defined as the change of the physical properties of a material by chemical reactions through condensation or addition polymerization or by crosslinking (e.g. vulcanisation). Usually, it is accomplished by the action of heat and catalysts, alone or in combination, with or without pressure.

Each adhesive is then characterized with a couple time/temperature necessary to complete the adhesive bonding. In general, the higher the temperature, the lower the time to complete the cure process. However, under a certain temperature, the cure is not possible. In our case, this cure temperature should be low enough to avoid any damage of the batteries.

Outgassing

Adhesives are particularly sensitive to the outgassing. Even on Earth and at room temperature (RT), they release many pollutants during the cure process. In orbit, the combination of glue outgassing and ultra violet rays could lead to deposit on solar cells surfaces, resulting in a decrease of their efficiency by obscuring them.

Then, and to obtain a reliable solution, our choice will be limited to the adhesives recommended by ESA (22), or by Swisscube (66).

Temperature range

According to the thermal subsystem (35), temperature range from $-50°$ to $70°$ and the adhesive should sustain these conditions.

CTE

According to the adhesive handbook (23), the thermal cycling in LEO can cause the weakening of the adhesive, which can be explained with the difference of CTE between the structure and the adhesive. Typically, the adhesives' CTE range from 50 to 500 $\mu strain/K$. As it depends strongly on the nature of the adhesive, we can only say that the adhesive should have a CTE as close as possible to the adherents (23 $\mu strain/K$).

Thermal conductivity

Another weakness of the adhesive is their low thermal conductivity (typically 1 W/mK). This additional thermal resistance depends on the application surface and thickness of the joint, hence the adhesive itself. Once again, we cannot quantify precisely the requirement and the only rule is to choose an adhesive with a good thermal conductivity. Note that

this property is much more important for the solar panels than for hysteresis rods.

Toughness

During launch, the CubeSat shall sustain the dynamic load and shocks from the LV. However, the molecular structure of the adhesive can lead to the crazing effect which is a micro-weakening of the mechanical properties. This can result in a failure of the adhesive.

Several modifications of the molecular structure exist to minimized this problem. In particular, the addition of micro rubber balls helps to absorb much better the shocks and gives better properties. These adhesives are then called ”tough´´.

3.4.6.3 Adhesives proposed

According to (23), adhesives are usually limited to epoxy-based, polyimide and silicone. The principal characteristics of each one are shown in Table 3.8

Family	Characteristics		Limitations	Aerospace Use
	Advantages	Disadvantages		
Epoxy (modified with)				
• nylon • nitrile • novolac • phenolic	• High shear strength • Low shrinkage • Cure 120°C or 170°C (depends on formulation)	• Brittle • Low hot strength	• High temperature <170°C • Hot/wet environments	• Most widely used for metal and composite bonds
Silicone				
	• High heat resistance	• Low strength	• Higher temperature applications (>170°C, <300°C) • Low temperature applications (<100°C)	• Higher temperature applications (>170°C, <300°C) • Low temperature applications (<100°C)
Polyimide				
	• Very high heat resistance • Good electrically	• Rigid • High temperature cure • Possibly corrosive	• Limited to higher temperature applications (up to 300°C)	• Limited to higher temperature applications (up to 300°C)

Figure 3.8 – *General characteristics and properties of adhesives. Courtesy (23)*

Among several drawbacks, polyimide adhesives bring a rigidity that will be dangerous during vibration testing and a high cure temperature that would be critical to the electronic components. So, only the characteristics of the epoxy and silicones adhesives will be studied.

Epoxy

Epoxy is probably the most widespread adhesive used in spatial technology, especially for metals and composite bonding. As a matter of fact, it presents several advantages such as :

1. a wide range of mechanical properties;
2. low shrinkage during bonding process;
3. good adhesion to many different substrate;
4. no by-product creating during cure;

Moreover, elastomeric modifiers are often added to improve peel strength as well as moisture resistance. These new varieties are formulated to be tougher, i.e. having improved impact resistance and higher fracture surface energies. These particular properties are very important because the adhesive has to be flexible to resist in vibration. Thus, high shear strength can be combined with a flexible behaviour to enforce structural integrity during launch. Cure temperature is an other advantage of the epoxy bonding : it can generally range from room temperature up to 175°, depending on the form.

Weak point of epoxy adhesives is that they can become brittle due to the thermal cycling which is particularly important in LEO. Finally, the epoxy bond will not be subject to very hot/wet conditions. An example of typical spatial epoxy adhesive is the Epo-Tek 930 (21) and Epo-Tek H74 (66).

Silicones

Silicones are synthetic polymers with a wide range of properties. Their special molecular structures allow an unusual combination of organic and inorganic chemical properties. Among several properties, we can find :

1. A wide range of viscosities;
2. very good temperature resistance;
3. ability to withstand high temperatures for long periods, up to $200°C$;
4. resistance to UV and IR radiation;
5. resistance to oxydation.

Likewise epoxy adhesives, silicones can be classified as structural adhesive, even if their mechanical properties are less marked. Then, they are widely used in so called 'soft-structural applications' where adhesive strength is needed to maintain component integrity or where flexibility is necessary to accommodate strains or vibrations. An example of a 'soft-structural' application is assembly of solar cells. CSL provides silicones adhesives RTV-142, RTV-615 and RTV-651.

Discussion

Epoxy adhesives can be used to bond the solar panels on the main structure as they have high mechanical properties, but they need to be tough to ensure the structural reliability during launch and thermally conductive to keep the benefit of the aluminum panels' properties. The hysteresis rods could be bonded with a silicone which can facilitate the bonding process.

We have seen that is quite difficult to select a particular adhesive for space use regarding all the problems that could occur. In particular, the CSL recommends to test the adhesives under vibrations to assess their

structural behavior. Then, the first interesting test could be a random qualification testing with an epoxy adhesive bonding of the top solar panel on the CSK structure.

Another severe drawback of the use of adhesives is that they complicates strongly the integration process and that the disintegration is not possible once in place. Indeed, the use of conventional solar panels clips could damage the solar cells structure (see requirement **STRU-6-INTER-3**). A possibility could be a composite solution with an adhesive bonding of the upper and lower solar panels and the mechanical fastening of the side panels thanks to home made clips.

3.5 Batteries' PCB

At this point, it is worth recalling a particular requirement from the Chapter 2 :

- **STRU-3-ENV-3**: Batteries' PCB shall be thermally insulated from the electronic cards.

This section intends to verify this requirement. First, the batteries' PCB design will be briefly presented while its requirements will be defined. After that, a material will be selected.

3.5.1 Assembly design

The sixth PCB is directly drawn one's inspiration from Pumpkin's *PC* − 104 stacking (Figure 3.9). Four screws provide the flexural rigidity behavior, 4 spacers separate the EPS2 from the PCB and 4 "self-stopping´´ nuts ensure the reliability of the assembly. Screws and nuts are chosen in *M*3 format because they constitute compromise for the structural reliability while being a compact solution.

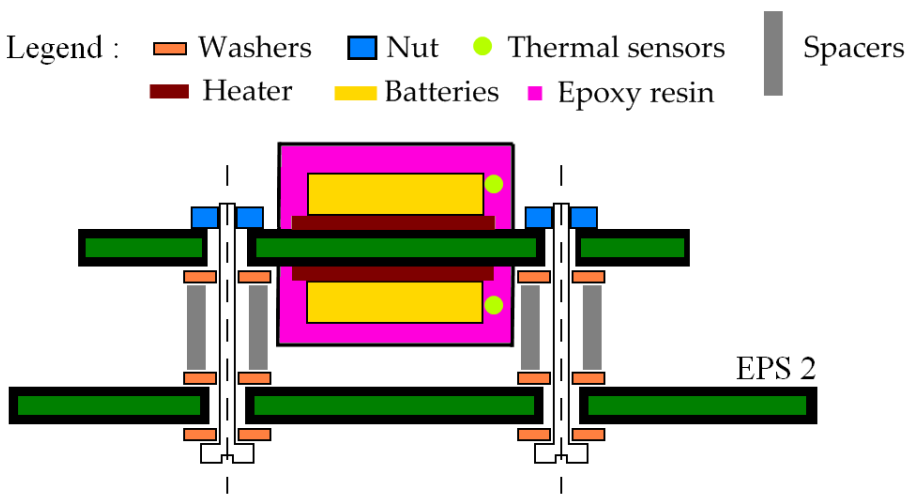

Figure 3.9 – *Sixth PCB details*

Mechanical purpose

Batteries are one of the heaviest components inside $OUFTI-1$, and dynamic loading could be a problem if a resonance appears during Vega's launch. Then, the general requirement can be stated :

- **STRU-1-LR-2**: the batteries assembly shall be a reliable mechanical assembly during launch.

And it can be defined more precisely :

- **STRU-1-LR-2-DES-1**: the screws, spacers and nuts shall be rigid.
- **STRU-1-LR-2-DES-2**: the screws, spacers and nuts shall be resistant.
- **STRU-1-LR-2-DES-3**: the screws, spacers and nuts shall have a toughness of at least 25 $MPa.m^{0,5}$.

STRU-3-ENV-3

Space vacuum suppresses the convection from the heat equation and the most important remaining process is the conduction. Then, the thermal conductivity between the EPS2 and batteries' PCB will be as low as possible. However, and to define a requirement, we can limit this value to 10 $W/m.K$. If this value leads to problematic heat transfer with the simulation (35), thermal washers can be added to the assembly.

- **STRU-3-ENV-3-DES-1**: the screws, spacers and nuts shall have thermal conductivity less than 10 $W/m.K$.

3.5.2 Material selection

An additional requirement is necessary. Indeed, all along the previous developments, we assumed that the final product, i.e. the screws, spacers and washers, were already available. However, it is important to take this point during the material selection to avoid any exotic solutions as "concrete screw´´.

- **STRU-1-LR-2-DES-1-DES-1**: the material selected shall allow the manufacturing of screws, spacers and nuts.

The objective is to minimize the mass. Actually, it is not incompatible with the KISS philosophy as the material has to be found in the form of final product e.i. screws and nuts, what take into account the cheap product's feature. This criterion will lead to a high performance solution, reliable from a mechanical point of view.

Once again, primary constraints can be taken as rigidity and strength. As the primal function is to ensure the assembly's mechanical reliability, these criterion seem to be the most suitable.

Finally, the functional limitations can be defined in table 3.8. The lower temperature is a bit different than from the solar panels (35) : the center of the satellite will be warmer and reach $-20°C$. The upper limit is set by the EPS1 transistor that can reach 90°.

Property	Range/value
Toughness	25 $MPa.m^{0,5}$
Temperature	$[0°C - 80°C]$
Thermal conduction	$\leq 10\ W/m.K$

Table 3.8 – *Batteries PCB's screws, nuts and spacers operating limits*

Beam, stiffness-limited design at minimum mass $\quad M_{rigidity} = \frac{E^{1/2}}{\rho}$

Beam plate, strength-limited design at minimum mass $\quad M_{resistance} = \frac{\sigma_{y0}^{2/3}}{\rho}$

The performance index can be found in reference (3). Screws can be viewed like beams with free section area, so :

Results from these definitions are presented in Figure 3.10 and 3.11.

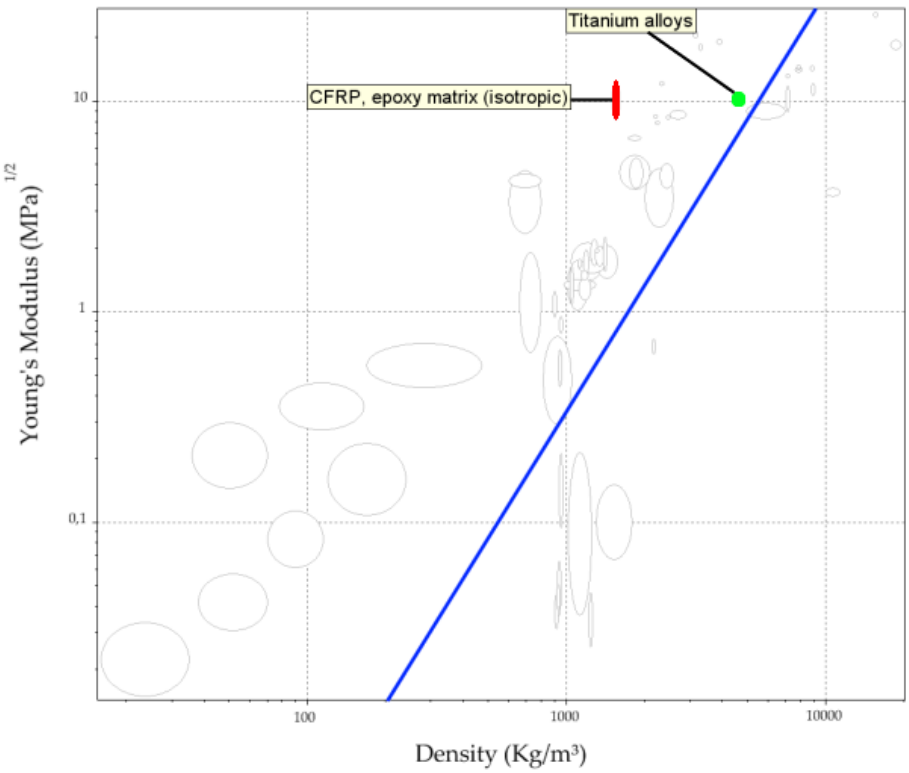

Figure 3.10 – *Design at minimum mass, rigidity*

Titanium seems to be the best solution, both from a mechanical and thermal point of view. Titanium has good space experience and good corrosion resistance while having useful combination of low density and high strength. Moreover, it does not require a protection in space environment.

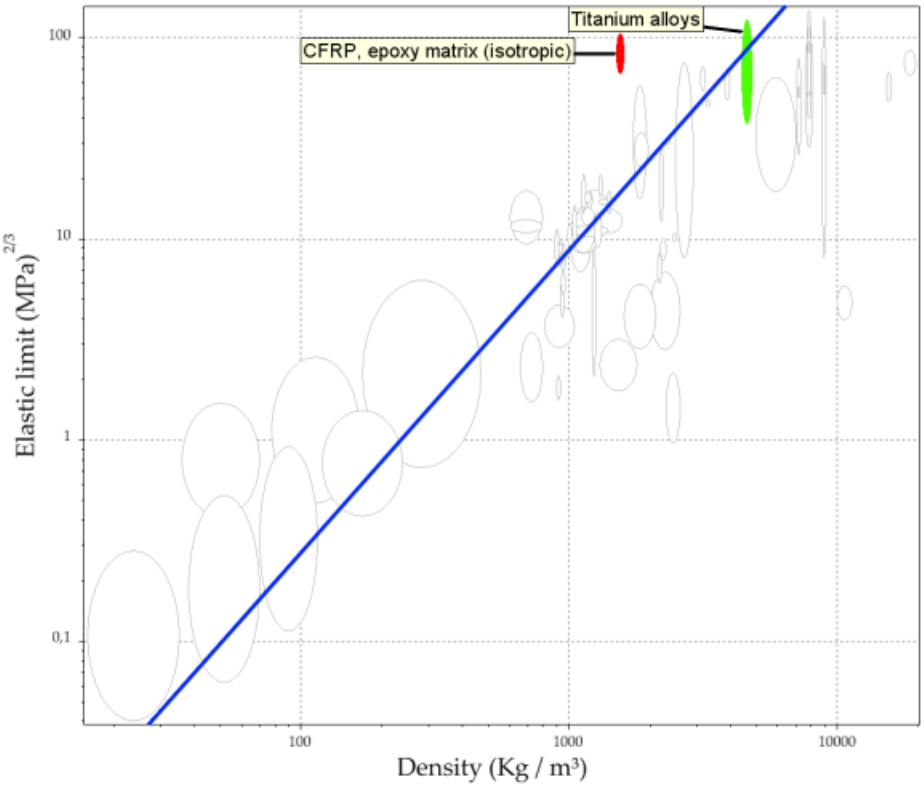

Figure 3.11 – *Design at minimum mass, strength*

3.5.3 Validation

The result directly ensures the three structural requirements and the thermal conductivity. Moreover, a complete set of screws and end product made of this material is available. As recommended by ESA, a $Ti\ 6Al\ 4V$ or more commonly Ti grade 5, will be used for screws, spacers and nuts. In this way, our 5 requirements are fully satisfied.

3.6 Finite element analysis

3.6.1 Introduction

The finite element analysis (FEA) is a powerful mathematical tool to study many problems in mechanical engineering. This method models and simplifies the real problem in order to obtain its structural features. Its main purpose is to facilitate the structural analysis by limiting the modeling's efforts. All the simulations proposed will be performed with Samcef and Samcef Field (69), a Finite Element Software made in Liège.

The main purpose of these FEA is the study of the structural behavior of $OUFTI-1$ aboard Vega Maiden Flight. This section investigates first the static loading case and the modal analysis. The structural integrity of the batteries' PCB will be investigated and finally, a harmonic response calculation will be presented. The detailed model description will be done before each analysis as well as the different loading cases.

3.6.2 Static analysis

As described in reference (7), the spacecraft is subjected to quasi-static loads during flight. This study's aim is to define weither the main structural parts are able to withstand the steady state acceleration and to calculate the factor and margin of safety.

Loading

Reference (56) defines the current CubeSats accommodation on the launcher as represented in Figure 3.12. P-Pods are lay down horizontally on the launcher's interface and are mounted radially.

The maximal quasi-static acceleration is $6,3\ g$ along the launcher's longitudinal axis, during the lift-off. The maximal lateral acceleration is due to the dynamic pressure and is $1,2\ g$ along the lateral axis. With a FOS (Factor Of Safety) of $1,8$, these accelerations become $11,5\ g$ and $2,25\ g$ respectively.

As lateral loads may act in any direction simultaneously with longitudinal loads, the structural model uses 3 static accelerations in the 3 spatial directions. Among various combination of static loads, two particular cases will be simulated :

1. CubeSat's axis X represents the launcher's longitudinal axis while Y and Z represent the lateral axis. (noted "case 1´´).

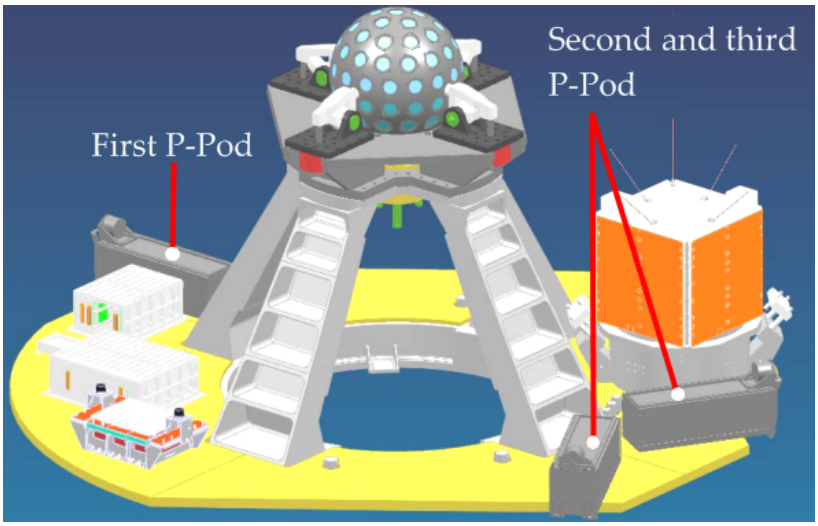

Figure 3.12 – *P-Pods configuration inside Vega*

2. CubeSat's axis Y represents the launcher's longitudinal axis while X and Z represent the lateral axis. (noted "case 2´´).

These simulations are representative of real conditions as the P-Pod is always in the horizontal position. The worst lateral case is defined in Figure 3.13. The CubeSat in position 1 undergoes the launcher's longitudinal acceleration on X in case 1 and on Y in case 2. Along the P-Pod axis, CubeSat in position 1 shall support not only its own weight but also the weight of the 2 overlying picosatellites. The associated lateral forces is then $2\ x\ 1(kg)\ x\ 2,25(g)\ x\ 9,81 = 44,15\ N$ rounded to $45\ N$.

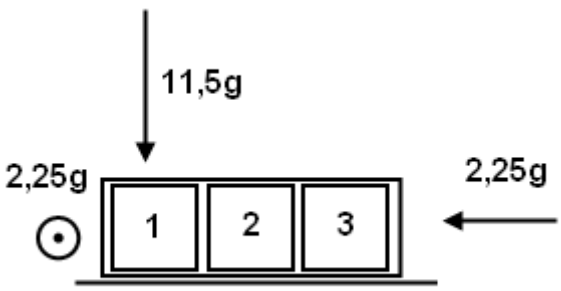

Figure 3.13 – *Worst lateral case*

Then, the worst case 1 and 2 can be summarized as :

1. Case 1 simulates an acceleration of $11,5\ g$ along X, $2,25\ g$ for both Y and Z. Four additional forces of $\frac{45}{4} = 11,25\ N$ are placed on the 4 base plate's feet.

2. Case 2 simulates an acceleration of $11,5\ g$ along Y, $2,25\ g$ for both X and Z. Four additional forces of $\frac{45}{4} = 11,25\ N$ are placed on the 4 base plate's feet.

Note that an additional security is defined in both cases : the lateral acceleration resultant applied to the whole model is $\sqrt{2 \cdot 2,25} = 3,2\ g$ instead of only $2,25\ g$. Moreover, the aforementioned steady-state accelerations occur during different phases of the flight, i.e. the longitudinal acceleration is maximal during the third stage acceleration while the lateral loads are maximum during lift-off. The resulting model is therefore conservative.

3.6.2.1 Model

To limit the modeling efforts, only the relevant structural parts will be taken into account.

All CSK structural parts are modeled using shells components. The low thickness of the plates ($1,52\ mm$) and the chassis ($1,27\ mm$), are negligible with respect to the other dimensions ($100\ mm$). Material properties of the $Al - 5052\ H32$ is obtained via CES.

The deployment switch and all others geometrical prominent shapes are neglected in this analysis whereas linear structural behavior is assumed. The endless screws are used as stainless steel beams of an average $2,5\ mm$ diameter with $8\ cm$ length.

The electronic cards are modeled as shells ($1,6\ mm$ thick). According to reference (65), a typical modeling simplification consists of neglecting the geometry of electronic components but by smearing their properties on the shell representing the PCB. Then, a global mass smearing is used by distributing the whole mass on the entire area of PCB. The PCBs are assumed to be isotropic with a Young's modulus of $18,5\ GPa$ (66). The 4 titanium screws of the batteries' PCB are modeled as beams of $2,5\ mm$ diameter. The stiffening effect of spacers are neglected but their mass are used.

The connections between the elements are considered as extremely rigid. In reality, the pieces will be bolted and glued together resulting in extremely rigid unions validating this assumption.

The mounting of a CubeSat within the P-Pod is detailled in reference (10). Then, the boundaries conditions within the P-Pod are taken as follow :

- The 4 end plate's feet are clamped to simulate the effect of the top and bottom panel on $OUFTI - 1$ feet.
- The 4 corner are locked on a line to simulate the rails.

3.6.2.2 Results

The main results are summarized in table 3.9. Figure 3.14 presents the displacements in the first case. The structure is pushed as a rigid body in a parallel direction to the P-POD while both upper and lower plated are deformed at the feet location. The maximum displacement occurs on the

Loading	Max. displacements (mm)	Max. Von-Mises stress (MPa)
X case	$0,053$	9
Y case	$0,052$	$8,99$

Table 3.9 – *Static FEA results*

base plate, at the forces' application points. It has a value of $0,053$ mm. The second case presents the same results. This can be explained with the global symmetry of the CSK structure.

The maximal Von Mises stress appears on the CSK end plate, at the joint with the chassis (Figure 3.15). The maximal equivalent stress on the beams are only around 5 MPa as they are less loaded.

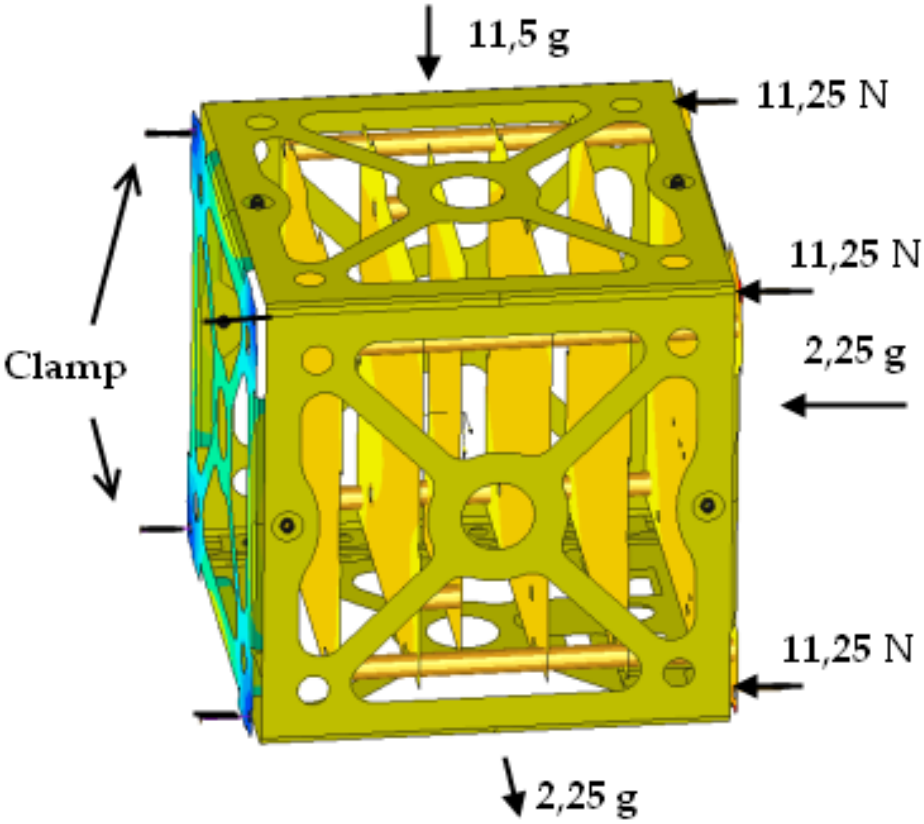

Figure 3.14 – *Displacements on the structure;*

According to the reference (20), we can define the margin of safety (MOS) :

$$MOS = \frac{allowableload}{appliedload\ x\ FOS} - 1 \tag{3.7}$$

With a yield stress of 150 MPa and a FOS of $1,8$, the MOS in X and Y case is $8,26$ in both cases. This means that $OUFTI - 1$ can support a load $8,26$ times higher before entering the plastic zone.

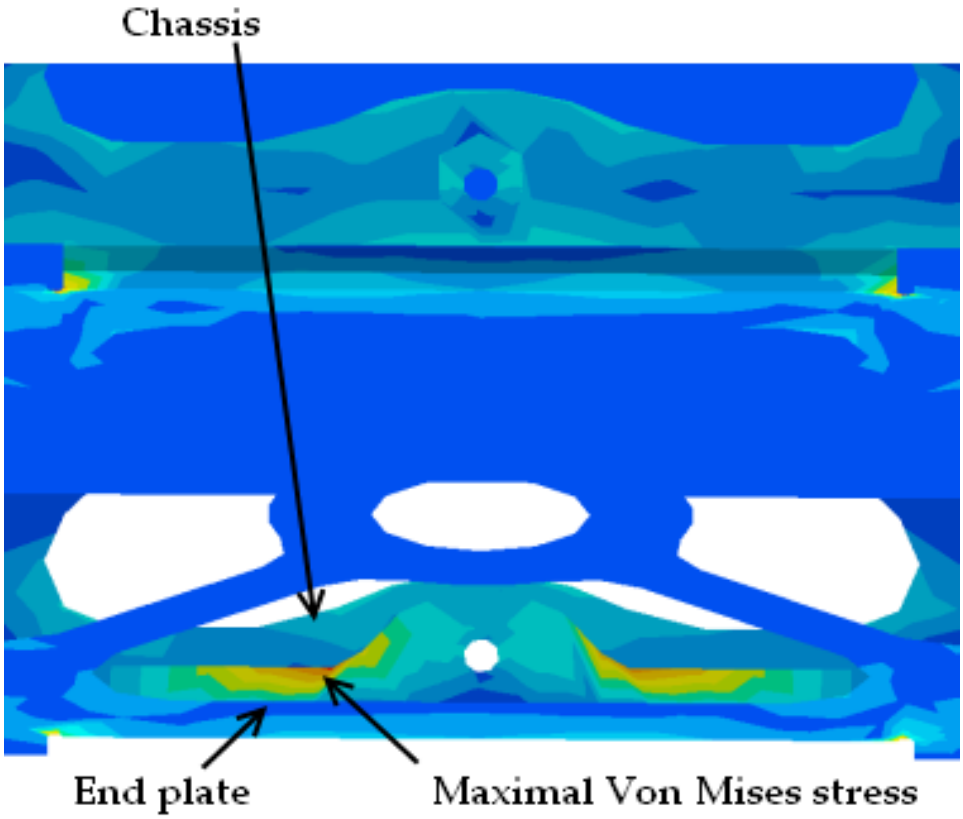

Figure 3.15 – *Maximal Von Mises stress on the structure*

3.6.3 Modal analysis

On the long-term, the FE modal analysis intends to forecast the dynamic behavior of $OUFTI-1$ flight model. In so far as this is the first steps of the modeling, only the Pumpkin's structure will be considered in this section and a complete modal survey will be presented on the same structure, in the next chapter.

3.6.3.1 Model

The model is similar to the static model but the electronic cards and the endless screws are not considered. In particular, components such as the deployment switch or the stainless steel ringlets on $-X$ are not considered. It will be seen later that these components have a significant effect on the modal behavior.

No boundaries conditions are applied and a linear structural behavior is assumed. Damping is not considered in the FEM.

3.6.3.2 Results

6 modes are included in the modal basis under 1000 Hz. First numerical results are shown in table 3.10.

Mode	Punctual connection (Hz)
1	522,6
2	591
3	604,3
4	643,2
5	709,5
6	796

Table 3.10 – *Modal parameters under 1000 Hz*

The first frequency comes around 530 Hz while the 3 next are closer and range from 590 to 670 Hz. Fifth frequency comes near 715 Hz and the last is situated not far from 800 Hz.

The CSK structure presents 2 typical modes :

1. Under 1000 Hz, each mode involves a vibration in phase of the panel's arms.
2. Above 1200 Hz, these vibrations change in a more complex deformation and the arms can vibrate out of phase.

Both kind of vibrations are shown in Figure 3.16.

First 6 modes can be briefly described with the panels involved in the vibration as well as their phases. The denomination "in phase´´ means that the panels engaged in the description are getting closer or moving away of the geometric center in the same time.

Mode 1 : 522 Hz

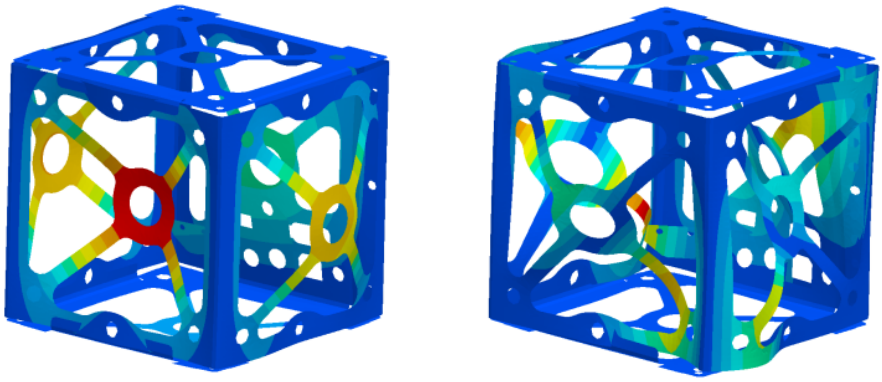

Figure 3.16 – *Typical vibration of the CSK structure's panels*

The first mode is characterized by the oscillations in phase of $+/-Y$ while $+X$ is out of phase compared to them. $-X$ has only a slight deformation.

Mode 2 : 591 Hz
The second mode is quite similar to the first one. $+/-Y$ are out of phase while $+X$ is in phase with $+Y$, but with less intensity. Others panels remain almost fixed.

Mode 3 : $604,3$ Hz
The third mode presents oscillations in phase of $+/-Y$ and $+X$. $+/-Z$ panels vibrate with a very slight deformation.

Mode 4 : $643,2$ Hz
The fourth mode has dominant oscillations on $+/-X$ but out of phase. $+/-Z$ are in phase and have vibrations quite important.

Mode 5 : $696,3$ Hz
The mode 5 has a local vibration of the panel $+Z$ while the other faces remain almost fixed.

Mode 6 : $808,8$ Hz
The last mode is also characterized by a local vibration of the $-Z$ face, with a slight deformation of $-X$.

All these modes are represented in Figures 3.17, 3.18 and 3.19. It is quite interesting for the experimental free-free modal survey to understand that these modes are always localized on the faces' center and that the feet are fixed.

3.6.4 Batteries PCB model

An important issue concerns the height of the batteries' PCB. Indeed, its structural deflection could lead to a collision between the batteries and electronic devices on EPS1 or EPS2.

The main purpose of this section is to develop a dynamic analysis of the batteries' subassembly to determine the batteries' displacement along

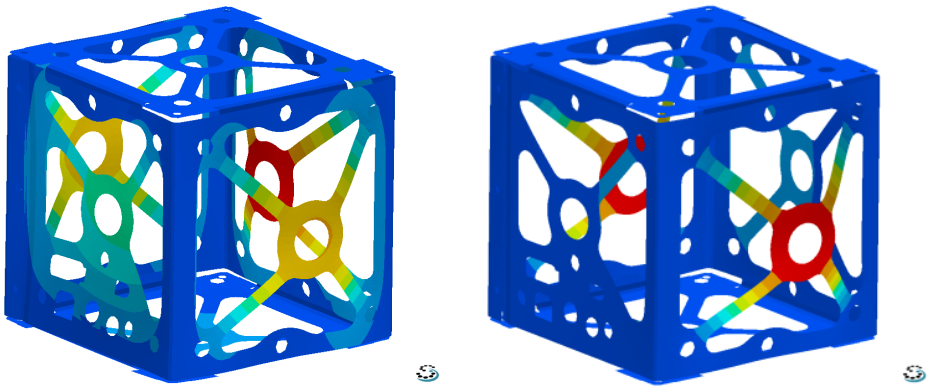

Figure 3.17 – *Left plot : first mode of vibration; right plot : second mode*

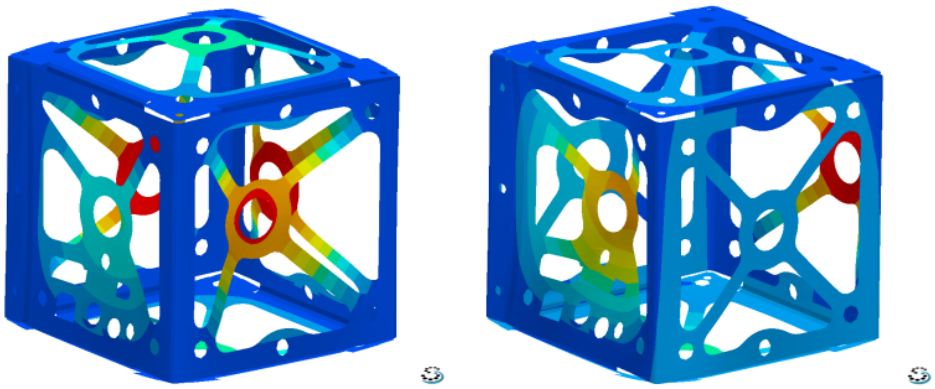

Figure 3.18 – *Left plot : third mode of vibration; right plot : fourth mode*

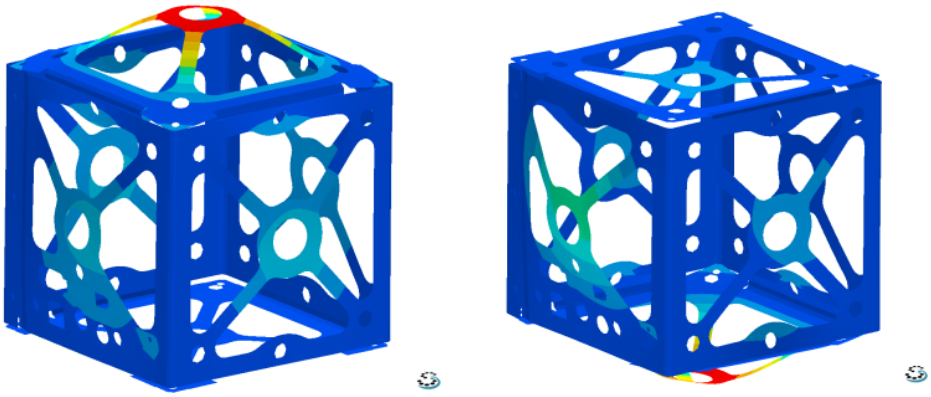

Figure 3.19 – *Left plot : fifth mode of vibration; right plot : sixth mode*

Z axis. The results should ensure that they will not touch or damage any electrical components on both EPS.

3.6.4.1 Model

As this study has been done during preliminary design, only a first approach to the problem will be presented. It follows the PCB's modeling techniques described in reference (65) by using a global distribution of mass over the entire PCB.

The model is constituted of 6 parts : the EPS2's PCB, the batteries' PCB and the 4 screws while spacers, nuts and thermal washers are neglected in first approach.

The distance from the batteries to the EPS1 and EPS2 are given in table 3.11. The sixth PCB is situated in a middle position between the highest component above EPS1 (4 mm) and the highest component under EPS2 (1 mm). The Kokam $603870H$ represents the worst case with its greatest external dimensions.

Batteries	Above EPS1	Under EPS2
Kokam 603870H	6,9	3,4
Kokam 554374H	8	4,5

Table 3.11 – *Distance from batteries to EPS1 and EPS2*

The screws can be modeled as titanium circular beams with a diameter of $2,5\ mm$ ($M3$). Their tips' circumferences are connected on PCBs' holes thanks to 8 rigid fixations, exactly as in the static analysis.

Each PCB is modeled as shells of $1,6\ mm$ thickness and a global mass smearing is used while the stiffness contribution of electronic devices (e.g. soldered joint, adhesive) is neglected. This technique has been chosen for its better accuracy during preliminary study and because it gives a conservative model.

In particular :

1. EPS2 card weights 64 gr and has $83,65\ cm^2$ of area. So, $\rho = 4480\ kg/m^3$ and is rounded to 4500.
2. Batteries and their PCB weight 113 gr, with an area of $47,5\ cm^2$ and then $\rho = 14860\ kg/m^3$, rounded to $15000\ kg/m^3$.

As explained in the static analysis, the PCBs are assumed to be isotropic with a Young's modulus of $18,5\ GPa$ (66). This approximation is sufficient in a first approach even if, in reality, the PCBs are made of composite material and present a significant amount of anisotropy.

According to reference (58), a modal damping of 2% is a quite representative value for a PCB because there exists a strong friction between

the composite's layers. As this parameter strongly conditions the structural deflection, only 1% will be included in the model to keep a security margin of 1%.

Finally, the connection to the endless screw can be modeled as fixed in the 3 spatial directions. The rotational stiffness exists but cannot be measured with a high degree of confidence in a preliminary design. Thus, the rotational degree of freedom are let free which will give a structural deflection overestimated.

3.6.4.2 Loading

Even if the only test requested is the random vibrations, it can be interesting to simulate the worst case in structural dynamic : the harmonic response of the structure.

The harmonic response analysis allows to predict and verify whether the proposed design will successfully resist harmful effects of forced vibrations such as the resonance. This study is much more reassuring than the random vibration due to the steady-state effect of vibrations and its constant dynamic amplification.

Therefore, a sinusoidal load is considered. Its frequency sweeps within the range of the random spectrum, $[20 - 2000]$Hz, and all the eigenfrequencies which lie within the selected range are included in the calculation of the forced response. Indeed, this is at the frequencies at which the model can undergo the most severe damage.

The acceleration is defined in such a way that the harmonic analysis reflects the random vibration test. The root mean square (RMS) level of the qualification test, which is 14 g ($1g = 9,81\ m/s^2$) (56), seems to be the solution. With a FOS of $1,25$, the acceleration becomes $17,5\ g$.

The worst case is defined in Z direction. Indeed, the mass of the batteries' PCB reduces the first natural frequency of the assembly in Z direction. The mode shape associated to this frequency is critical because of the combination of a low frequency with a structural deflection along Z. Only the harmonic response in Z will then be considered.

3.6.4.3 Results

First of all, Samcef defines the modal parameters (frequency and shape) that will be used to calculate the harmonic response. As expected, the first mode presents a deflection on both PCBs along Z axis and comes at 250 Hz (see Figure 3.20).

The steady state response calculation indicates a maximal structural deflection of $0,3\ mm$ in $-Z$ on the batteries' PCB at 250 Hz. The structural deflection of EPS1 has to be taken into account. In the same conditions, it is limited under $0,3\ mm$ because it is lightweight than the assembly EPS2/batteries. This leads to a higher frequency and then, to a lower displacement. But for the calculus, let us use $0,3\ mm$ in $+Z$.

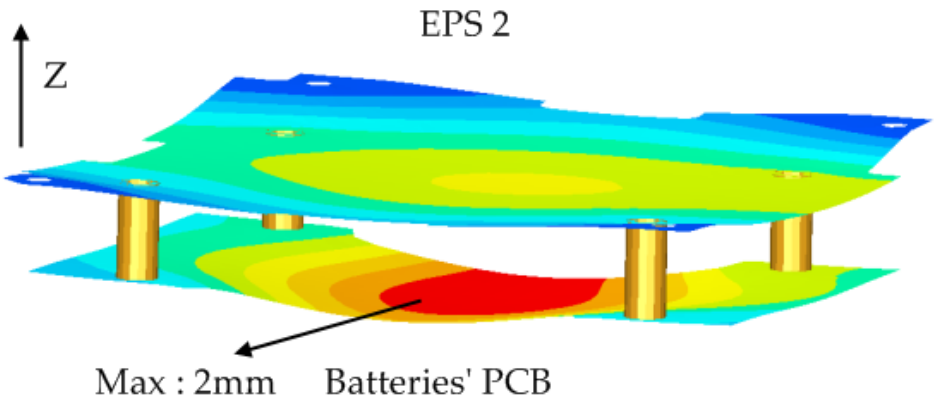

Figure 3.20 – *First mode of batteries' PCB*

The spacers between both cards (EPS1 and EPS2) can be considered extremely rigid in their longitudinal axis : there is no relative motion between EPS1/EPS2. The maximal distance between batteries and EPS1 is then decreases of $0,3 - (-0,3) = 0,6\ mm$ at resonance. Even if a FOS of 3 is used, the total displacement between the lower batteries and EPS1 is $1,8\ mm$. Because of there is $2,9\ mm$ between these latter, we can conclude on the reliability of the design.

On the other hand, the maximal Von Mises stresses are located at the connection between EPS2 and the titanium screws. They can undergo 31 MPa at the resonance (Figure 3.21), which is not a problem for the titanium screws.

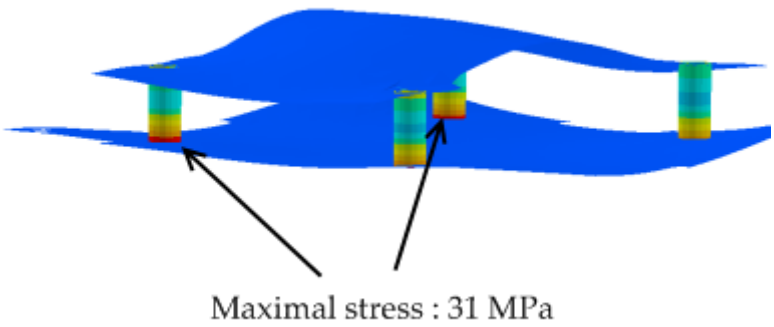

Figure 3.21 – *Maximal Von mises stress on the batteries' PCB*

3.7 Concluding remarks

This chapter brings some certifications on the structural reliability of $OUFTI-1$. First, it has demonstrated the mass requirements (**STRU-MR-1** and **STRU-MR-2**) and the inertia calculation necessary for the ADCS

(31) and MIAS (9) analysis. The solar panels' design was established and a material was chosen in accordance to the environmental, design and configuration requirements. The panels' thickness was also chosen to ensure 1 year mission lifetime and a brief description of the adhesives requirements was done. The batteries' PCB was also studied to be thermally insulate from its environment and to withstand the launch vibration. Finally, some FEA were performed to simulate the structural behavior of $OUFTI-1$ during launch. The first analysis has ensured the mechanical reliability under quasi-static loads while the main modal features were identified. The batteries' PCB height was calculated to avoid any collision with both EPS.

From this list of results, we can conclude that, at this level of development, the satellite $OUFTI-1$ is a reliable solution in accordance with the configuration, design, environmental and launch requirements.

Vibration testing 4

4.1 Introduction

The main problems associated to the previous simulations can be their constant simplifications which can lead to loss of important information. The results provided by the FEA could then be distorted or give a fuzzy idea of the real structural behavior.

On the contrary, the different tests available in structural dynamic allow a complete identification of the structural's parameters. Their purpose is to identify the real behavior of the structure and to update the mathematical model's parameters.

This chapter starts with the presentation of a free-free modal survey on the CSK structure. The modal FEA will then be correlated to the modal survey with 2 different methods : Least-Squares Complex Exponential(LSCE)/Least-Squares Frequency Domain(LSFD) and Ibrahim Time Domain(ITD). The model performed in the previous chapter will be updated. After the study of the Test Pod boundary conditions, the first results of the shaker random tests on the structural model of $OUFTI-1$ will be shown and discussed. Finally, the unscrewing effect will be presented.

4.2 Free-free modal survey

4.2.1 Objective

The free-free modal survey purpose is to characterize the dynamic behavior of CSK structure and to correlate the corresponding FEM. This analysis stands for the primary validation of the CSK structure. Further investigations will be performed next year and the model does not need a detailed finishing. Only the modal features under 1000 Hz will be identified and correlated.

4.2.2 Experimental procedure

The CSK structure analyzed is constituted of the 3 metallic parts (i.e. the base plate, the chassis and the end plate), the deployment switch on the base plate and the 8 feet. The tests were performed with the equipment of "Laboratoire d'identification des structures´´ at ULg.

Three mains parameters are defined when performing a free-free modal survey : the acquisition system, the support and the type of excitation. Each of them has a strong influence on the final results and correlation. They have to be chosen carefully.

Acquisition system

The acquisition system has to take measurements on the structure without disturbing it. Even if an accelerometer as light as $0,4\ gr$ is used, the shift in frequency can be 15 Hz and 20 Hz on the first and second frequency (Figure 4.1). Hopefully, the acquisition of modal parameters can be performed using the laser transducer. Its main advantage is its ability to take measurements with a laser beam without touch the CSK structure. However, this system restrains the allowable kind of support because it requires an accurate pointing.

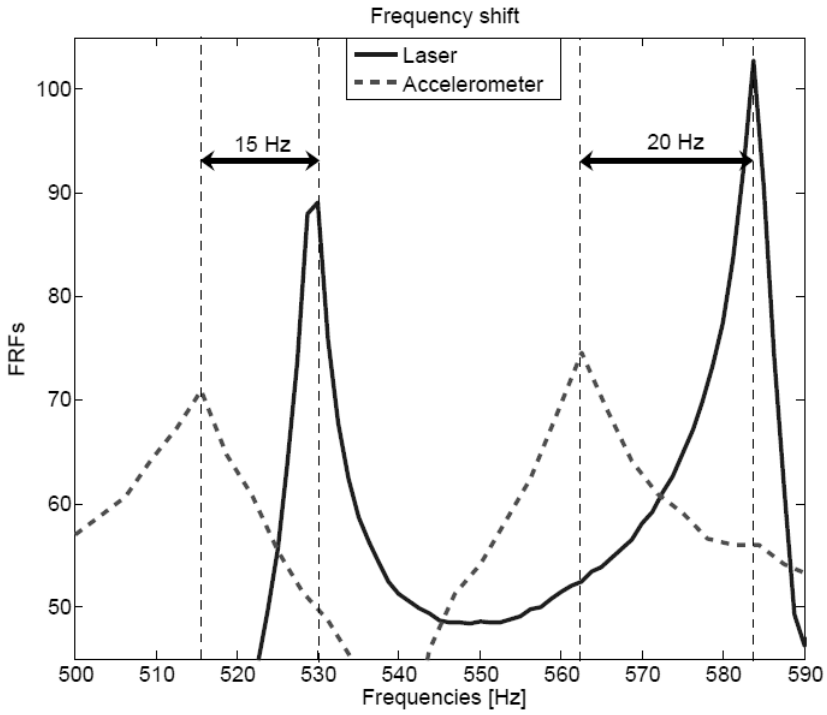

Figure 4.1 – *Frequency shift due to the accelerometer*

Support

The support is chosen to give a rigid body mode at a low frequency such that it can be distinguished from the real mode of the structure. As previously mentioned, the laser restrains the different support because it needs an accurate pointing on the structure. The structure is put down on its base plate's feet and on a rigid plastic foam (see Figure 4.2). As presented in the previous modal analysis, this does not affect the measurements because the feet are almost situated on vibrations' antinode.

In this configuration, only 5 of the 6 faces are accessible to the laser

in one analysis. A complete study will be performed on $+/-X$, $+/-Y$ and $+Z$. $-Z$ will be measured separately to get additional information.

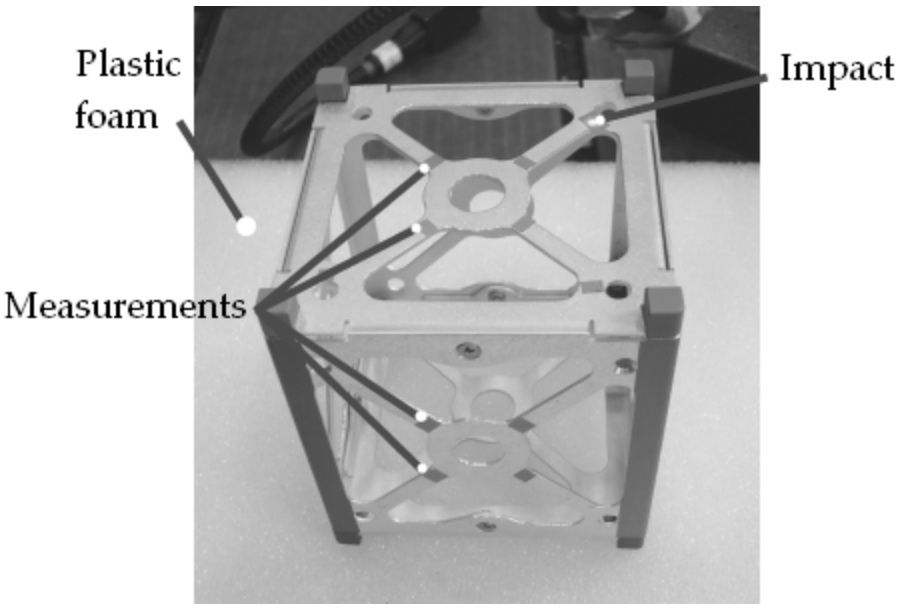

Figure 4.2 – *CSK structure placed on the support*

Excitation

The main criterion for the selection of the excitation are : simplicity, rapidity and inexpensive. The hammer excitation has been chosen. It shortens the experiment's setup and allows the study of a wide range of frequencies. The hammer chosen is the smallest available in the vibration laboratory. Its tip is made of stainless steel, a material hard enough to get a flat power spectral density (PSD) in the range $[0-1000]$ Hz.

It will be noted that no impact averaging has been performed. Actually, perform a series of impacts on the same point is difficult with a CubeSat. This is a small structure and any difference in the impact location has a significant effect on the results : they are better without any average. The frequency sampling is 5120 Hz and the resolution $1,25$ Hz.

Ideally, the spatial and the frequency contributions are necessary to excite a mode. However, the CubeSat response is good enough in the 3 spatial directions, even if the excitation is performed in only one direction. The structure is then impacted in Z axis, on the end plate and at the beginning of a diagonal arm (Figure 4.2).

The measurements are performed with 4 points per face, all situated on the diagonal just before the central hole (Figure 4.2). The points of impact and measurements remain the same for the analysis on $-Z$.

4.2.3 Results and identification

This section presents the results of experimental measurements. A brief analysis of the frequency response function (FRF) will be carried out and the identification with LSCE will be presented.

Frequency response function

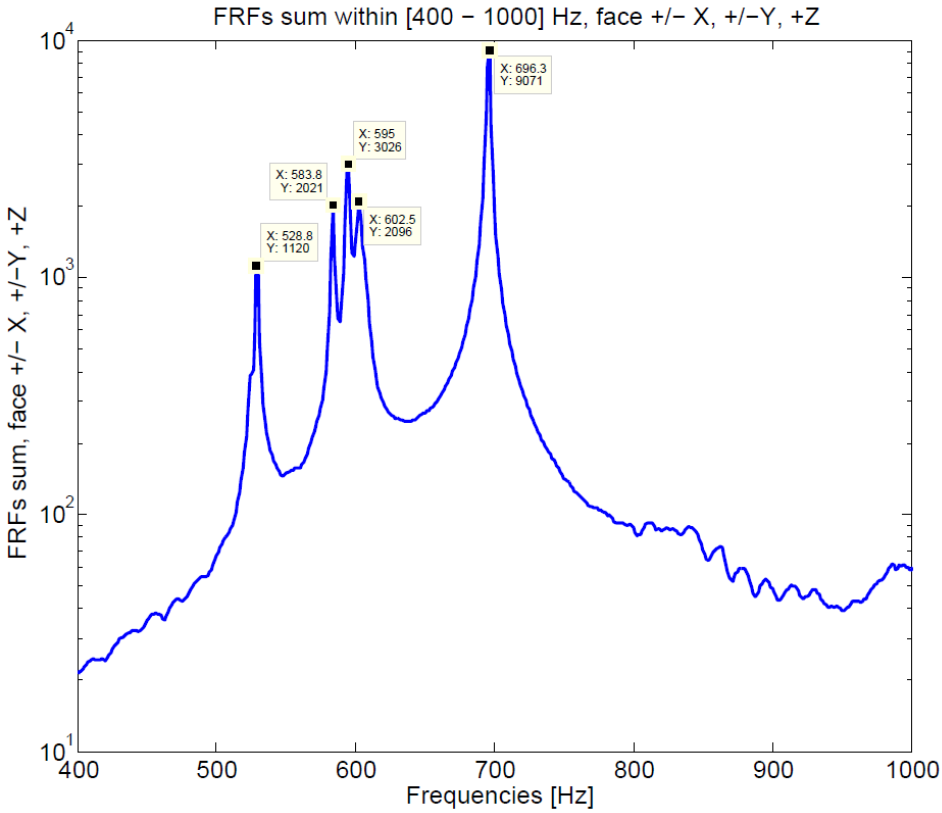

Figure 4.3 – *Sum of the FRFs on 5 faces of the CSK structure*

Figures 4.3 and 4.4 represent the sum of the FRFs on the CSK structure's within $[400\ 1000]\ Hz$. 5 frequencies appear on $+/-X$, $+/-Y$, $+Z$ and one additional on $-Z$. The table 4.1 summarizes the frequencies and compares them to the modal FEA.

Mode	Experimental (Hz)	Samcef (Hz)	Error (%)
1	528,8	539,3	1,9
2	583,8	602,1	3,1
3	595	610,5	2,6
4	602,5	669	11
5	696,3	727,3	4,4
6	808,8	814,4	0,7

Table 4.1 – *Frequency comparison between the experimental and numerical analysis*

In order to compare the frequencies in the table, it is assumed that the

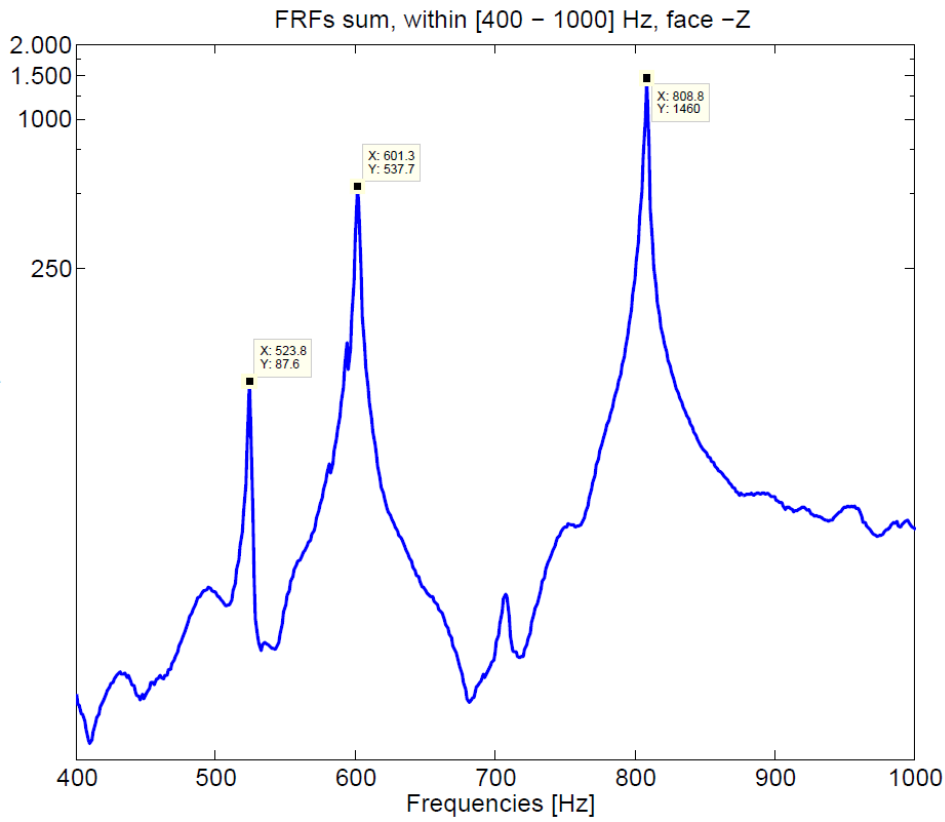

Figure 4.4 – *Sum of the FRFs on -Z face of the CSK structure*

order in which the modes appear is the same for the experimental analysis and for the Samcef simulation. This hypothesis will be verified later.

From this table, it can be seen that only the fourth frequency has a significant difference of 11% with its experimental homologous. The others frequencies show in average an error of less than 5% and no additional frequency appears compared to the Samcef model. Furthermore, both experiment and modal FEA do not have any frequency between $[850 - 1200]\ Hz$.

LSCE Identification

A popular form of curve-fitting experimental data is the LSCE method. It calculates the damping and natural frequencies in the time domain by making use of impulse response functions (IRFs) obtained from FRFs by an inverse Fourier transform. A critical issue is the selection of the correct model order O_q which is related to the number of assumed degree-of-freedom. If the analyst assumes a model order higher than the one actually present in the data, computational modes will result from the forced fulfillment of the specified model order rather than from dynamic system properties (42). The stabilization diagram presents the solutions computed with an increasing model order. In this way, the physical modes can then be easily separated from spurious modes by looking for poles which ap-

pear at nearly identical frequencies for the different model orders considered.

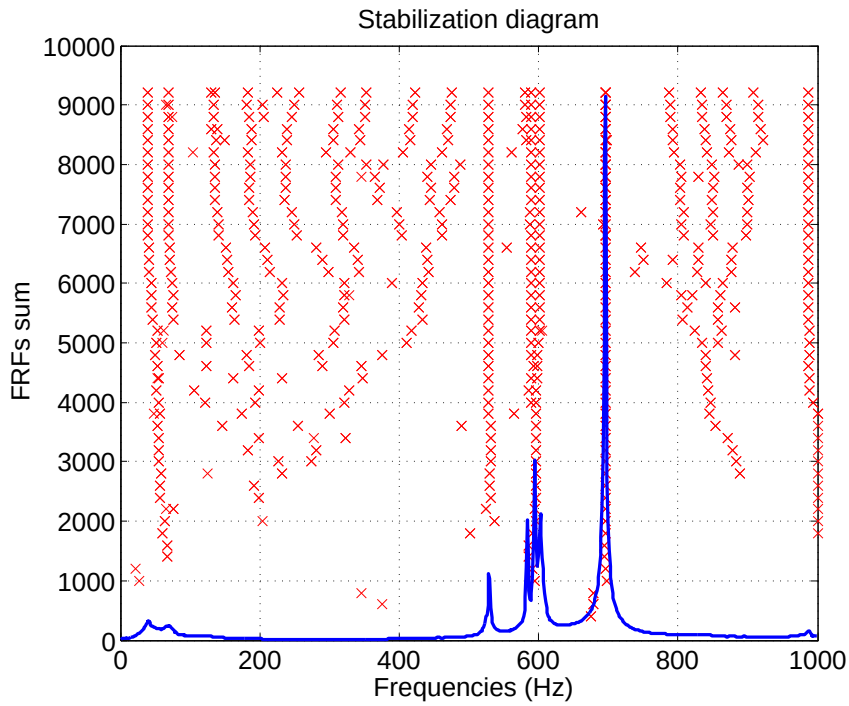

Figure 4.5 – *Stabilisation diagram on panel +/-X, +/-Y, +Z*

The LSCE identification leads to the stabilization diagram presented in Figure 4.5. It calculates the poles on the FRFs sum of $+/-X$, $+/-Y$ and $+Z$ until the order 20. The five frequencies identified during the FRF analysis are stabilized. A second stabilization diagram has also been performed on the FRFs sum of $-Z$ (not represented) and the additional pole (808 Hz) is identified. The frequencies presented in Table 4.1 are then validated.

LSFD/ITD

LSCE method does not yield the modes shapes. In order to estimate these latter, a second method called LSFD is considered and takes advantage of the knowledge of the natural frequencies and damping ratios (42). This method formulates the least-squares problem in the frequency domain and leads to the modes shapes thanks to the decomposition of the frequency response function.

Ibrahim Time Domain method is a method ables to get the modal parameters (i.e. natural frequencies, damping factor and modes shapes) from temporal series. It considers free response time histories from the structure under test in order to determine its modal characteristics. This method has been introduced to avoid problems, e.g. modal interference of closely spaced modes, encountered using frequency domain.

In order to validate the experimental modal features and start a corre-

lation procedure on reliable basis, a comparison between LSFD and ITD identification has been performed.

Once the modes being defined with both methods, they can be compared by using the modal assurance criterion (MAC). The MAC is a widely used technique for comparing mode shapes (42). It gives quantitatively a good idea of the closeness between two families of mode shapes :

$$MAC(x_1, x_2) = (\frac{x_1^T \; x_2}{\|x_1\| \; \|x_2\|})^2 \tag{4.1}$$

MAC values oscillate between 0 and 1, a unitary value meaning a perfect correlation. In practice, a value greater than $0,8$ is acceptable to establish the correspondence between 2 modes.

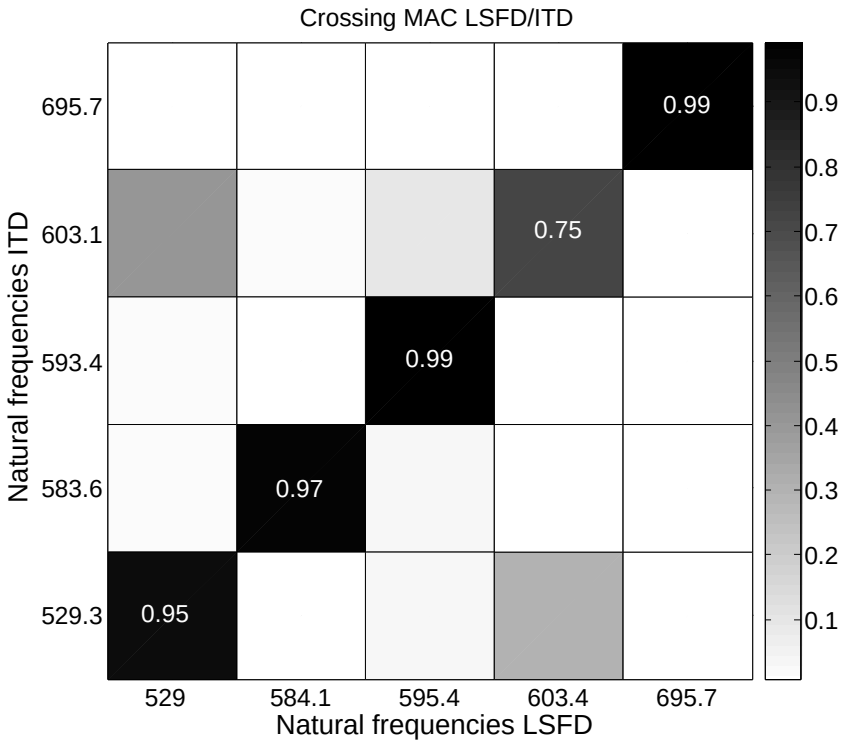

Figure 4.6 – *Crossing MAC matrix between LSFD and ITD results*

Note that even if measurements on $-Z$ are available, 4 points is not representative of the overall structural behavior. It will not be included in the MAC matrix. Modal parameters from LSFD and ITD are presented in Figure 4.6. Three remarks may be drawn regarding this figure :

- The natural frequencies are similar. The maximal relative error is $0,3\%$ for the third frequency.
- The modes 1, 2, 3 and 5 have values upper or equal to $0,95$. This indicates a very good discrimination and a reliable modal identification.
- The concordance is less good with the mode 4 ($0,75$).

The last comment leads to the conclusion of a difficult modal identification on the mode 4 as its characteristics are not well defined. A value better than $0,75$ during the correlation should be difficult to discuss because the lack of knowledge about its real shape. The LSFD representation of mode 4 is given in Figure 4.7. The dominant deformations on $-X$ could explain the bad correlation with this particular mode. Actually, $-X$ presents an excrescence because it supports the data ports of communications. This implies a contact on a larger area and a friction much more pronounced. The resulting mode shapes present an important complex behavior.

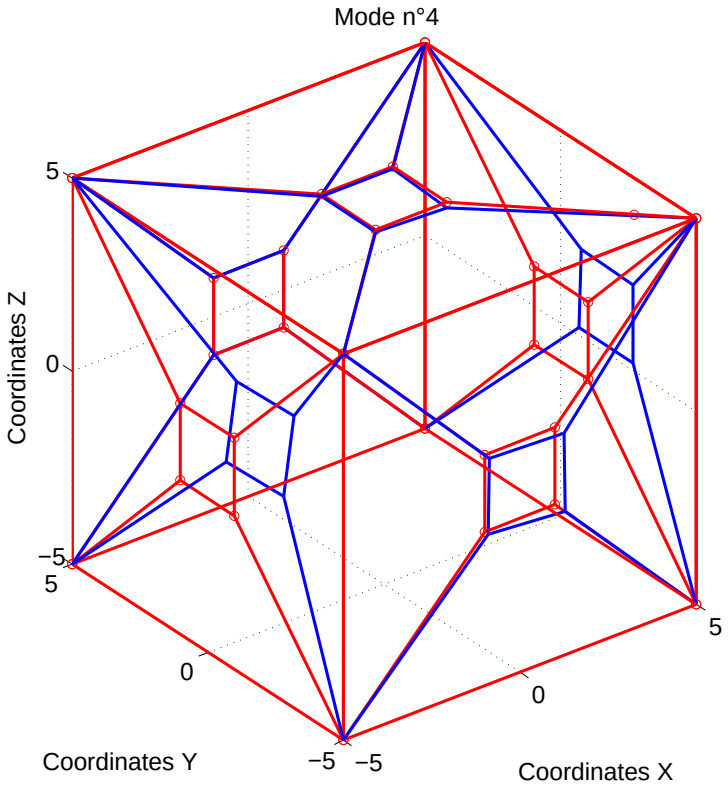

Figure 4.7 – *LSFD mode 4*

As the FEM does not use any damping, its modes shape are real and the approximation of the real LSFD modes shapes can lead to bad correlation.

With these results validation, we expect obtain a model with a mean value of MAC's diagonal greater than $0,85$ and each diagonal's terms with a value greater than $0,8$, except with mode 4.

4.3 Correlation

4.3.1 LSFD/Samcef

Figure 4.8 presents the crossing MAC between LSFD modes shapes and first Samcef model.

The modes 2 and 3 present values of $0,96$ and $0,9$. These values are representative of good modeling quality. Mode 1 and 5 have a value of

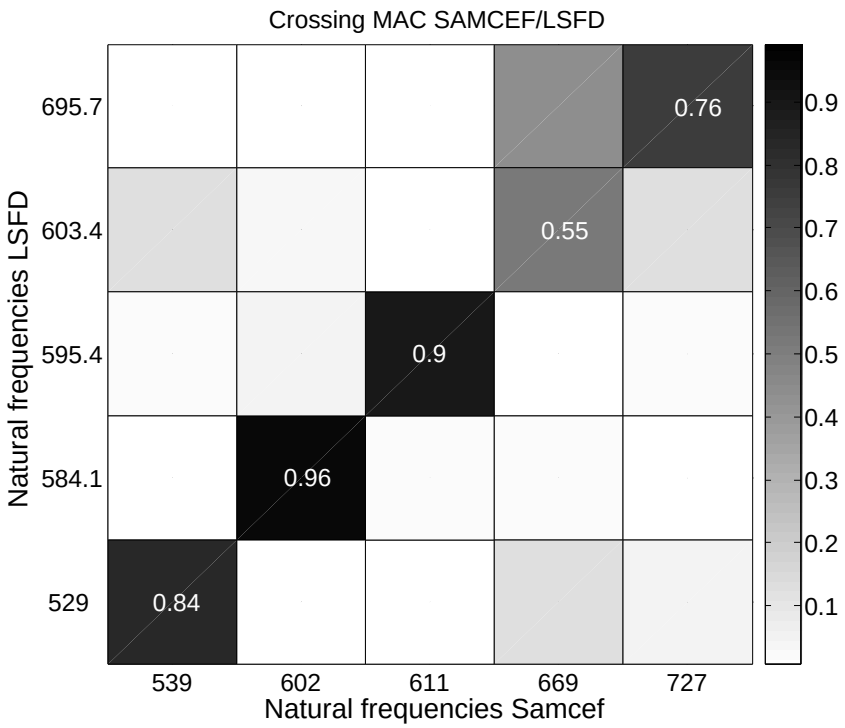

Figure 4.8 – *Crossing MAC between LSFD results and Samcef simulation*

$0,84$ and $0,76$ respectively but they could be improved with additional modeling considerations. As expected, the mode 4 has a low value of $0,55$.

Other typical causes of bad correlation such as noisy data, presence of non linearities and bad modal identification can be turned down as 2 different modal identification have been tested. In order to get a better modeling, some investigations on the modeling error/uncertainties have been performed.

In particular, 2 improvements are considered :

1. Two types of connections between shells;
2. the addition of deployment switch and stainless steel ringlets' mass on the base plate.

4.3.2 Connections modeling

Due to the lack of knowledge about some physical parameters, several simplifications have been introduced in the first FEM.

Actually, a first important issue remains on the fixation's modeling between chassis and plates. These connections could be considered extremely rigid because we are only interested in the first vibration modes. However, the contacts between shells are not well defined. Then two limiting cases will be simulated :

1. Use of connections in one point, like a ”bad´´ screw;
2. use of connections on the screw’s diameter, like a ”perfect´´ one.

Table 4.2 summarizes the results of both mathematical models. A good reality representation is situated between them. This modification has a good influence on the modes shapes and on the MAC matrix (not represented).

Mode	Experimental (Hz)	”Bad screw´´(Hz)	”Perfect screw´´ (Hz)
1	528,8	522,6	539,3
2	583,8	591	602,1
3	595	604,3	610,5
4	602,5	643,2	669
5	696,3	709,5	727,3
6	808,8	796	814,4

Table 4.2 – *Comparison of 2 modeling connections*

4.3.3 Lumped mass

With the first FEM, the deployment switch mass was not taken into account. Its mass, 3 grams, could have a significant effect on the deformation of $-X$.

Furthermore, the chassis is screwed on $-X$ with 3 fasteners instead of one on other face. A stainless steel ringlet used to connect the upper screw on the base plate is situated on a node of vibration. Then, its mass ($0,5\ gr$) will also be taken into account.

Finally, the RBF pin is guided within a thin tube on the base plate to switch off the deployment switch included on FM430 2.8. Its mass will be taken into account ($1,8\ gr$). Without any other demonstration, these lumped mass have a positive influence on the results.

4.3.4 Results

LSFD

The best results are obtained with a connection on the overall screw diameter and the addition of the deployment switch, thin tube and stainless steel ringlet mass. The improved crossing MAC between LSFD/Samcef is presented in Figure 4.9. The mean value is $0,86$ while all terms (except mode 4) are greater than $0,8$. This better correlation can be linked to the attenuation of vibrations on $-X$.

ITD

The comparison between the final Samcef model and the ITD mode shapes is presented in Figure 4.10

The results follow the same trend than with the LSFD identification. The improved modeling under Samcef presents a mean value of $0,88$ on

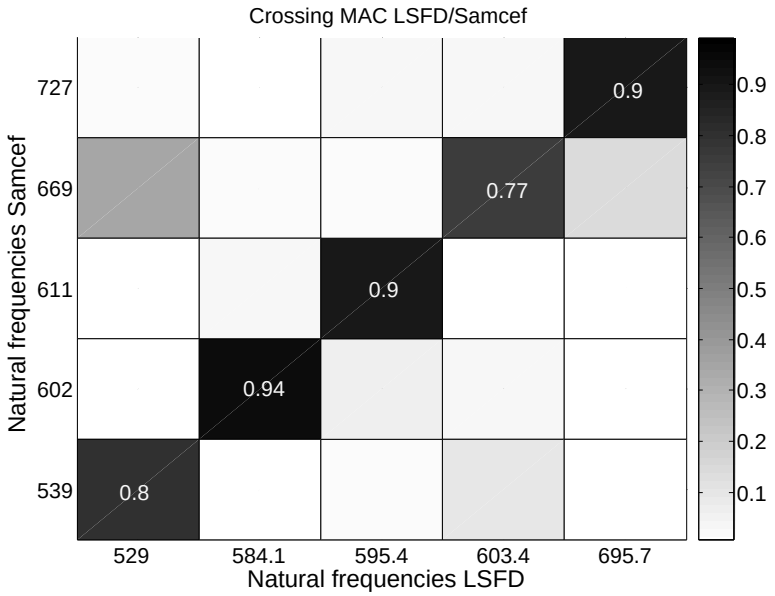

Figure 4.9 – *Crossing MAC between LSFD identification and Samcef modeling improved*

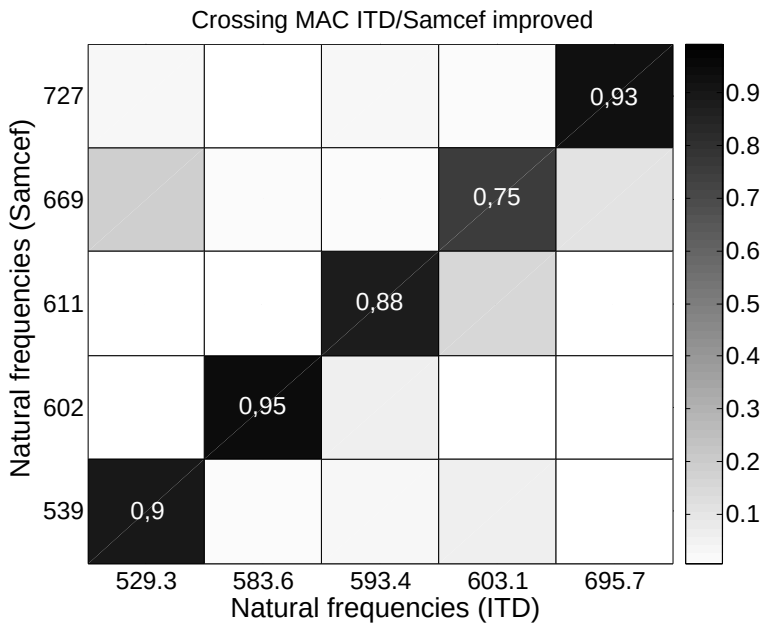

Figure 4.10 – *Crossing MAC between ITD identification and Samcef modeling improved*

the diagonal while all terms are greater or equal to $0,88$. Only the mode 4 remains under $0,8$.

Summary

We have seen that 6 frequencies were identified but only the 5 first modes were investigated. The modal identification performed with both LSCE/LSFD and ITD methods concludes to the same results excepted with the mode 4. This bad correlation has been explained as a greater deformation on $-X$ which cannot be easily discriminated. The modal correlation between the improved FE modeling and the LSFD/ITD results has shown good results.

On the basis of those results, we can validate our model.

4.4 Shaker testing

4.4.1 Objective

This section presents the first sine sweep and random tests performed on a structural model (SM) of $OUFTI-1$. The main purpose is to obtain information concerning the behavior of the electronic cards under harsh launch's vibrations.

More precisely, those tests intend to :

1. Analyze the influence of the boundary conditions introduced by the equipment, and more particularly, the effects of the integration inside the test pod.
2. Measure the vibrations' level on the electronic cards and the effects of the components' type used on it.
3. Analyze the unscrewing effect and its impact on vibration analysis.

On basis of the results, several guidelines could be drawn to product the final electronic cards.

Firstly, the SM will be described in details and the differences with the flight model will be highlighted. The procedure and setup used during tests will be described. The equipment, i.e. shaker, test pod and interface, will be briefly presented to give a technical background. Finally, the results will be presented, discussed and some guidelines to design the electronic cards will be proposed.

4.4.2 Structural model

The SM is constituted of :

1. The CSK structure that is identical to the flight model.
2. Four electronic cards that come from computer's motherboards cut to the PC-104 external dimensions.

3. One flight model of the electronic card (ECFM) with its PC-104 connector.

4. The endless screw, the spacers and the midplane standoffs to connect the electronic cards to the structure.

All the electronic cards are connected like the current flight system configuration (see Figure 2.20) and the ECFM is placed in third position, i.e. it simulates the EPS1, as represented in Figure 4.11.

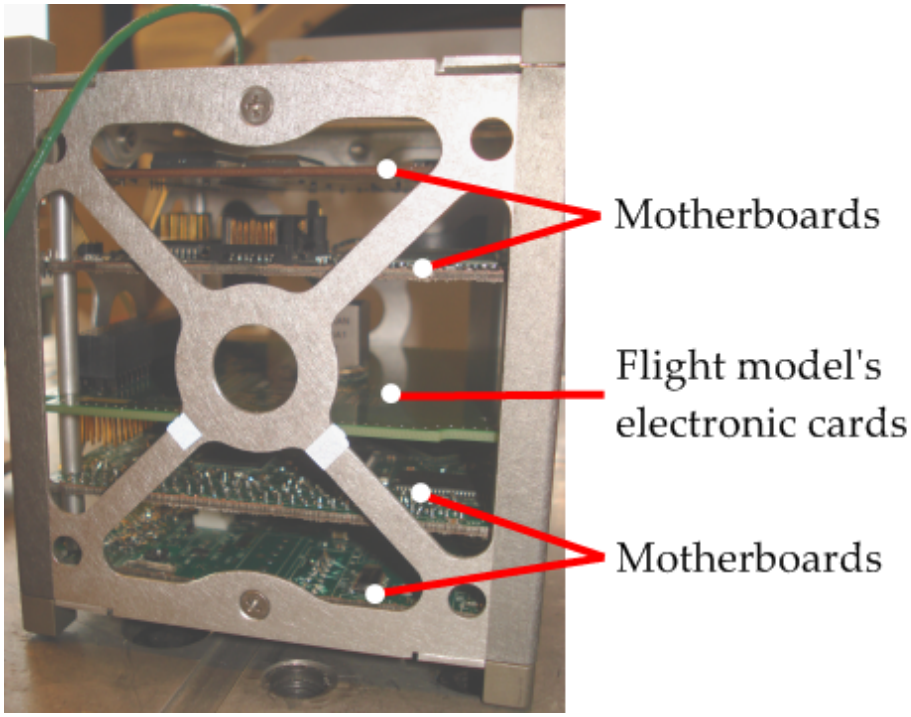

Figure 4.11 – *Mechanical engineering model tested*

Compared to the complete flight model, the SM does not integrate the batteries and their PCB, rods and permanent magnet, solar panels and antennas' deployment mechanism. Furthermore, the motherboards do not integrate the PC-104 connector.

4.4.3 Equipment

Test-pod

According to the Test-Pod User's Guide (10), the Test-Pod represented in Figure 4.12 is to be used by CubeSat developers as an environmental simulation of the P-POD deployer. The Test-Pod interior is designed to simulate the environment inside the P-POD deployer. It allows CubeSat developers to test their satellites to the environment inside the P-POD deployer rather than designing to the launch vehicle loads.

The mounting procedure and technical data related to its own vibration frequency are also referenced the User's Guide (10).

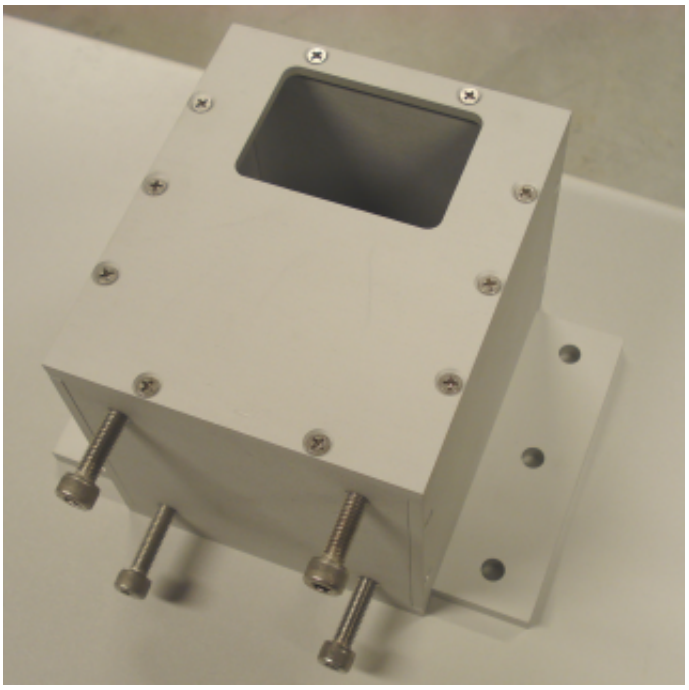

Figure 4.12 – *Test-Pod*

Shaker

The tests will be performed on a shaker G&W 26 *kN* belonging to the University of Liège. Its main technical characteristics are summarized in Table 4.3.

Properties	Value	Unit
Frequency range	[5 2000]	Hz
Maximum peak force	26,6	kN
Maximum RMS force	26,6	kN
Maximum shock force	53,4 (6ms)/42,4(11ms)	kN
Maximum acceleration (shaker)	40	g
Maximum acceleration (shaker + table)	23,3	g
Maximum velocity	1,52	m/s
Maximum displacement	25,4	mm
Moving mass	68,1	kg
Table mass	48,2	kg
Admissible mass	500	kg

Table 4.3 – *Main properties of the shaker 26 kN; Courtesy (50)*

Interface

The shaker's vibration table needs a suitable interface to connect the Test-Pod. According to reference (78), this interface has to answer to some technical criterion :

1. Support will simulate as close as possible the boundary conditions

of the ARES interface. At the moment, the latest conditions are given in the ICD (56).

2. The modal deformation of the support will not influence the tests. A rule of good practice (78) is to have a first vibration frequency $1,5$ time higher than highest test frequency(2000 Hz).

3. Shaker must be able to provide the power to the test and the support will be as lightweight as possible.

4. The interface shall be usable on the G&W 26 kN, Ling 80 kN and Ling 88 kN at CSL.

5. The interface shall be reusable.

The shaker's interface is designed using the technical references (36), (17) and (10). The result is presented in Figure 4.13.

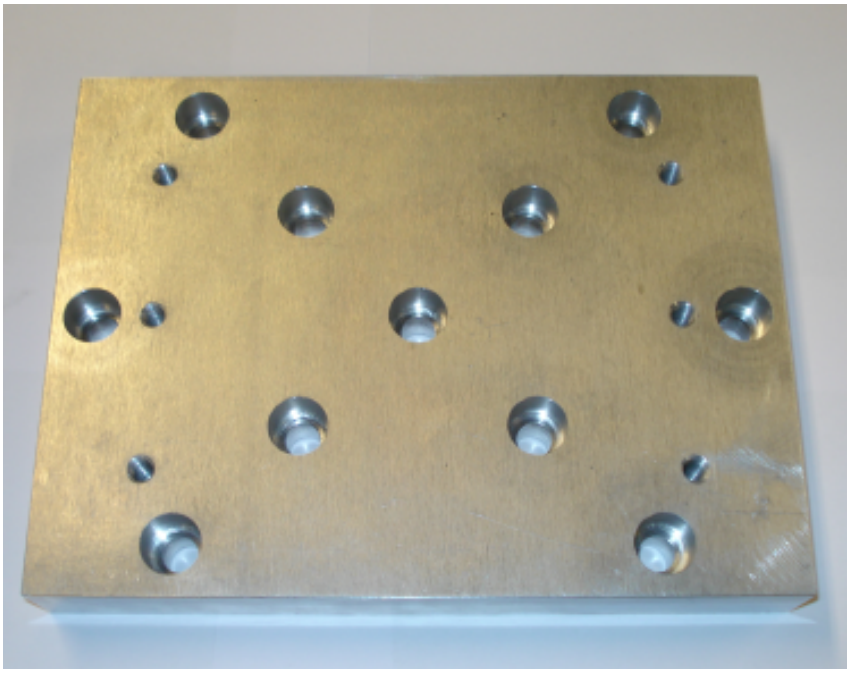

Figure 4.13 – *Interface between Test-Pod and shaker*

This support is representative of the mounting condition on the LARES (see Figure 3.12) and is designed to be used on the 3 shakers. The modal FEM shows a lower frequency of 6800 Hz, which is at $3,4$ times higher than 2000 Hz.

It weights $3,2$ kg and is made of aluminum $Al - Si - 1$, a light, machinable and easily available material. A common formula used to assess the acceleration available on a shaker is based on the Newton's second law :

$$a = \frac{Maximum force}{M_{total}} \tag{4.2}$$

According to the Table 4.3 on which the preliminary tests will be performed, one has :

$$a = \frac{Maximum force}{M_{mobile} + M_{table} + M_{interface} + M_{Test-Pod} + M_{CubeSat}} = 212,6\ m/s^2 \tag{4.3}$$

As the G&W is the less powerful of the 3 shakers, we conclude that the equipment is suitable. Finally, note that this support has been tested before first shaker's run.

4.4.4 Tests

4.4.4.1 Boundaries conditions within Test-Pod

Procedure

As represented in Figure 4.14, the CubeSat's corners are guided by Test-Pod's rails. The pusher plate is then screwed on to place the spring plungers in contact with the top plate.

This test intends to perform a sensitive analysis of the height H. It has to be calculated as described in the Test-Pod user's guide. The influence of this height can be transformed in equivalent torque on the fasteners :

1. They are tighten using hands. There is no control on the torque (Noted case 1).
2. They are torqued in an alternating pattern to $1,5\ Nm$ thanks to a dynamometer (value prescribed in the Test-Pod user guide (10), noted case 2).
3. They are torqued in an alternating pattern to $2,5\ Nm$ (Noted case 3).

About 1/2 screw's turn differentiates the first and the third case.

An accelerometer is placed on the ECFM using wax. The FRFs will be identified with a sine sweep $0,5\ g$, along CubeSat's Z axis. The sweep rate is 2 octaves/min, within the frequency range $[20\ 2000]\ Hz$.

Results

Figure 4.15 represents the 3 different cases. Under 500 Hz, the 3 conditions are equivalent. Above this frequency, the first case (continuous line) begins to diverge significantly while the 2 others remain similar. It can be noted that it exists slight differences between $1,5\ Nm$ and $2,5\ Nm$ torques at higher frequencies, even if the curves follow the same trend.

Two conclusions can be drawn :

1. The hand tightening does not give relevant boundary conditions and shall never be used to test the satellite under "real´´ integration conditions.
2. The boundary conditions ensured with a torque of $1,5$ or $2,5\ Nm$ present the same results.

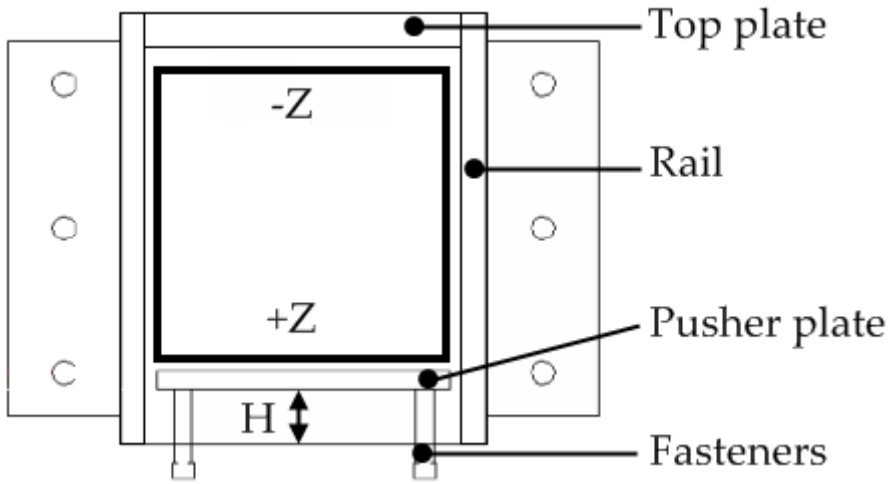

Figure 4.14 – *CubeSat integrated within the Test-Pod*

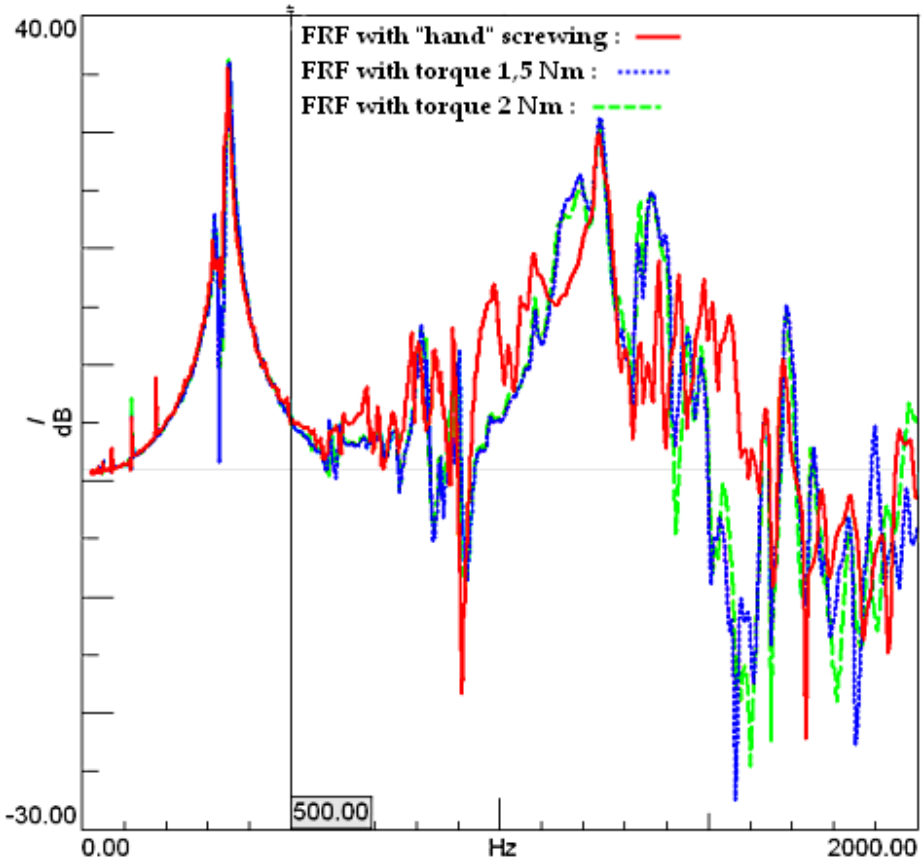

Figure 4.15 – *Integration with different couple on the screws*

Moreover, the first case is submitted to another problem : the unscrewing effect. This one will be studied later. To avoid any unscrewing or excessive compression of spring plungers, the torque will be set to $1,5\ Nm$ during all the following tests.

4.4.4.2 Random test

Procedure

Random vibration analysis focuses on determining the statistics response of an oscillator or structure to input forces that are definable only in terms of their statistics. The discipline of random vibration is born of the need to understand how structures respond to dynamic loads that are too complex to model deterministically.

The random vibration spectrum aboard Vega is defined in Table 4.4. It is decomposed in 3 levels of equal intensity. The lowest level ranges from 20 and 60 Hz. A second plateau exists between 70 and 200 while the CubeSat will undergo the most important vibrations from 300 to 700 Hz. Above this latter, the energy included in the input signal falls.

Frequency	**Acceptance PSD (g^2/Hz)**	**Qualification PSD (g^2/Hz)**
20	$0,029$	$0,0727$
60	$0,029$	$0,0727$
70	$0,04$	$0,1$
200	$0,04$	$0,1$
300	$0,08$	$0,2$
700	$0,08$	$0,2$
2000	$0,008$	$0,02$
Duration	2 minutes/axis	$2,5$ minutes/axis
RMS value	$8,81$	$13,98$

Table 4.4 – *Random vibration spectrum*

According to ESA's approach (28), the random tests are performed by following a particular procedure :

1. a first sine sweep of $0,5\ g$, 2 octaves/min within the range $[20\ 2000]\ Hz$.
2. a random test based on the acceptance/qualification level of Vega (56) ($8,8\ g\ RMS/14\ g\ RMS$).
3. a second sine sweep of $0,5\ g$, 2 octaves/min within the range $[20\ 2000]\ Hz$.

The main purpose of this test is to analyze the accelerometer's influence on the PCB's vibrations.

Both cases are performed in the same conditions. The SM is integrated within Test-Pod and the fasteners are screwed on to $1,5\ Nm$. Two accelerometers are used :

1. A micro "PCB´´ accelerometer whose weight is $0,4\ gr$ (sensitivity : $4,58\ mV/g$).
2. a "Dytran´´ accelerometer of $11,7\ gr$ (sensitivity : $10\ mV/g$).

They are placed at the ECFM's center (Figure 4.16) to test their influences on the PCB's natural frequency.

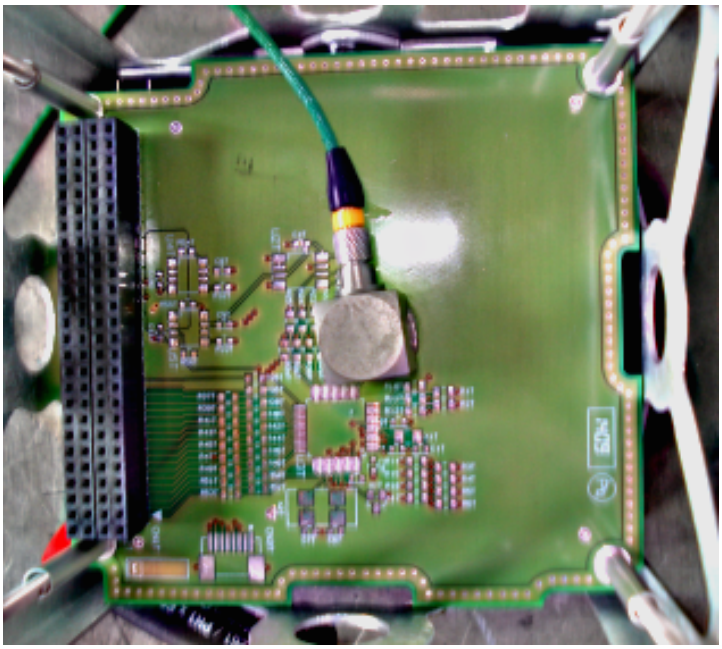

Figure 4.16 – *Accelerometer Dytran at the ECFM's center*

Results

2 temporal series are compared in Figure 4.17. The dotted line is associated to smallest accelerometer whereas the continuous line is associated to the Dytran accelerometer. Both are representative of typical vibrations samples on electronic cards at the acceptance level. Two observations can be drawn :

1. The vibrations' peak value range from 100 to 300 g. Note that some samples indicate more than 400 g.
2. The peak value with the "PCB´´ accelerometer is 2 times the peak value from "Dytran´´ measurements.

Because of these levels, the electronic cards should be studied to mitigate the vibrations' effect on components. The next section discusses 2 solutions.

Discussion

The first comment leads to particular attention on the choice of the electronic devices and on their location on the cards. Indeed, components such as quartz or connectors are sensitive to the vibration environment

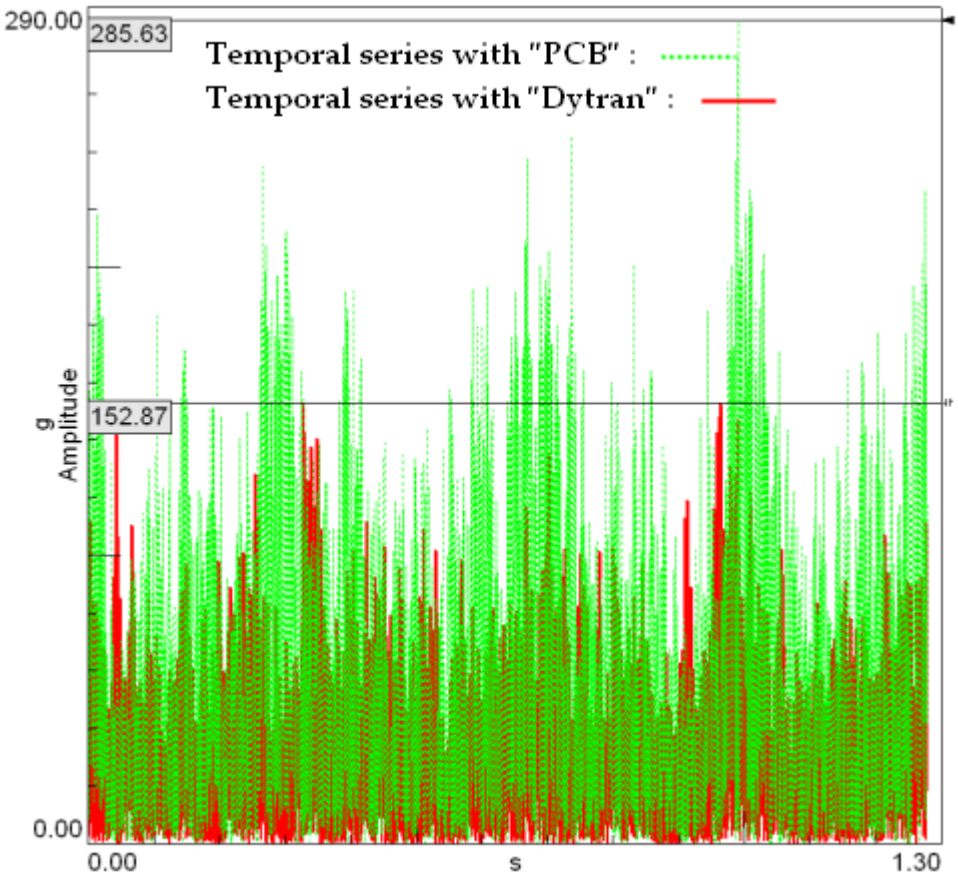

Figure 4.17 – *Temporal series during acceptance test*

because their technology involves fragile material or fixations on the cards. At least 4 means exist to mitigate the vibration effects :

- Electronic components can be chosen in the "automotive´´ category. These components are designed to resist to harsh vibration environment in mechanical industry (e.g. on motors controlled with electronics). Typically, they can support from 20 to 50 g.
- Sensitive components can be placed on locally stiffened area to limit the dynamic amplification of the cards and ensure a maximal rigidity. For instance, the connectors on our electronic cards (Figure 2.21) are located near the endless screw, where the card is fixed.
- In addition to the soldering or brazing, the components can be bonded on the electronic cards. According to reference (2), a guideline can be the bonding of components heavier than 3 gr (e.g. planar transformer on EPS2).
- If the dynamic amplification is too great, more complex damping technology can be considered (48). For instance, the addition of visco-elastic "damper´´ to the external surface of the circuit article or the use of internal damping layer are 2 common techniques to shield electronics against harsh vibrations.

For the second comment, let us recall the main relationship of the spectral calculus for stationary signals :

$$S_{xx}(w) = |H(w)|^2 S_{ff}(w) \tag{4.4}$$

where $S_{xx}(w)$ is the output spectral density, $S_{ff}(w)$ the input spectral density and $H(w)$ the frequency response function (16). To mitigate vibrations effects on electronic devices, the product in the right member has to be reduced.

According to the equation 4.4, the Figures 4.18 and 4.19 should be linked through input spectral density defined in Table 4.4. Let us compare this relation to our experimental results.

The sine sweep indicates that the $11,3$ grams of difference between "PCB´´ and "Dytran´´ accelerometers induce a frequency shifting around 130 Hz. The natural frequencies are 469 Hz and 333 Hz respectively. According to Table 4.4, the input PSD is equivalent for both frequencies.

On the other hand, the ratio between output PSD is equal to 4 (Figure 4.18). This difference can be explained with the frequency response functions of Figure 4.19 which presents a ratio of 2 between peaks' value.

Then, the equation 4.4 presents 2 common means to mitigate the vibrations level on electronic cards :

1. as in the previous example, the FRF peak value can be reduced
2. the system's natural frequencies are modified in such a way to place its resonances within the low range of the input PSD or above 700 Hz.

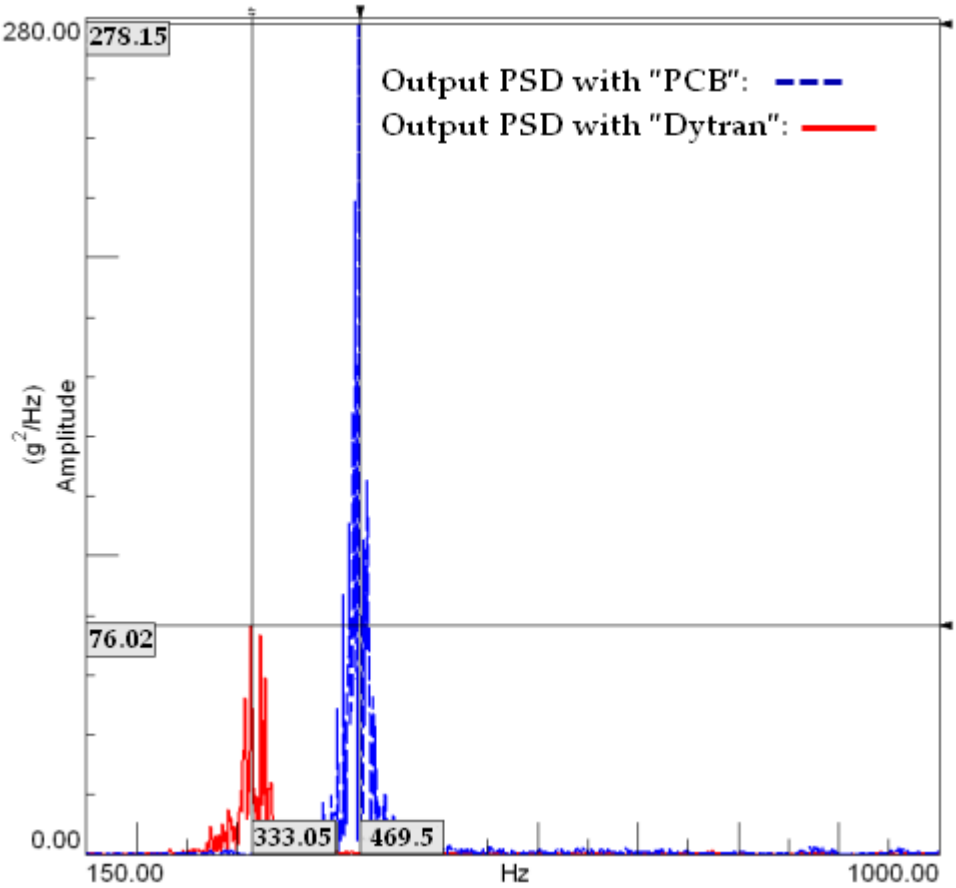

Figure 4.18 – *Comparison of output PSD with both accelerometers*

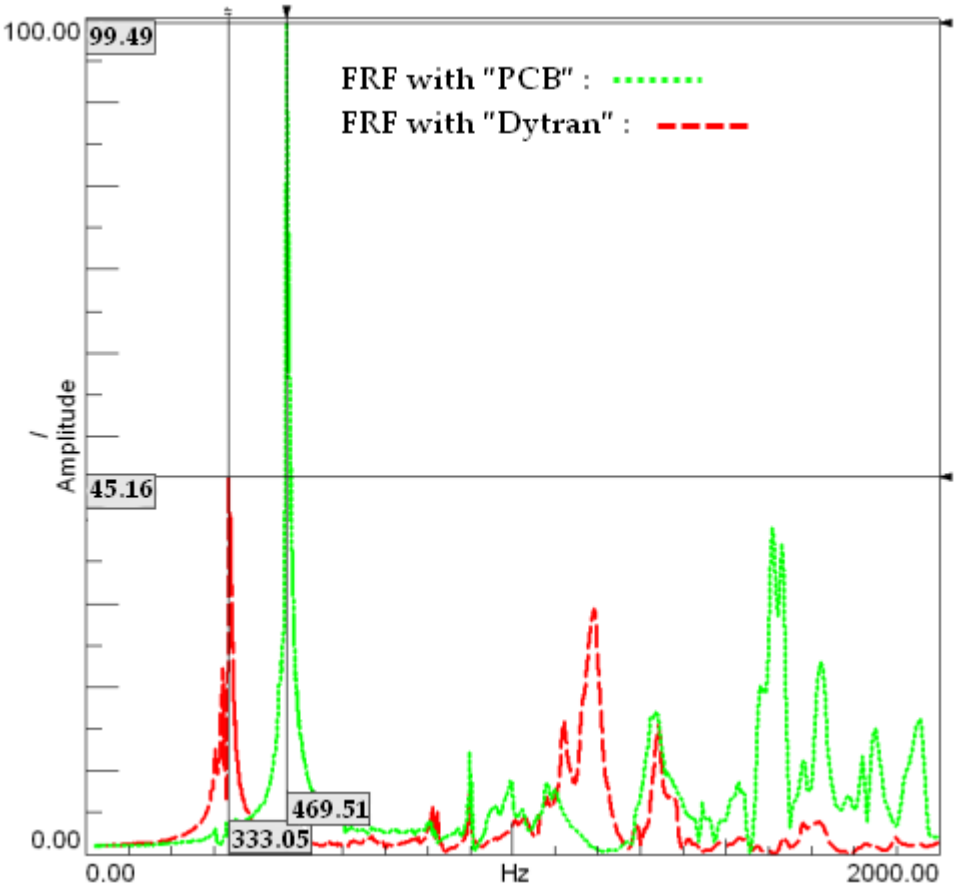

Figure 4.19 – *FRF with both accelerometer*

A solution to achieve this latter comment could be to ballast the cards if this can be allowed by the mass budget. However, one should keep in mind that the satellite shall have no resonance under a particular frequency, not yet defined by ICD. The dynamic amplification as a function of mass, damping and stiffness is much more complex than a linear relationship. A smart analysis should then be performed to combine the mass budget, a limited value of FRF, a lower first natural frequency in accordance to the previous requirements (i.e. radiations shielding) .

4.4.4.3 Unscrewing effect

Procedure

A common problem under harsh vibrations is the unscrewing effect. Actually, the screws, bolts and nuts are so shaken that they can unscrew and fall within the P-Pod.

In addition to the problems cause to the loss of stiffness on the main structure, these fasteners could travel and damage others fragile devices (e.g. solar cells, antennas) within the P-Pod. This effect can also interfere with a modal correlation as the structure is modified during tests. Finally, ESA requires a pass/fail criteria between first and second sine sweep analysis of the previous random test : the frequency of the final resonance peaks shall not change by more than 5%, and their amplitudes shall not change by more than $3dB$.

The purpose of this test is to defined weither the structural model of $OUFTI-1$ is subjected to the unscrewing effect.

Results

Figure 4.20 presents 2 sine sweeps conformed to the ESA approach, before and after the qualification testing (14 $gRMS$). A shift in frequency of 20 Hz (5%) appears while the frequency response function decreases with a factor 2 (3 dB).

This effect can be associated to the unscrewing effect during vibration tests. An example of this particular problem is the unscrewing of a midplane standoff during another test (Figure 4.21). If the screw is not so well attached, the vibrations induce a relative motion between 2 parts which leads to the progressive unscrew of fasteners. On the contrary, it should be noted that unscrewing mitigates the vibrations effect as the system's FRF decreases.

A common mean to counteract this phenomenon is to bond with a silicone adhesive the fasteners and screws on the flight model. Another solution consists to use a dynamometer key to obtain a controlled torque on the chassis' screws.

Guidelines

This section summarizes some guidelines for future vibration tests on basis of these experiences.

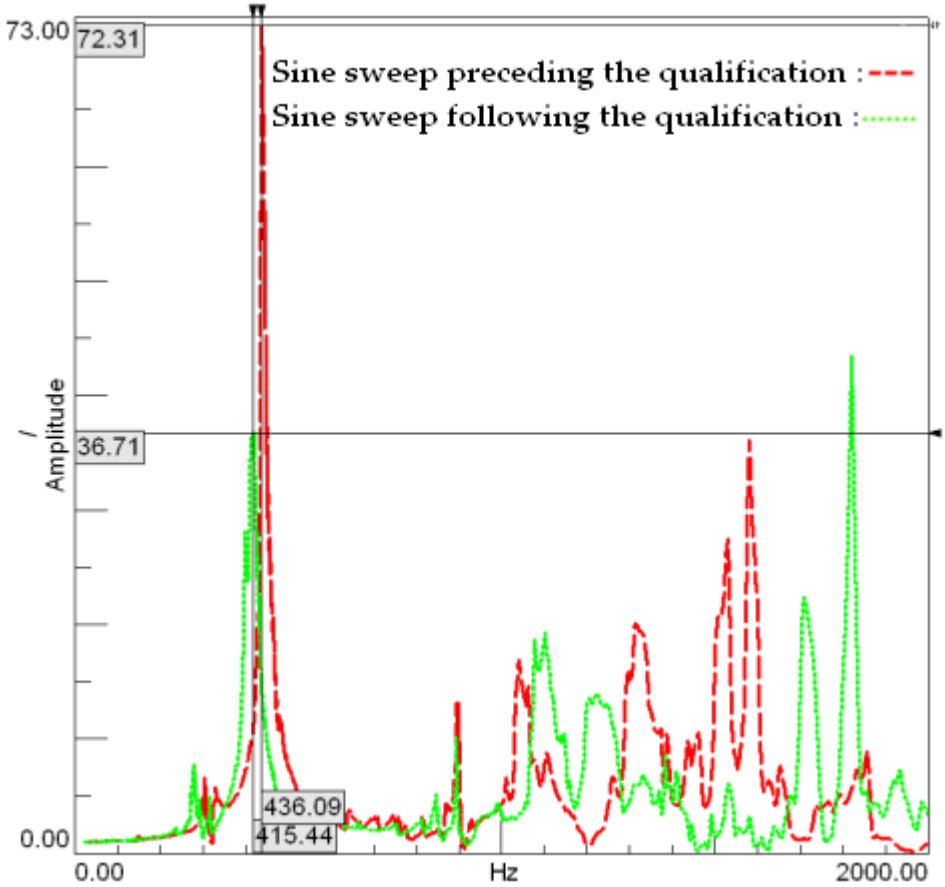

Figure 4.20 – *Frequency shift due to the unscrewing effect*

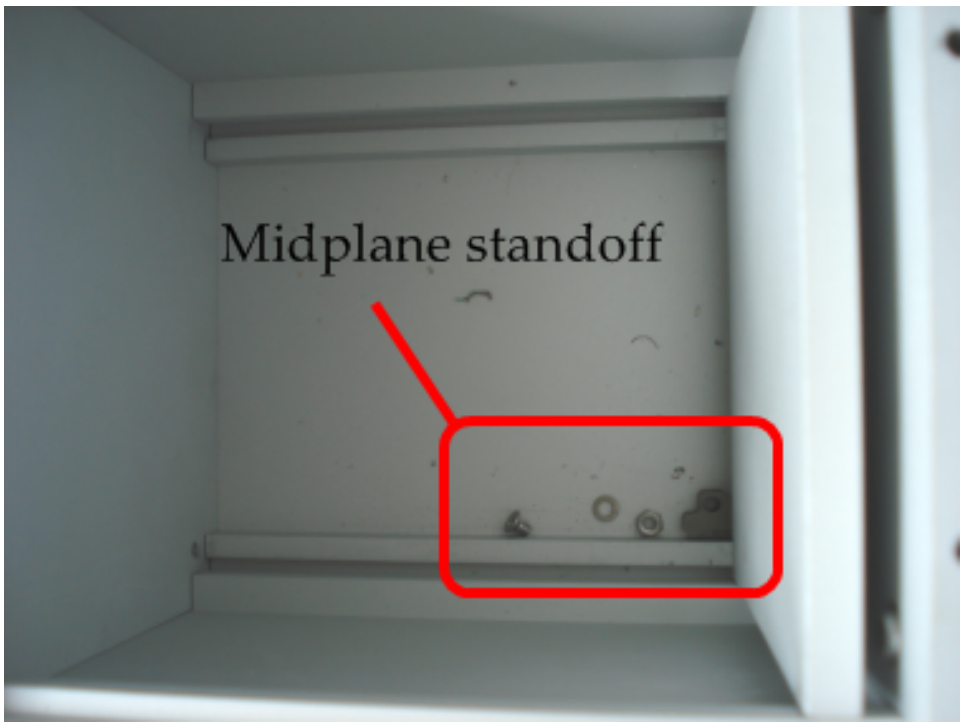

Figure 4.21 – *A midplane unscrewed during the qualification testing*

- The boundary conditions within Test Pod should be ensured with a torque of $1,5\ Nm$ on the pusher plate's fasteners.
- All electronic devices should be chosen in the automotive category.
- All electronic devices heavier than $3\ gr$ should be bonded in addition to the soldering or brazing.
- Sensitive components should be located near stiffened areas. However, and if the components are also sensitive to the radiations, a compromise between its radiation shielding (i.e. on the center near the batteries) and the vibrations mitigations should be used. A particular case could be to shield locally the components against radiations.
- Electronic cards' damping should be considered in the worst cases.
- If possible, electronic cards should be stiffened or ballast, in accordance with the mass budget and the frequencies' requirements.
- The screws and all the assembly mechanically attached should be torqued with a dynamometer key, especially if user expects a correlation under harsh vibration environment.
- The screws and all the assembly mechanically attached should be bonded on the flight model.

4.5 Concluding remarks

This chapter has presented the modal identification of the CSK structure. The experimental procedure was explained and the results discussed. Two methods were used to identified the modal parameters. A correlation was then investigated and a final model that respect our objectives was proposed.

The first vibrations tests with a structural model were performed. The boundary conditions within the Test Pod were studied and a rule concerning the pusher plate's fasteners was formulated. The structural model has been tested under random vibrations and some guidelines were drawn to the future layout of electronics cards. Finally, the unscrewing effect was studied and basic precautions were stated.

Conclusions 5

This master thesis developed the structural analysis and flight system configuration of $OUFTI-1$. The objective was to design a suitable and reliable mechanical structure, in accordance with typical requirements and functions of a satellite in orbit. This section discusses the results and the project in general.

5.1 Summary of the accomplished work

The first part of this work constituted a presentation of the CubeSat standard and general requirements associated to this definition. The structural part's functions were drawn. A basic list of requirements were then given to respect our objectives.

Chapter 2 presented both mechanical and electrical components as well as their functions. The technical constraints concerning the flight system configuration were given, and the strong effect of environmental requirements on the overall design was highlighted. A configuration conforms to these constraints was developed and discussed.

Chapter 3 developed an accurate mass budget and demonstrated the fulfillment of the mass requirement. Inertia and center of gravity were assessed to provide reliable information to ADCS and MIAS subsystems. The complete solar panels design was performed in accordance to the design requirements. A particular material, the aluminum, was chosen to ensure the structural reliability and the fulfillment of the environmental constraints (e.g. thermal, radiative). The panels' thickness was defined to shield the spacecraft equipment during 1 year.

Then, first finite element analyses were performed to ensure the structural requirements during launch. In particular, the batteries' PCB was studied to sustain the dynamic loads and protect the electronic components on both EPS. A static case and a modal analysis were also performed.

Finally, the chapter 4 presented the modal survey of the CSK structure and its correlation to the modal analysis. Preliminary vibration tests were performed and some guidelines to the future electronic cards layout were stated.

At this point of the project, the structural subsystem fulfills all the defined objectives. Indeed, the environmental constraints, the design and mass requirements as well as the structural integrity are ensured through this work. The future work could then be developed on this basis.

5.2 Perspectives

This section intends to give some guidelines to the future work on the structural subsystem. Chapter after chapter, problems are highlighted in accordance to the future project's developments.

Concerning the flight system configuration, the next problem will be the complete analysis of the EMC with the cards. They should be verified in anechoic room and the conclusions should confirm the actual cards' order. On the other hand, the accurate antennas' radiance diagram should be taken into account to locate precisely the permanent magnet. The integration procedure has to be continued, and the new developments has to be integrated.

The accurate mass budget should be updated to obtain a more and more refined definition of the mass consuming. The theoretical definition of COG and inertia terms should also be verified as soon as a complete engineering model will be available. The EPS should chose definitively the batteries and the PCB electrical layout to allow a final design. Additional FEM will be also necessary during the future work. In particular, the modal analysis with the electronic cards and a random analysis should be performed.

Finally, the experimental modal survey of CubeSat and its electronic cards should be performed and correlated to its finite element model. In addition to this, further investigations on the vibrations mitigations on electronic cards could be drawn.

5.3 Personal point of view

If the real objective of this project was "fun and education´´, it was definitely achieved.

$OUFTI-1$ provided me with a unique opportunity to confront myself with a real space project. This master thesis allowed me to venture off the beaten track while learning a lot of lessons. $OUFTI-1$ constituted an interesting difference in my degree course with a hands-on project performed in a multidisciplinary team.

I learned a lot from the industrial framework : the external constraints (e.g. delivery time, availability of products), the work within a team with a pleasant atmosphere, and almost the difference between theory and practice, even if both are necessary one to the other.

This project gave me the opportunity of my first trip to California and to ESTEC in the Netherlands. I talk with the Belgian cosmonaut Frank De Winne, and I met many interesting people.

I have learned a lot from all my friends, project managers and professors, both from human and technical point of view. On the other hand,

work with students from engineering schools was also a very good experience, their approaches being complementary to the university's.

The conclusions of all of this could be simply "I learned´´. My technical background is now much more important than I expected. I have another approach to projects. From the master thesis writing to the thoughtful finding of technical solutions, I have also learned to be much more calm, rigorous and pragmatic. So, I just want to say to the future students : Just go on!

Appendix

Contents

A PC-104 LAYOUT

B Solar panels design

Batteries datasheets

C

Interface design

D

Bibliography

[1] F. Aguado, "Status on xatcobeo," *CubeSat Developers' Workshop*, Apr 2009. (Quoted page 58.)

[2] J. Aldeguer, "Conception de cartes pour équipements spatialisables," Alcatel Space, Cannes, France, Tech. Rep., Aug 2005. (Quoted pages 56 et 99.)

[3] M. Ashby, *Materials Selection in Mechanical Design*. Butterworth-Heinemann, 1999. (Quoted pages 51, 52, 53 et 65.)

[4] ——, *Materials, Engineering, Science, Processing and Design*. Elsevier, 2007. (Quoted page 51.)

[5] AzurSpace, "Azurspace's website," http://www.azurspace.com/. (Quoted pages 5 et 24.)

[6] V. Bashbush, "Characterization of the internal and external environments of the cubesat p-pod and test pod," California Polytechnic State University, San Luis Obispo, California, United States of America, Tech. Rep., Jan 2004. (Quoted page 3.)

[7] C. Berna and M. Luron, *Vega User's Manual*, Ariane Espace, Jan 2002. (Quoted pages 6, 8, 9 et 67.)

[8] V. Beukelaers, "Compte rendu de la réunion radiation au centre spatial de liège," ULg, Liège, Belgique, Tech. Rep., Feb 2009. (Quoted pages 55 et 56.)

[9] ——, "From mission analysis to space flight simulation of the oufti-1 nano-satellite," ULg, Liège, Belgique, Tech. Rep., May 2009. (Quoted pages 27, 56 et 78.)

[10] J. Brown, "Test pod user's guide rev 6," California Polytechnic State University, Tech. Rep., jun 2006. (Quoted pages 69, 91, 93 et 94.)

[11] U. CalPoly, "Cp-x website," http://polysat.calpoly.edu. (Quoted page 4.)

[12] ——, "Cubesat community website," http://cubesat.atl.calpoly.edu. (Quoted page 4.)

[13] J. Chan, "Kumu a o cubesat project," *CubeSat Developers' Workshop*, Apr 2009. (Quoted page 4.)

[14] ClydeSpace, "Clydespace's website," http://www.clyde-space.com/. (Quoted page 14.)

[15] A. De Rooy, "The degradation of metal surfaces by atomic oxygen," *ESA - Estec*, Nov 1985. (Quoted page 54.)

[16] C. De Silva, *Vibration and shock handbook*. Taylor & Francis, 2005. (Quoted page 99.)

[17] J. Debongnie, *Conception Mécanique*. Aees, 2005. (Quoted page 93.)

[18] A. Denis, "Références techniques de cubesats récemment lancé," *ULg*, May 2008. (Quoted page 3.)

[19] L. Dusseau, "Robusta, un satellite pédagogique," *EDP Science*, Jan 2009. (Quoted page 2.)

[20] N. ECSS, "Ecss-e-30 part 2a - space engineering, mechanical part 2 : structural," ESA, Tech. Rep., Apr 2000. (Quoted page 70.)

[21] ——, "Ecss-q-70-71a rev. 1 - data for selection of space materials and processes," ESA, Tech. Rep., June 2004. (Quoted pages 54 et 62.)

[22] ESA, "Esa materials website database," http://esmat.esa.int. (Quoted pages 54 et 60.)

[23] ESTEC, *Adhesive Handbook, ECSS-EHB-32-11 Draft 2*. ESA, 2007. (Quoted pages 58, 59, 60 et 61.)

[24] ——, *Materials Handbook, ECSS-HB-304 Draft 2*. ESA, 2007. (Quoted page 54.)

[25] ——, "Space engineering, technical requirements specifications," ESTEC, ECSS normalisation, Tech. Rep., 2009. (Quoted page 6.)

[26] N. Evrard, "Conception et réalisation du système de mesures du nanosatellite oufti-1," Institut Gramme, Tech. Rep., Jun 2009. (Quoted page 22.)

[27] P. Fortescue and al., *Spacecraft Systems Engineering*. Wiley, 2003. (Quoted pages 54 et 56.)

[28] P. Galeone, "Approach for the structural tests for the qualification of the cubesats/p-pods," *ESA-ESTEC*, Apr 2009. (Quoted pages 8 et 96.)

[29] *CES Selector*, Granta Design Limited, Jan 2008. (Quoted page 55.)

[30] L. Halbach, "Oufti-1 project requirements, mission and system definition," *ULg*, Feb 2009. (Quoted page 4.)

[31] S. Hannay, "Attitude determination and control system of student nanosatellite oufti-1 of university of liege," ULg, Tech. Rep., May 2009. (Quoted pages 7, 19, 29, 43 et 78.)

[32] J. Hardy, "Implémentation du protocole ax.25 à bord du nanosatellite oufti-1," Institut Gramme, Tech. Rep., Jun 2009. (Quoted page 23.)

[33] P. Haris, "Pc104 plus specification, v2.2," PC104 consortium, Tech. Rep., Jan 2007. (Quoted pages 17, 21 et 27.)

[34] R. Henrard, "Design et implémentation du système de télécommunications du nanosatellite oufti-1," Institut Supérieur Industriel Liégeois, Tech. Rep., May 2009. (Quoted pages 23 et 27.)

[35] L. Jacques, "Thermal design of the oufti-1 nanosatellite," ULg, Tech. Rep., May 2009. (Quoted pages 6, 23, 24, 28, 49, 60 et 64.)

[36] S. Jardon, "V2i, plan de table des shakers ling 80, gw 26 et ling csl," V2i, Tech. Rep., Jul 2008. (Quoted page 93.)

[37] A. Kalman, "Pumpkin's website," http://www.cubesatkit.com/. (Quoted pages 5, 13 et 14.)

[38] ——, "Overview of the cubesat kit," Pumpkin Inc., Tech. Rep., Jan 2004. (Quoted pages 13 et 14.)

[39] ——, "Cubesat kit spring plunger feet," Pumpkin Inc., Tech. Rep., May 2005. (Quoted page 16.)

[40] ——, "Csk midplane standoff kit," Pumpkin Inc., Tech. Rep., Mar 2008. (Quoted page 18.)

[41] ——, "Cubesat kit. fm430 flight module, rev c," Pumpkin Inc., Tech. Rep., Jun 2008. (Quoted page 27.)

[42] G. Kerschen and al., *Experimental Modal Analysis*. LTAS, 2008. (Quoted pages 83, 84 et 85.)

[43] C. Key, *Materials selection list for space hardware systems*. NASA, 1988. (Quoted pages 7, 47 et 54.)

[44] J. Lecomte, *Sélection des matériaux*. LTAS, 2008. (Quoted page 51.)

[45] P. Ledent, "Design and implementation of on-board digitaly controled electrical power supply of student nanosatellite oufti-1 of university of liege," ULg, Tech. Rep., May 2009. (Quoted pages 22 et 23.)

[46] ——, "Test report, vacuum tests for varta and kokam batteries," ULg, Liège, Belgique, Tech. Rep., May 2009. (Quoted page 27.)

[47] S. Lee, "Cubesat design specification rev. 11," *California Polytechnic State University*, Feb 2008. (Quoted pages 3, 6, 7, 8, 9, 14 et 47.)

[48] J. MacCutcheon, "Internally damped circuit articles," Minesota mining and manufacturing co., Tech. Rep., Sep 1996. (Quoted page 99.)

[49] F. Mahy, "Design and implementation of on-board telecommunication system of student nanosatellite oufti-1 of university of liège," ULg, Tech. Rep., May 2009. (Quoted pages 22, 23 et 27.)

[50] F. Marin, "V2i, shaker's characteristics," V2i, Tech. Rep., Sep 2008. (Quoted page 92.)

[51] U. of Applied Sciences Aachen, "Compass 1 website," http://www.cubesat.de/. (Quoted page 4.)

[52] U. of Dresde, "Tud - faculty of computer science," http://www.inf.tu-dresden.de. (Quoted pages 23 et 28.)

[53] U. of Louisiana, "Cape's website," http://cape.louisiana.edu. (Quoted page 4.)

[54] U. of Technology Delft, "Delfi-c3's website," http://www.delfic3.nl. (Quoted page 4.)

[55] U. of Toronto, "Can-x2 website," http://www.utias-sfl.net. (Quoted page 4.)

[56] J. Pedersen, "Vega cubesats icd iss 0 rev 4 draft," *ESA*, pp. 18–25, Feb 2009. (Quoted pages 6, 7, 8, 9, 47, 67, 76, 93 et 96.)

[57] G. Pierlot, "Oufti-1's integration procedure," ULg, Tech. Rep., Mar 2009. (Quoted page 38.)

[58] J. Pitarresi, "Dynamic modeling and measurements of personal computer motherboards," University of New-York, Tech. Rep., Feb 2008. (Quoted page 75.)

[59] E. Porter, "Cell specification data, slpb 554374h," Kokam, Tech. Rep., Feb 2007. (Quoted page 23.)

[60] ——, "Cell specification data, slpb 603870h," Kokam, Tech. Rep., Feb 2007. (Quoted page 23.)

[61] A. Reif, "Cubesat control document," Pumpkin Inc., Tech. Rep., Dec 2003. (Quoted pages 7, 13 et 14.)

[62] ——, "Cubesat kit pcb specification," Pumpkin Inc., Tech. Rep., Sep 2003. (Quoted page 21.)

[63] ——, "Cubesat kit system chart," Pumpkin Inc., Tech. Rep., Aug 2007. (Quoted page 40.)

[64] ——, "Solar panel clips set data sheet rev. a," Pumpkin Inc., Tech. Rep., May 2007. (Quoted pages 31 et 46.)

[65] G. Richardson, "Analysis of simplified fe models of pcbs exposed to random vibrations," University of Southampton, Tech. Rep., Feb 2008. (Quoted pages 69 et 75.)

[66] G. Roethlisberger, "Swisscube structural design and flight system configuration, phase b," EPFL, Lausanne, Switzerland, Tech. Rep., Feb 2007. (Quoted pages 3, 31, 60, 62, 69 et 75.)

[67] J. Safrany, "Anodisation de l'aluminium et de ses alliages," *Les techniques de l'ingénieur*, Feb 2003. (Quoted page 55.)

[68] Samtec, "High speed rugged/power, micro interconnects," http://www.samtec.com/. (Quoted page 22.)

[69] *Samcef User Manual*, Samtech, Rue des chasseurs ardenais 4000 Liège, Oct 2008. (Quoted page 67.)

[70] H. Schnirch, "Plf 463759c technical specification," Varta, Tech. Rep., Aug 2007. (Quoted page 23.)

[71] Shibayama and al., "Identification of the center-of-gravity and inertia terms of 3-dimensional body," Oct 2006. (Quoted page 45.)

[72] G. Strobl, "Evolution of fully european triple gaas solar cell," *Seventh European Space Power Conference*, May 2005. (Quoted page 24.)

[73] ——, "Solar cells 3g28 data sheet," Azurspace, Tech. Rep., apr 2007. (Quoted pages 27 et 46.)

[74] D. Systemes, "Dassault systemes : Catia - plm solution," http://www.3ds.com/products/catia/welcome/. (Quoted page 10.)

[75] D. Teney, "Design and implementation of on-board processor and software of student nanosatellite oufti-1 of university of liège," ULg, Tech. Rep., May 2009. (Quoted page 22.)

[76] Thales, "Thales website," http://www.thalesaleniaspace.com. (Quoted pages 5 et 57.)

[77] P. Thirion, "Design and implementation of on-board electrical power supply of student nanosatellite oufti-1 of university of liege," ULg, Tech. Rep., May 2009. (Quoted pages 22, 24 et 28.)

[78] J. Tock, "Règles de conception d'un support d'expérience pour essais vibratoires," ULg, Tech. Rep., Jun 1992. (Quoted pages 92 et 93.)

[79] K. Trusco, "Cga633450b technical specification," Panasonic, Tech. Rep., Jan 2007. (Quoted page 23.)

[80] B. Twiggs, "Making it smaller," *CubeSat Developers' Workshop*, Apr 2009. (Quoted page 2.)

[81] J. Wertz, "Conception et réalisation du système de déploiement des antennes du nanosatellite oufti-1," Institut Gramme, Tech. Rep., Jun 2009. (Quoted page 20.)

[82] I. Yang, "Elevated sockets datasheet," Samtec, Tech. Rep., Sep 2008. (Quoted page 22.)

[83] ——, "Socket strip datasheet," Samtec, Tech. Rep., Sep 2008. (Quoted page 21.)

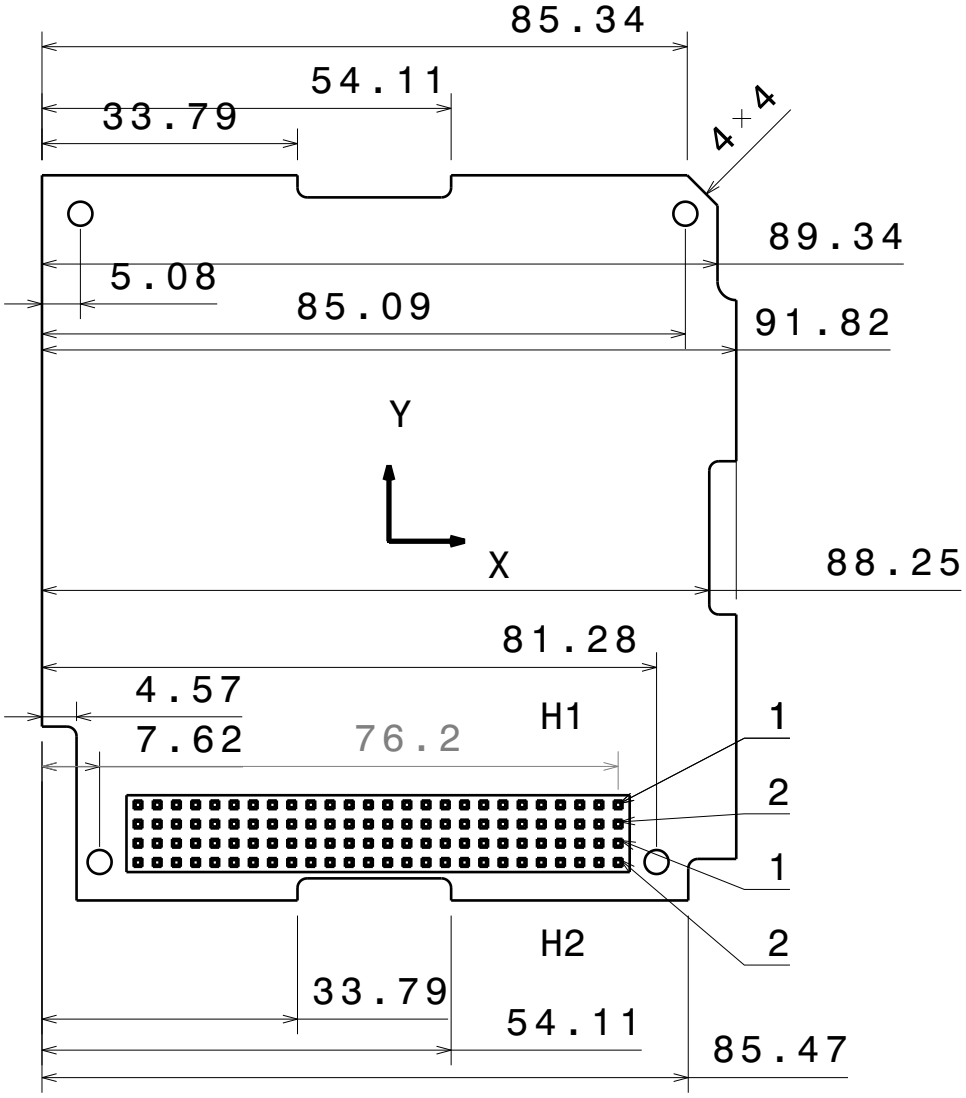

Vue de face
Echelle : 1:1

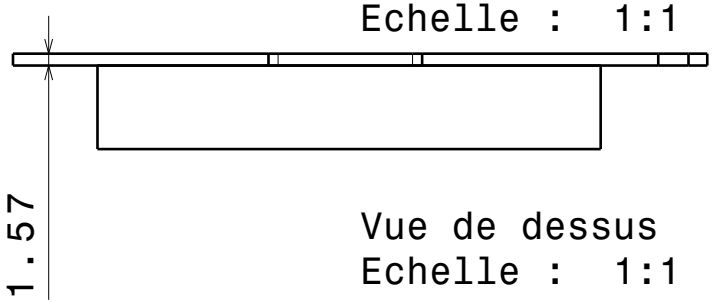

Vue de dessus
Echelle : 1:1

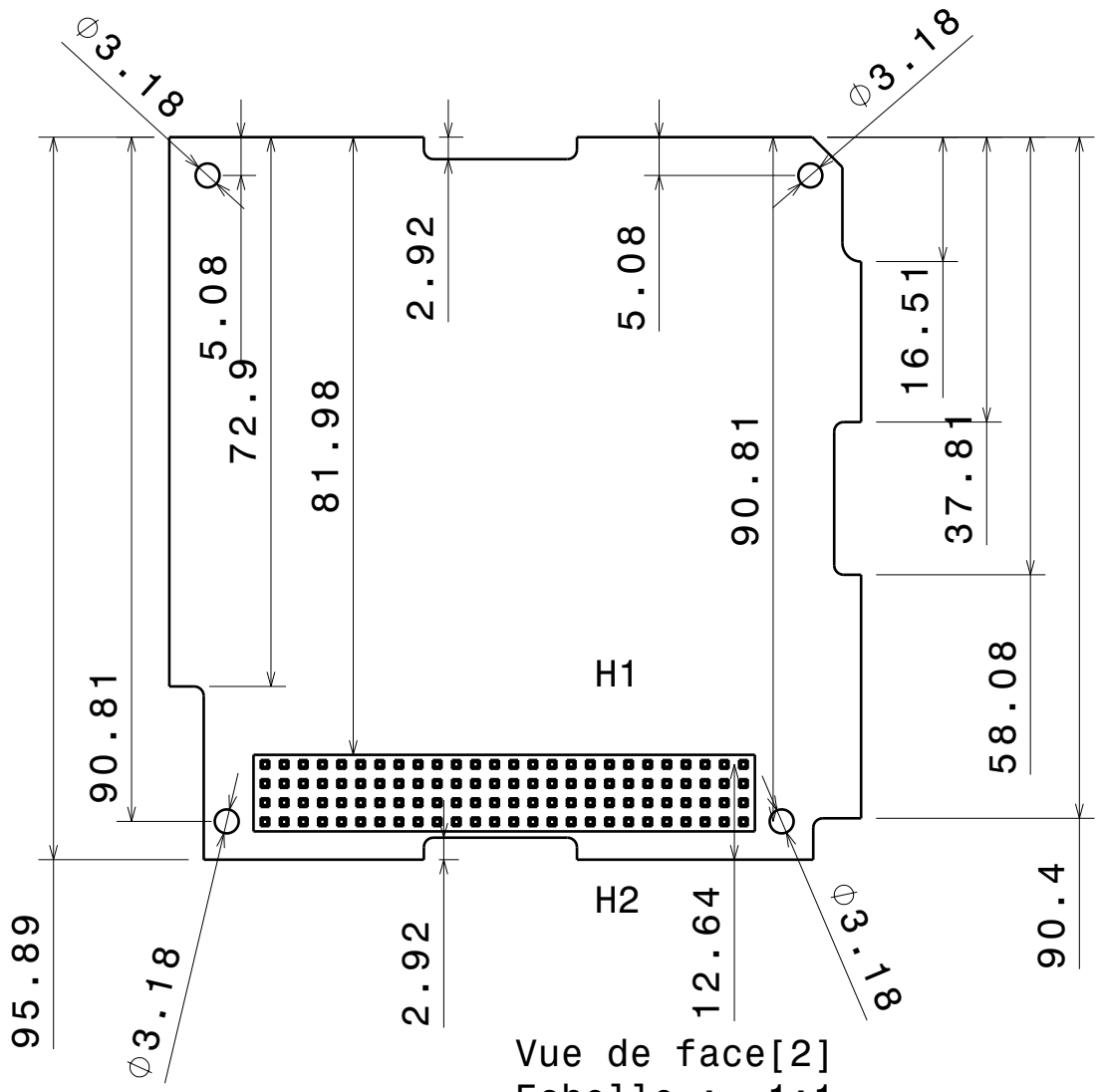

Vue de face[2]
Echelle : 1:1

Tolérances non référencées : +/- 0.05mm	Nb.	Désignation	Matériel
	1	Carte	GFRP FR4
	Ech 1:1	PC104 +	Nom : Pierlot G.
Note : /	ULg, LTAS		Date : 06/03/2009

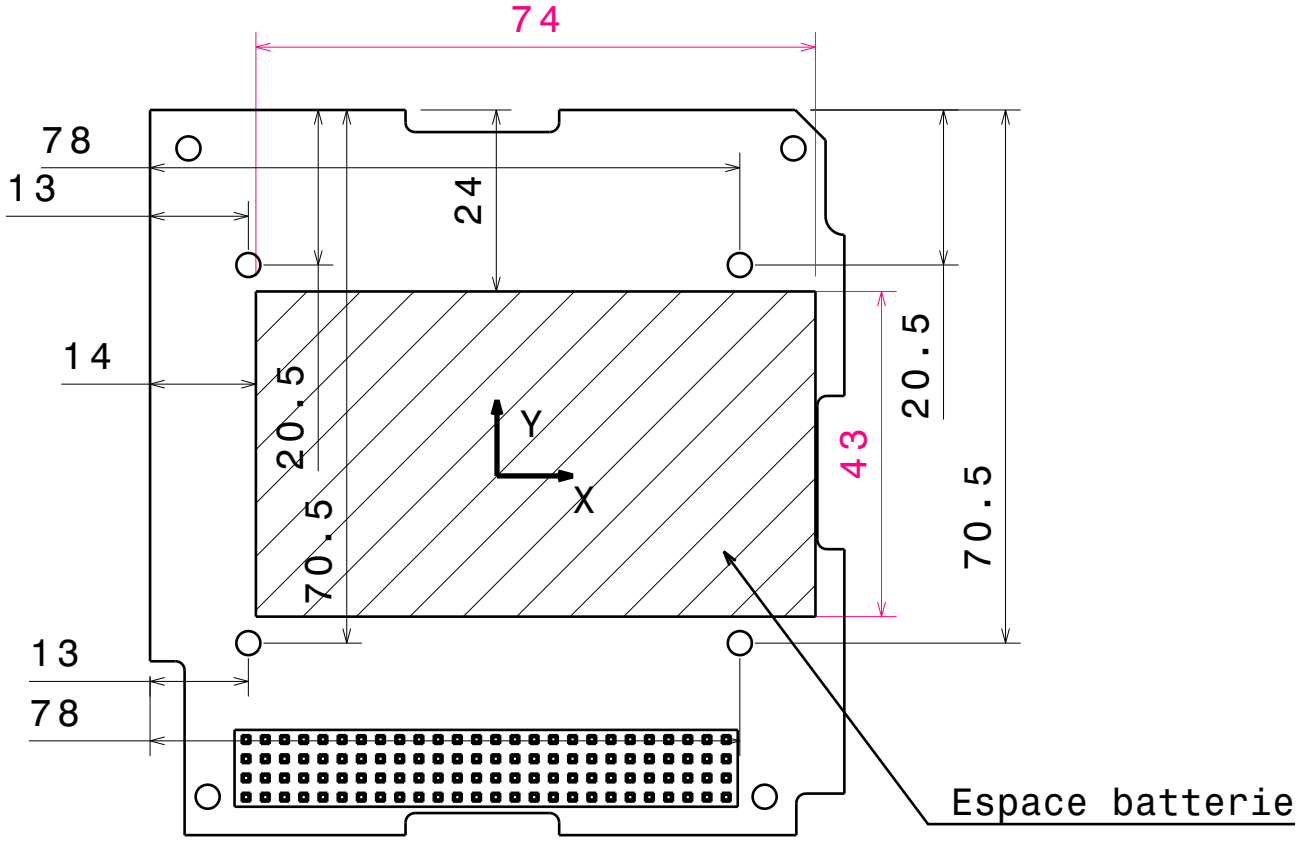

Vue de face
Echelle : 1:1

Les dimensions générales restant les mêmes,
seuls les 4 trous du PCB batteries sont annotées
La zone de l'espace batterie limite la hauteur
des composants à 4mm

Tolérances non référencées : +/- 0.05mm	Nb.	Désignation	Matériel
	/	Carte	GFRP FR4
	Ech 1:1	PC104 + EPS2	Nom : Pierlot G.
Note : rev1	ULg, LTAS		Date :14/03/2009

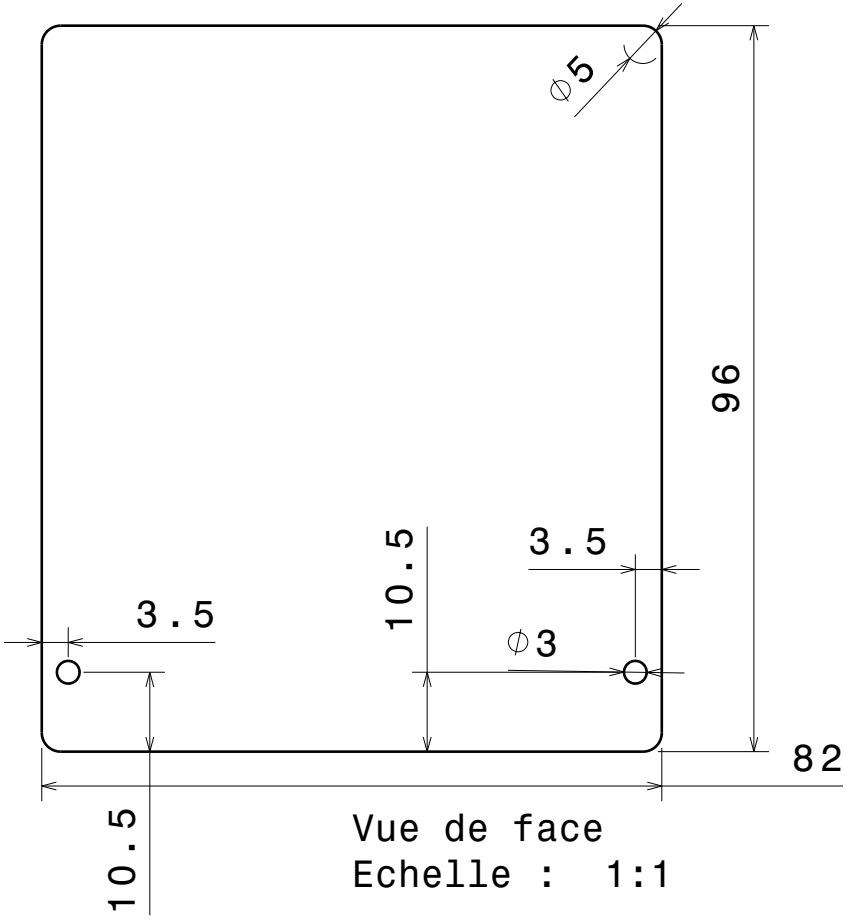

Vue de face
Echelle : 1:1

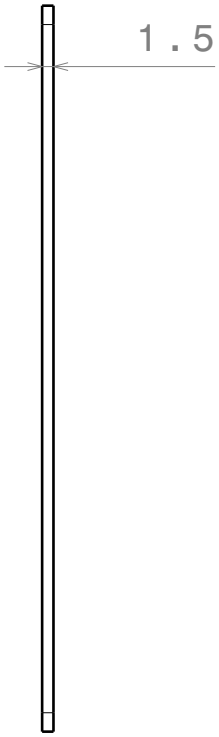

Vue de gauche
Echelle : 1:1

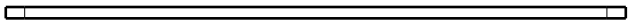

Vue de dessus
Echelle : 1:1

Tolérances non référencées : +/- 0.05mm	Nb.	Désignation	Matériel
	3	Panneau solaire	Al 7075-T73
	Ech 1:1	+X,+/-Y	Nom : Pierlot G.
Note : /	ULg, LTAS		Date : 25/01/2009

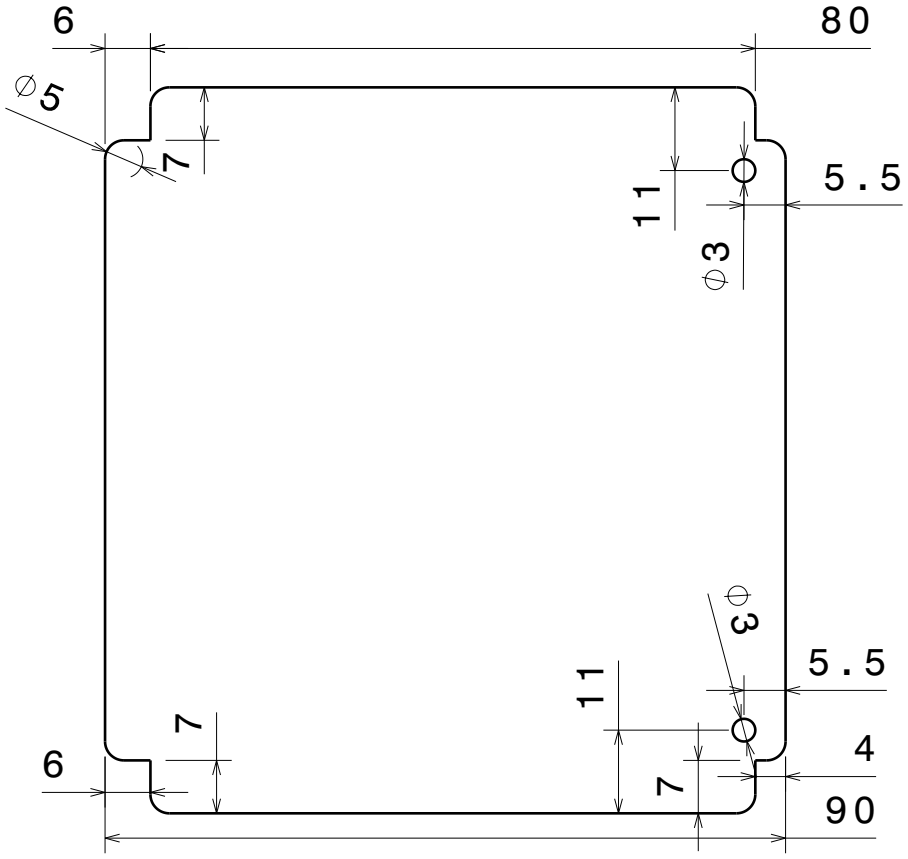

Vue de face
Echelle : 1:1

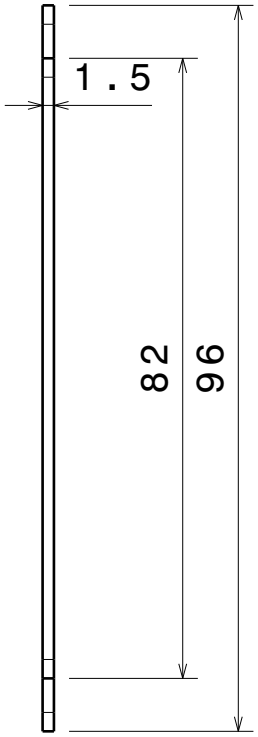

Vue de gauche
Echelle : 1:1

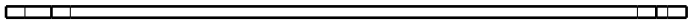

Vue de dessus
Echelle : 1:1

Tolérances non référencées : +/- 0.05mm	Nb.	Désignation	Matériel
	1	Panneau solaire	Al 7075-T73
	Ech 1:1	+Z	Nom : Pierlot G.
Note : /	ULg, LTAS		Date : 25/01/2009

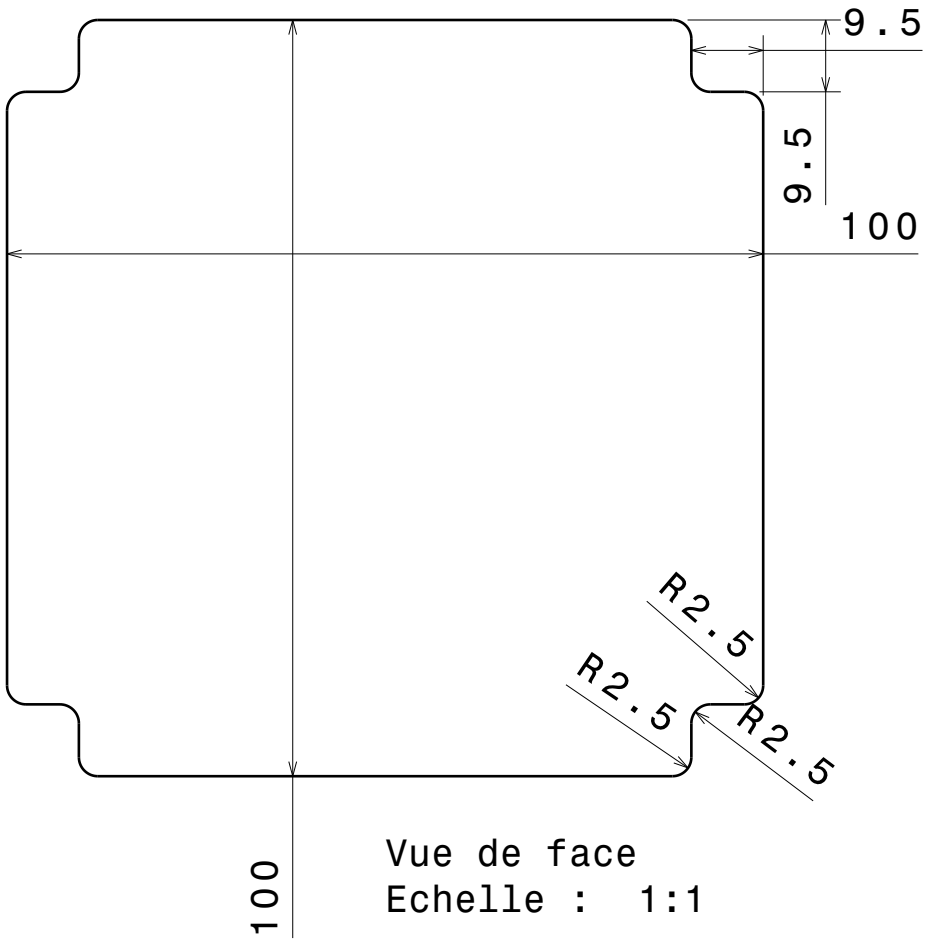

Vue de face
Echelle : 1:1

Vue de gauche
Echelle : 1:1

Tolérances non référencées : +/- 0.05mm	Nb.	Désignation	Matériel
	1	Panneau solaire	Al 7075-T73
	Ech 1:1	-Z	Nom : Pierlot G.
Note : /	ULg, LTAS		Date : 25/01/2009

Cell Specification Data

SLPB 554374H

Kokam Co., Ltd.

Cell Specification

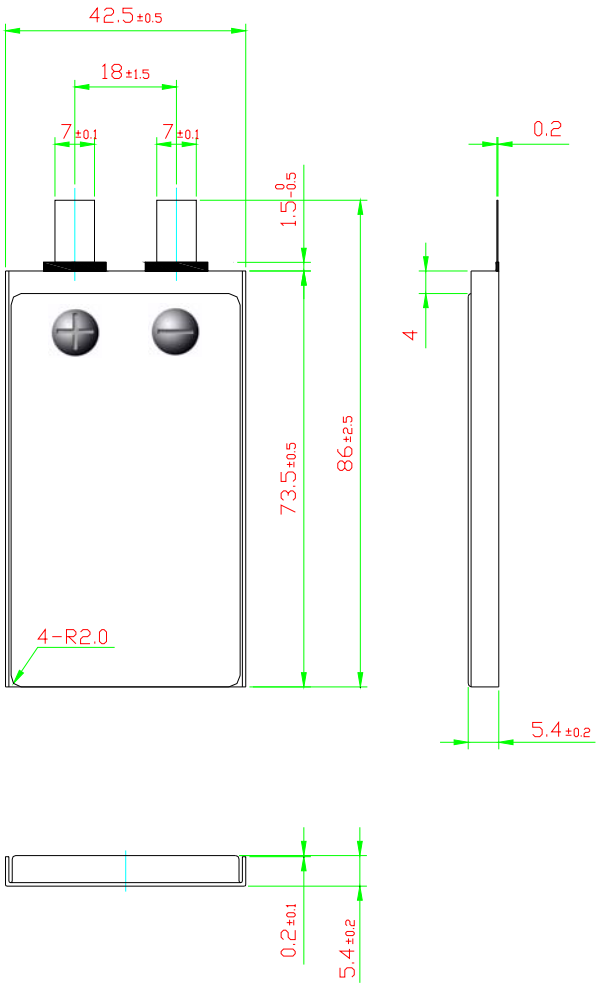

Typical Capacity[1)]		1.25 Ah
Nominal Voltage		3.7 V
Charge Condition	Max. Current	2.5 A
	Voltage	4.2V ± 0.03 V
Discharge Condition	Continuous Current	18.75 A
	Peak Current	37.50 A
	Cut-off Voltage	2.7 V
Cycle Life		> 500 Cycles
Operating Temp.	Charge	0 ~ 40 ℃
	Discharge	-20 ~ 60 ℃
Dimension	Thickness (mm)	5.4 ± 0.2
	Width (mm)	42.5 ± 0.5
	Length (mm)	73.5 ± 0.5
Weight (g)		32.0 ± 1.0

1) Typical Capacity : 0.5C, 4.2~2.7V @25°C

Cell Specification Data

SLB 603870H

Kokam Co., Ltd.

Cell Specification

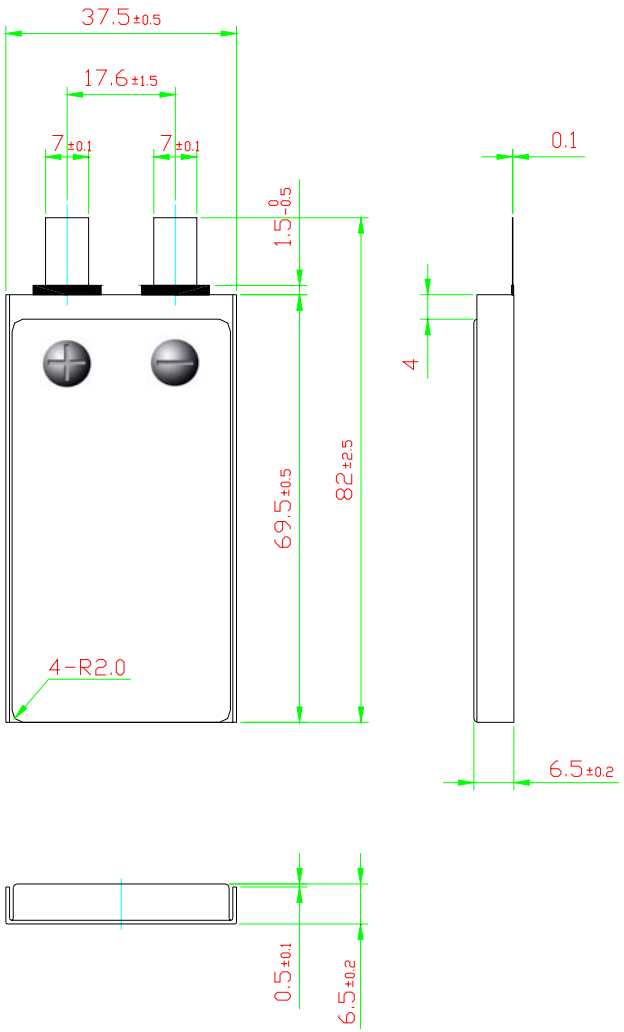

Typical Capacity[1)]		1.5 Ah
Nominal Voltage		3.7 V
Charge Condition	Max. Current	3.0 A
	Voltage	4.2V ± 0.03V
Discharge Condition	Continuous Current	12.0 A
	Peak Current	24.0 A
	Cut-off Voltage	2.7 V
Cycle Life		> 500 Cycles
Operating Temp.	Charge	0 ~ 40℃
	Discharge	-20 ~ 60 ℃
Dimension	Thickness (mm)	6.5 ± 0.2
	Width (mm)	37.5 ± 0.5
	Length (mm)	69.5 ± 0.5
Weight (g)		32.0 ± 1.0

1) Typical Capacity : 0.5C, 4.2 ~ 2.7V @25°C,

Cell Specification Data

SLPB 723870H4

Kokam Co., Ltd.

Cell Specification

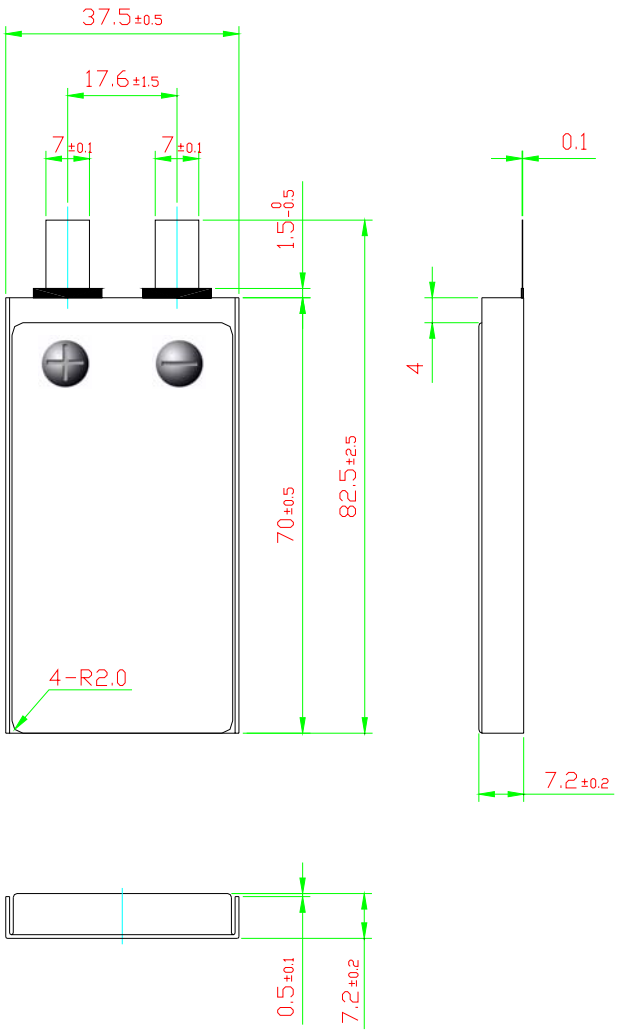

Typical Capacity[1)]		1.5 Ah
Nominal Voltage		3.7 V
Charge Condition	Max. Current	3.0 A
	Voltage	4.2V ± 0.03 V
Discharge Condition	Continuous Current	30.0 A
	Peak Current	60.0 A
	Cut-off Voltage	2.7 V
Cycle Life		> 500 Cycles
Operating Temp.	Charge	0 ~ 40 ℃
	Discharge	-20 ~ 60 ℃
Dimension	Thickness (mm)	7.2 ± 0.2
	Width (mm)	37.5 ± 0.5
	Length (mm)	70.0 ± 0.5
Weight (g)		37.0 ± 1.5

1) Typical Capacity : 0.5C, 4.2 ~ 2.7V @25°C

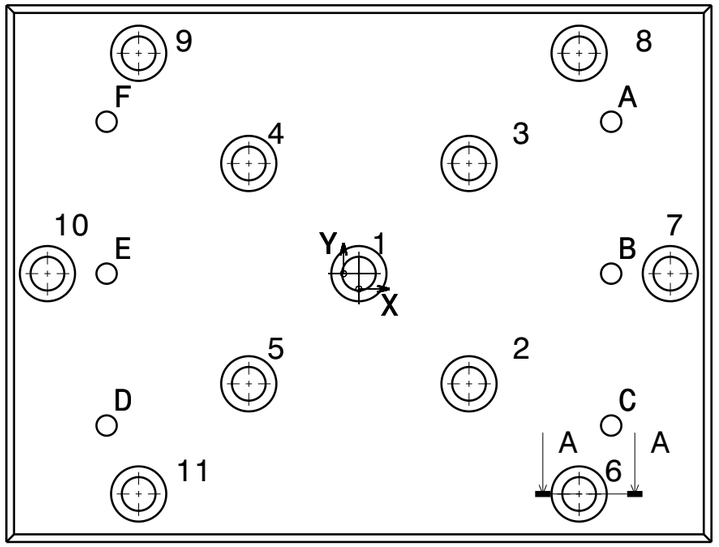

Vue de face
Echelle : 1:2

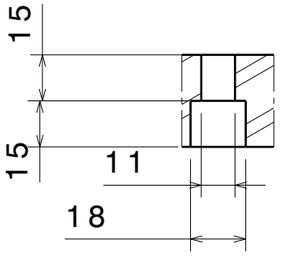

Coupe A-A
Echelle : 1:2

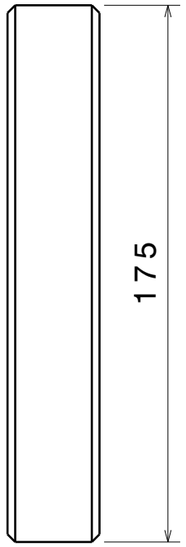

Vue de gauche
Echelle : 1:2

REF.	X	Y	Diamètre
1	0	0	11
2	35.92	-35.92	11
3	35.92	35.92	11
4	-35.92	35.92	11
5	-35.92	-35.92	11
6	71.84	-71.84	11
7	101.6	0	11
8	71.84	71.84	11
9	-71.84	71.84	11
10	-101.6	0	11
11	-71.84	-71.84	11

REF.	X	Y	Diamètre
A	82,3	49,53	6,65
B	82,3	0	6,65
C	82,3	-49,53	6,65
D	-82,3	-49,53	6,65
E	-82,3	0	6,65
F	-82,3	49,53	6,65

Les trous A,B,C,D,E,F sont taraudés M8
Les trous de 1 à 11 sont passant

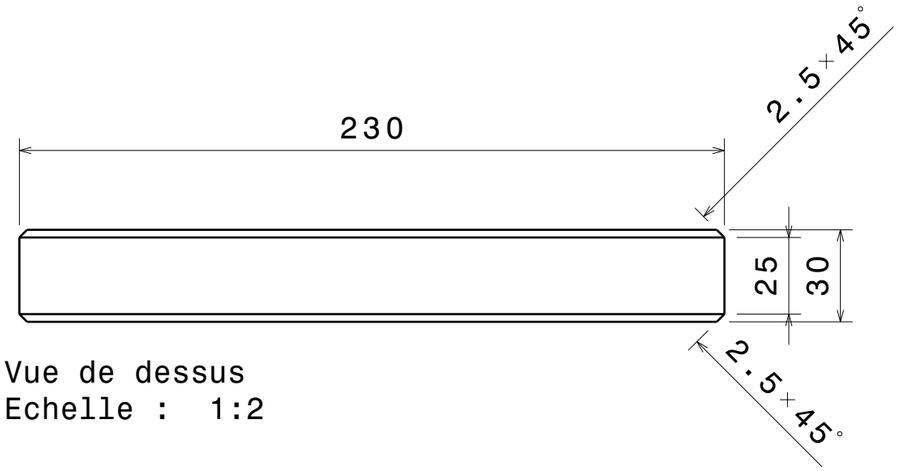

Vue de dessus
Echelle : 1:2

Tolérances non référencées : +/- 0.1mm	Nb.	Désignation	Matériel
	1	Support	Aluminium
	Echelle 1:2	Interface test-pod	Nom : Pierlot G.
Note : /	ULg, Département aérospatial		Date : 01/01/2009

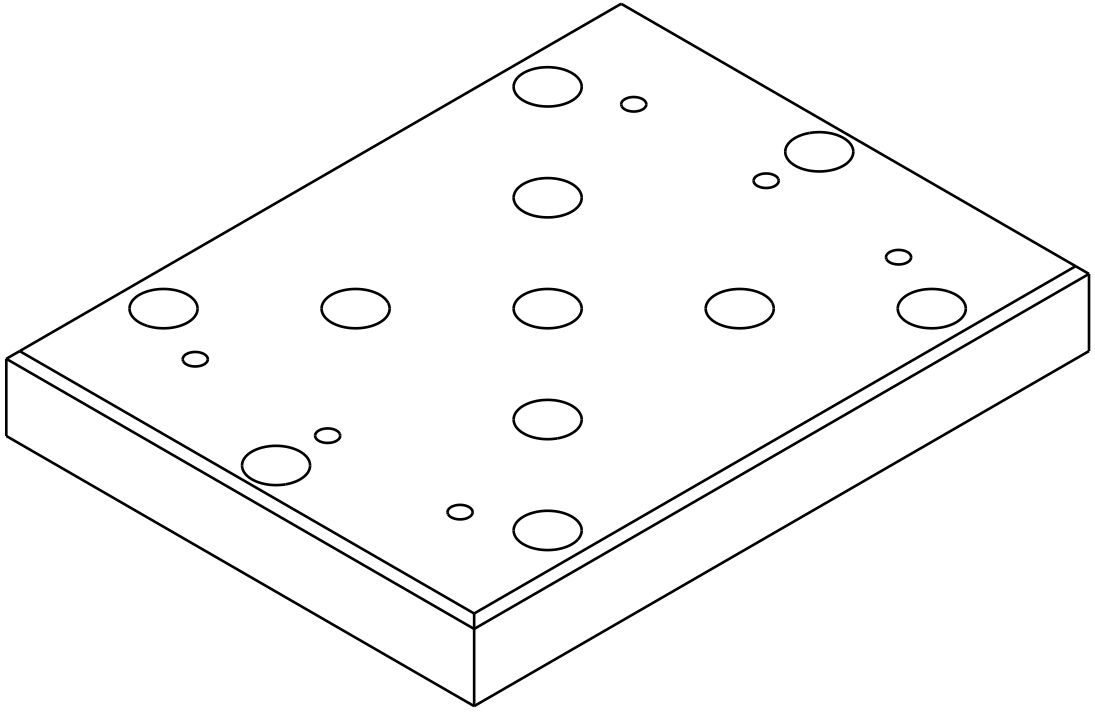

Vue isométrique
Echelle : 1:2

Tolérances non référencées : +/- 0.1mm	Nb.	Désignation	Matériel
	1	Support	Aluminium
	Echelle 1:2	Interface test-pod	Nom : Pierlot G.
Note : /	ULg, Département aérospatial		Date : 01/01/2009